

**Examining the role of *Mco4* in *Drosophila* iron transport**

by

Areeg Abd Elhafiz

A thesis submitted in partial fulfilment of the requirements for the degree of

Master of Science

In

Molecular Biology and Genetics

Department of Biological Sciences

University of Alberta

©Areeg Abd Elhafiz, 2022

## ABSTRACT

Iron is involved in many aspects of life and is essential for survival and normal development. The role of iron in the body is crucial for many processes, including oxygen transport, steroid hormone synthesis, and DNA repair. However, iron transport in *Drosophila melanogaster* is less characterized compared to mammalian systems. The mechanism behind how dietary iron is absorbed and transported throughout the body is not entirely clear. Three independent RNA-Seq experiments performed by former Ph.D. students from the King-Jones lab identified significant upregulation of the *Drosophila melanogaster* gene multicopper oxidase 4 (*Mco4*) under iron-deprived conditions. This signifies *Mco4*'s possible involvement in the cell's response to low iron conditions. *Mco4* is the ortholog of yeast *Fet3* and is predicted to encode a multicopper ferroxidase. Fet3p works in conjunction with the transport protein Ftr1p and is required for high affinity iron import. Accordingly, this thesis proposes *Mco4* to function as a high affinity iron importer under low iron conditions in *Drosophila*. The cellular localization and tissue distribution of *Mco4* has not been reported before. Therefore, I generated an *ex vivo* overexpression construct and a transgenic line to study the localization of *Mco4* in cells and tissues. In both experiments, I found *Mco4* to be localized in the cell membrane, similar to its ortholog Fet3p. To further understand its function, I generated a complete *Mco4*-loss-of-function line using CRISPR/Cas9. Analysis of the *Mco4* null mutant flies was found to significantly reduce the survival rate when these mutants were reared on a low iron diet. To my knowledge, this is the first time a complete loss of *Drosophila Mco4* function has been reported. Based on these findings, it would seem likely for *Mco4* to play a key role in the cell's response to low iron levels as a potential ferroxidase.

## ACKNOWLEDGMENTS

This thesis would not have been possible without the support of numerous people around me, especially with the impact the COVID-19 pandemic has had on all aspects of our lives. I would like to first begin by expressing my sincere gratitude to my supervisor, Dr. Kirst King-Jones, for accepting me into his lab for my master's program. Without his guidance and support throughout my program, this thesis would not be possible. It is immeasurable how much I've learned, and I am incredibly grateful for having had this opportunity. My sincere gratitude also goes to my current and past lab mates, who have been understanding and helpful during the extent of my program. I want to particularly thank Dr. Wen Liu, a postdoc in our lab, for guiding me personally through generating my constructs and being patient with his explanations for the many questions I had. I would also like to thank Dr. Andrew Waskiewicz from my committee for his feedback and input during my committee meeting and throughout my master's program.

I would like to thank the Molecular Biology Service Unit (MBSU) team, Cheryl for being so kind and helpful with her assistance and Troy for lending his knowledge in explaining RNA-Seq and RT-qPCR validation analysis. A special thanks to Dr. Lakshmi, my undergraduate professor at UMS, whose support allowed me to pursue this path. I acknowledge that all the illustrations I have presented in this thesis are created using the BioRender tool.

An extended gratitude to all the friends I've made throughout these formative years. The life of a master's student is so stressful, as you already know and meeting up together occasionally was the highlight of my week. Thanks for being great listeners, for the insightful conversations we've shared and for making this journey so memorable. You guys have been amazing, and I will surely miss each and every one of you.

Above all, I want to thank my family and especially my mother for her unconditional support, patience and care throughout my academic pursuit. I am grateful for their unwavering moral support and encouragement. Thank you for always listening, caring and having faith in me. Lastly, I would like to end this section with a favourite quote of mine.

"Success is peace of mind in knowing you did your best." - John Wooden

# TABLE OF CONTENTS

	Page
TABLE OF CONTENTS.....	iv
LIST OF TABLES.....	viii
LIST OF FIGURES AND ILLUSTRATIONS .....	ix
LIST OF ABBREVIATIONS.....	xi
CHAPTER	
<b>Chapter 1 Introduction .....</b>	<b>1</b>
1.0 Overview.....	1
1.1 Dietary Source of Iron .....	3
1.2 Iron Trafficking in Mammals.....	3
1.3 Mammalian Multicopper oxidases .....	5
1.31 Ceruloplasmin .....	5
1.32 Hephaestin .....	5
1.33 Zyklopen .....	6
1.4 Iron Imbalance Generates Free Radical Species .....	7
1.5 Regulation of Intracellular Iron in Mammals .....	7
2.1 Iron Trafficking in Yeast .....	9
2.2 Regulation of iron in Yeast .....	10
3.1 Iron Trafficking in <i>Drosophila</i> .....	11
3.2 <i>Drosophila</i> Multicopper oxidases .....	15
3.21 Multicopper oxidase 1 .....	15
3.22 Multicopper oxidase 2 ( <i>Straw</i> ).....	15
3.23 Multicopper oxidase 3 .....	16
3.24 Multicopper oxidase 4 .....	16
3.3 Regulation of iron in <i>Drosophila</i> .....	17

4.1	The <i>Drosophila</i> Prothoracic Gland as a Model for Studying Iron Metabolism .....	19
4.2	Heme Synthesis.....	21
5.0	Overview of the Secretory Pathway Involving Membrane-bound Proteins .....	24
6.0	Research objectives .....	26
<b>Chapter 2</b>	<b>Materials and methods.....</b>	<b>27</b>
2.1	<i>Drosophila</i> husbandry and maintenance .....	27
2.2	Preparation of embryo collection plates .....	27
2.3	Iron-supplemented medium .....	28
2.4	Iron-chelated medium .....	28
2.5	Survival study .....	28
2.6	Staging, Dissection and Slide preparation .....	28
2.7	Tissue Immunostaining: BRGC & Gut samples.....	29
2.8	DNA extraction from adult flies by DNAzol.....	29
2.9	DNA extraction from a single adult flies for transgenic insertion validation.....	30
2.10	RNA extraction from isolated PG and whole-body larval samples using TRIzol and the QIAGEN RNeasy® Mini Kit (cat.nos.74104).....	31
2.11	Gel extraction using the QIAquick® Gel Extraction kit (cat.nos.28704).....	31
2.12	DNA extraction using the Thermo Scientific GeneJET Plasmid Miniprep Kit (#K0503).....	32
2.13	Midiprep using the QIAGEN® Plasmid Midi Kit (cat.nos.12145).....	32
2.14	Purification of PCR products .....	33
2.15	Preparation of Competent cells .....	33
2.16	Transformation .....	34
2.17	Colony PCR .....	34
2.18	Gibson Assembly Reaction .....	35
2.19	Generation of constructs for S2 cell transfection.....	35
2.20	Generation of a transgenic <i>UAS-Mco4</i> line .....	35
2.21	Generation of the <i>Mco4</i> null mutant CRISPR line .....	36
2.22	Transfection of S2 Cells.....	36
2.23	Cell Immunodetection .....	37

2.24	cDNA Synthesis .....	37
2.25	Quantitative Real-Time PCR (qPCR).....	38
2.25.1	Primer validation .....	38
2.25.2	qPCR protocol.....	38
2.26	Statistics .....	39
2.27	Ferric iron staining .....	39
2.28	Centrifuge .....	39
<b>Chapter 3</b>	<b>Preliminary data generated in our lab suggests Mco4 may act as a high affinity iron importer .....</b>	<b>46</b>
<b>Chapter 4</b>	<b>Characterizing Mco4 function in <i>Drosophila</i> .....</b>	<b>53</b>
4.1	Individually analyzing the PG-specific knockdown of all four <i>Drosophila</i> multicopper oxidases using RNAi.....	53
	Results.....	54
4.21	RT-qPCR evaluation of RNA-Sequencing data .....	55
4.22	Analysing the effects of PG-specific <i>Mco4</i> knockdown .....	58
	Results.....	59
4.23	Analysing the effects of ubiquitously knocking down <i>Mco4</i> function .....	61
	Results.....	61
4.24	Intestinal iron staining of <i>tubulin&gt;Mco4<sup>RNAi-1</sup></i> gut using Perl's Prussian Blue stain...65	
	Results.....	66
4.25	Validating RNAi lines using RT-qPCR.....	68
	Results.....	68
	<b>Discussion.....</b>	<b>69</b>
<b>Chapter 5</b>	<b>Determining the subcellular localization of Mco4 in the cell.....</b>	<b>72</b>
5.1	Determining Mco4 localization <i>ex vivo</i> using S2 cells.....	76
	Results.....	76
5.2	Determine Mco4 localization using a transgenic line.....	78
	Results.....	79

<b>Discussion.....</b>	<b>82</b>
<b>Chapter 6 Generating an <i>Mco4</i><sup>-/-</sup> null mutation line via CRISPR/Cas9 .....</b>	<b>84</b>
6.1 Validating <i>Mco4</i> <sup>-/-</sup> line through RT-qPCR.....	87
Results.....	87
6.2 Examining the survival rates of <i>Mco4</i> <sup>-/-</sup> populations .....	88
6.3 Examining whether <i>Mco4</i> <sup>-/-</sup> flies display red autofluorescence.....	89
Results.....	90
6.4 Perl's Prussian Blue staining of whole guts isolated from <i>Mco4</i> <sup>-/-</sup> larvae.....	93
Results.....	93
<b>Discussion.....</b>	<b>94</b>
<b>Chapter 7 Summary and significance .....</b>	<b>96</b>
<b>Chapter 8 Future Directions .....</b>	<b>100</b>
8.1 Study <i>Mco4</i> null mutants under iron-chelated conditions over multiple generations .....	100
8.2 Identifying proteins that interact with Mco4 .....	100
8.3 Evaluate whether Mco4 contains a ferroxidase activity .....	102
8.4 Conclusion .....	103
<b>Literature Cited .....</b>	<b>104</b>

## LIST OF TABLES

Tables	Page
1.0 Summary of potential candidates involved in <i>Drosophila</i> iron transport ....	12
1.1 Comparison of human and <i>Drosophila</i> genes involved in iron homeostasis .....	13
2.1 List of <i>Drosophila</i> stocks .....	40
2.2 Immunostaining antibodies and staining reagent concentrations .....	41
2.3 List of primers .....	42
2.4 List of generated constructs .....	45
3.1 Summary of <i>Drosophila</i> MCOs fold changes in all three independent RNA-Seq experiments .....	49
3.2 Protein alignment of <i>Drosophila</i> MCOs with yeast Fet3p using BLASTP .....	49

## LIST OF FIGURES AND ILLUSTRATIONS

Figure	Page
1	Schematic representation of iron uptake and transport in mammals .....4
2	Schematic representation of iron regulation in mammals .....8
3	Schematic representation of iron transport in yeast .....10
4	Schematic representation of iron transport in <i>Drosophila</i> .....14
5	RIP-qPCR results for IRP1A <sup>C450S</sup> show Mco4 interaction .....18
6	Ecdysone biosynthesis in the PG .....20
7	Mutation in the <i>PPOX</i> gene ( <i>PPOX</i> <sup>13702</sup> allele) results in a porphyria-like phenotype .....22
8	Heme biosynthetic pathway .....23
9	Secretory pathway overview .....25
10	RNA-Seq experiment revealed upregulation of <i>Mco4</i> under dietary iron changes in Brain-Ring Gland Complex samples .....50
11	PG-specific disruptions of <i>AGBE</i> results in a porphyria-like phenotype and high <i>Mco4</i> upregulation. ....51
12	Transgenic expression of apo-IRP1A in the PG results in elevated <i>Mco4</i> expression .....52
13	Survival analysis of animals with PG-specific <i>Drosophila</i> multicopper oxidase (1-4) knockdown using RNAi .....55
14	RT-qPCR evaluations of high <i>Mco4</i> expression levels found in RNA-Seq data .....57
15	The survival rate of <i>Mco4</i> prothoracic knockdown flies reared on Nutri-Fly food .....59

16	Impairment of Mco4 function in the PG .....	60
17	The effect of a ubiquitous knockdown of <i>Mco4</i> on survival.....	63
18	Dissected midgut regions isolated from ubiquitous <i>Mco4</i> knockdown larvae reared on normal and iron-depleted conditions .....	64
19	Prussian blue larval gut staining of <i>tubulin&gt;Mco4<sup>RNAi-1</sup></i> larvae .....	67
20	RT-qPCR validation of <i>Mco4</i> RNAi lines.....	69
21	Predictions produced by both PSIPRED and SignalP 5.0 software .....	74
22	Sequence alignment of Mco4 and Fet3p .....	75
23	Plasmid constructs generated to study Mco4 subcellular localization <i>ex vivo</i> .....	77
24	Subcellular localization of Mco4 in S2 cells. ....	78
25	Transgenic line generated to study Mco4 subcellular localization.....	80
26	Subcellular localization of Mco4 in three different tissues .....	81
27	Schematic overview of CRISPR/Cas9 HDR-mediated <i>Mco4<sup>-/-</sup></i> line .....	86
28	Validation of <i>Mco4<sup>-/-</sup></i> line using RT-qPCR.....	88
29	The survival rate of <i>Mco4<sup>-/-</sup></i> flies on standard and iron-depleted food .....	89
30	Dissected PGs isolated from <i>Mco4<sup>-/-</sup></i> larvae reared on standard, and iron- depleted diets.....	90
31	Dissected midgut regions isolated from <i>Mco4<sup>-/-</sup></i> larvae reared on standard and iron-depleted diets.....	91
32	Dissected hindguts isolated from <i>Mco4<sup>-/-</sup></i> larvae reared on standard and iron-depleted food.....	92
33	Perl's Prussian blue staining of <i>Mco4<sup>-/-</sup></i> larvae reared on iron-depleted and iron-enriched food.....	93
34	Proposed model for high affinity iron transport in <i>Drosophila</i> during iron- deprived conditions .....	99

## LIST OF ABBREVIATIONS

<i>AGBE</i>	Alpha Glucan-Branching Enzyme
<i>attB</i>	Bacterial attachment site
<i>attP</i>	Phage attachment site
BPS	Bathophenanthroline Sulfate
BDSC	Bloomington Drosophila Stock Center
BRGC	Brain Ring Gland Complex
Co-IP	Co-Immunoprecipitation
CRISPR	Clustered Regularly Interspaced Short Palindromic Repeats
Dcytb	Duodenal Cytochrome b
DMT1	Divalent Metal Transporter 1
DSB	Double-strand break
DSCP	Drosophila Synthetic Core Promoter
EGFP	Enhanced Green Fluorescent Protein
ER	Endoplasmic Reticulum
FAC	Ferric Ammonium Citrate
Fe-S	Iron Sulphur Cluster
Fe <sup>3+</sup>	Ferric iron
Fe <sup>2+</sup>	Ferrous iron
FRET	Förster resonance energy transfer
FRT	Flippase Recombinase Target
gRNA	guide RNA
HDR	Homology Directed Repair
IRE	Iron Response Element
IRPs	Iron Regulatory Proteins
L3	Third instar larvae
MBSU	Molecular Biology Service Unit
MCO	Multicopper oxidase
min.	minutes

NHEJ	Non-homologous end joining
PAM	Protospacer adjacent motif
PG	Prothoracic Gland
<i>phm</i>	<i>phantom</i> (a <i>Drosophila</i> gene)
<i>phm22</i>	a <i>prothoracic gland-specific Gal4</i> driver based on the <i>phm</i> regulatory region
PCR	Polymerase Chain Reaction
<i>PPOX</i>	Protoporphyrinogen oxidase
PTTH	Prothoracicotropic hormone
RNAi	RNA interference
RNA-Seq	RNA sequencing
RIP-PCR	RNA-immunoprecipitation followed by PCR
RPKM	Reads Per Kilobase of transcript per Million reads mapped
<i>RP49</i>	Ribosomal protein 49
rpm	Revolutions per minute
RT	Room Temperature
RT-qPCR	Reverse Transcriptase qPCR
ROS	Reactive Oxygen Species
S2	<i>Drosophila</i> Schneider 2 cells
SG	Salivary gland
SP	Signal peptide
Tf	Vertebrate Transferrin
Tsf	<i>Drosophila</i> Transferrin
TfR1	Transferrin Receptor 1
TurboID	TurboID-mediated biotinylation
UAS	Upstream Activation Sequence
<i>w<sup>1118</sup></i>	wildtype
ΦC31	PhiC31 integrase

# CHAPTER 1

## Introduction

1.0 Overview. Iron is an essential trace element for an organism's growth and development. The role of iron in the body is crucial for many processes, including oxygen transport, iron-containing enzymes, steroid hormone synthesis, and DNA repair [1]. The ability of iron to gain and lose electrons is a feature that enables iron to be a suitable component of biochemical reactions such as oxygen transport and energy metabolism [2]. However, iron's capacity for electron transfer can result in the generation of toxic oxygen radicals (OH\*), which, when unregulated, can have devastating effects at the cellular level [1]. Consequently, iron concentration in the cell is by iron regulatory proteins to maintain homeostasis [3]. Iron is recycled by the body, with adults maintaining a balance of 3.5-5 g of stored iron and a loss of 1-2 mg of iron daily [4-5]. It is important that iron lost due to excretion by the body be replenished by dietary iron intake, 8 mg daily for adults [6-7]. This is because out of the 8 mg daily intake, only 1-2 mg of iron is estimated to be absorbed by the body, which accounts for iron lost to excretion [5,7]. The iron absorption rate is dependent on the iron body requirement and increases with the need [8]. An imbalance in iron homeostasis causes a wide range of human diseases, including hemochromatosis, anemia, and anemic hypoxia. It is estimated that anemia affects a third of the world's population [9], emphasizing the significance of studying iron metabolism to develop novel therapeutics in treating iron disorders. *Drosophila melanogaster* is an excellent model organism for studying various diseases since ~75% of human genes have homologs in *Drosophila* [10]. *Drosophila* has been effective in studying the impacts of iron dysregulation on the body [11]. However, the process through which *Drosophila* acquires iron from its diet is not entirely understood [12].

Ecdysone is an essential steroid hormone responsible for larval developmental transitions (L1, L2 and L3) in *Drosophila* [13]. The ecdysone biosynthesis pathway involves Halloween enzymes to metabolize cholesterol into ecdysone. Halloween enzymes, when mutated, result in the embryos displaying a defect to their exoskeleton, earning them the name the Halloween gene

family [14]. All but one Halloween enzyme requires iron cofactors, heme and Fe-S clusters [15]. Despite iron's vital importance in synthesizing ecdysone, how iron is imported into the cell, exported out of the cell and transported throughout the body is uncharacterized. The lack of conservation from vertebrate iron transport to *Drosophila* is apparent. The diversity in *Drosophila* mainly lies in the sub-cellular localization of ferritin, a multiprotein complex capable of storing thousands of iron atoms, the absence of ferroportin, the only known iron exporter and transferrin receptor necessary for iron uptake into the cell [16]. Vertebrate ferritin is mainly localized to the cytosol. In contrast, *Drosophila* ferritin is predominantly found in the secretory pathway (endoplasmic reticulum and Golgi complex) and the hemolymph [16]. The abundance of ferritin in the hemolymph is hypothesized to play a role in iron transport and export outside the cell [16]. On the other hand, yeast has two iron transport systems: Fet4p, a non-specific divalent metal/iron transporter and Fet3p/Ftr1p, a heterodimer that acts as a high affinity iron importer [17]. Yeast Fet3p is an ortholog of *Drosophila* Mco4, while no Ftr1p ortholog has been identified in *Drosophila*. The function of the *Drosophila* Mco4 gene is unclear but given that it is an ortholog to Fet3. It is predicted to function as a ferroxidase. We became interested in Mco4 because the gene was upregulated in three independent RNA-Seq experiments under iron-deprived conditions.

Thus, this research aims to examine and understand the possible role of Mco4 in *Drosophila* iron transport functioning as a potential ferroxidase. This thesis focuses on the cellular mechanism behind iron uptake and represented Mco4 as a possible high affinity iron importer. Through characterizing Mco4 localization in the cell and phenotypes associated with the loss or knockdown of Mco4 function in a tissue-specific manner. Finally, by understanding the cellular mechanisms involved in iron transport, we can shed new light on the physiology and pathophysiology of iron disorders.

This thesis focuses on iron uptake in *Drosophila*; however, it is essential to highlight iron uptake in other relevant species. To understand iron metabolism, one needs to consider cellular iron import, export, and regulation [18].

## 1.1 Dietary Source of Iron

Iron is vital for an organism's daily functions and is acquired from the diet. There are two dietary forms of iron, bound iron and unbound iron. Heme contains bound iron and is absorbed by the body more readily than non-heme (unbound iron). Heme is found mainly as a cofactor bound to the animal proteins hemoglobin and myoglobin [19]. Compared to heme, unbound iron is less efficiently absorbed and is found in plants and animal products as ferric iron ( $\text{Fe}^{3+}$ ) [19]. The body recycles internalized iron, and when in excess, iron is stored within ferritin, thus conserved by the organism [1].

## 1.2 Iron Trafficking in Mammals

Iron exists mainly in two oxidation states: ferrous iron ( $\text{Fe}^{2+}$ ) and ferric iron ( $\text{Fe}^{3+}$ ). Iron is absorbed from its dietary source in its  $\text{Fe}^{3+}$  state. However, for iron to be absorbed by the duodenal enterocyte (small intestine) and transported by transferrin in the circulatory system, it must be reduced to  $\text{Fe}^{2+}$  [18]. The ferrireductase duodenal cytochrome b (Dcytb) enzyme reduces  $\text{Fe}^{3+}$  to  $\text{Fe}^{2+}$ , at which point iron is transported through the luminal membrane into the enterocyte cytoplasm by the divalent metal transporter 1 (DMT1) [20-21]. DMT1 transports transitional metals, copper, zinc, cadmium and ferrous iron across the membrane [22-23]. Iron can also be absorbed as heme by the enterocyte heme transporter; however, DMT1 is the only known non-heme iron importer [18]. Iron can then be stored as ferritin or transported across the membrane and into the blood by ferroportin, a membrane protein [24-25]. Hephaestin then re-oxidizes iron as it exits the enterocyte to allow transport in the blood by transferrin (Tf) [18]. Hephaestin is one of the three human multicopper oxidases; the other two are Ceruloplasmin and Zyklopen. Circulating iron-bound transferrin (holo-Tf) binds to transferrin receptors of cells requiring iron for the cellular synthesis of heme and iron-sulfur clusters (Fe-S) (both are a type of protein cofactor). Upon binding, endocytosis occurs, and iron is released into the cell's cytosol through the DMT1 channel [26]. Iron is either oxidized to  $\text{Fe}^{3+}$  where it is then stored within the ferritin nano-cage [27], becoming inaccessible for oxidation or remains in the cytosol in a labile iron pool

(LIP) [26]. Ferritin has been reported to potentially play a role in transcription regulation, bind to DNA and protect DNA from oxidative damage [28]. Free iron is highly reactive and contributes to the generation of reactive oxygen species (ROS) via the Fenton reaction [29]. When iron from the LIP reaches the mitochondria, it is transported into the mitochondria through the Mitoferrin channel and is used to synthesize heme and Fe-S clusters [26]. However, how iron from the LIP reaches the mitochondria is uncharacterized (Figure 1) [30].

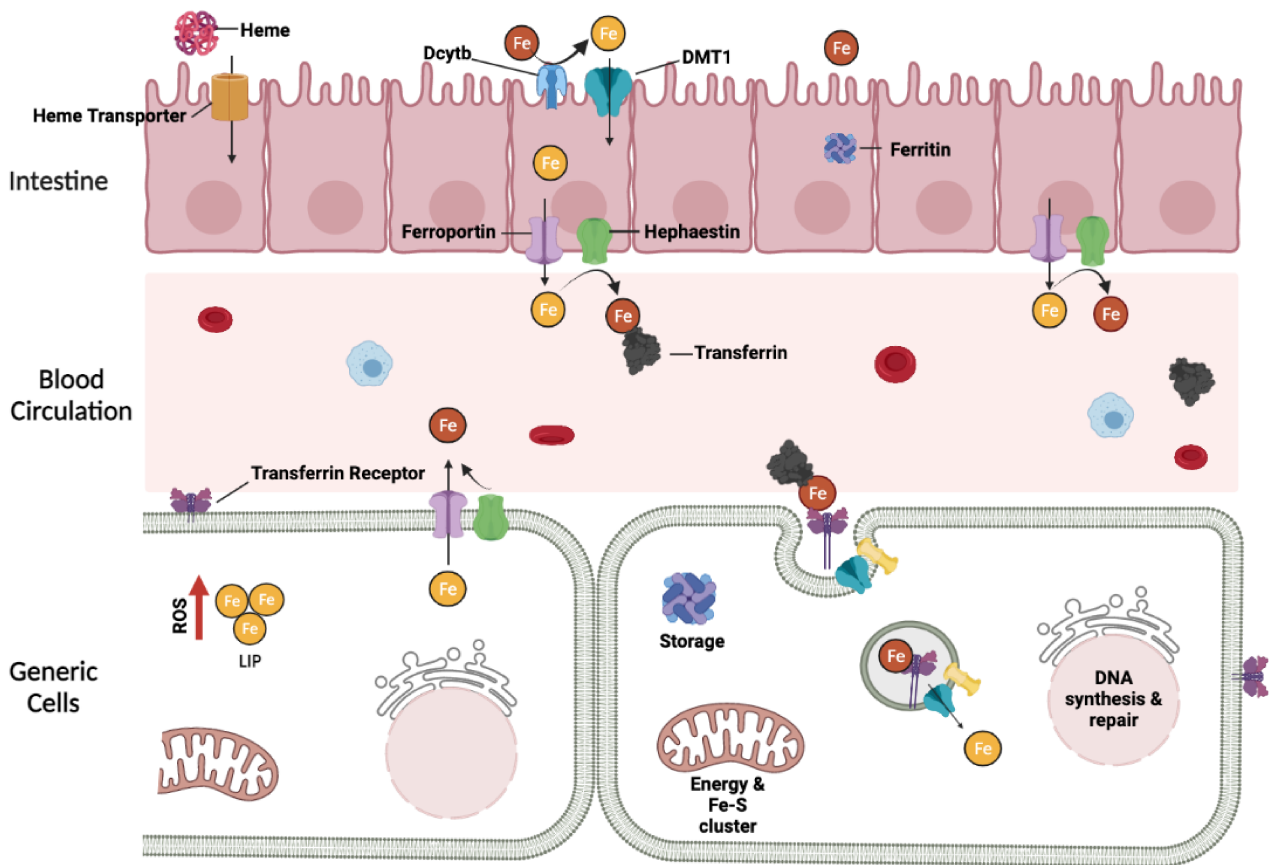


**Figure 1. Schematic representation of iron uptake and transport in mammals.** Dietary iron found in its unbound form,  $\text{Fe}^{3+}$  state (indicated as a red iron), is first reduced to its  $\text{Fe}^{2+}$  state (indicated as a yellow iron) by the enzyme Dcytb (blue). Once in the cell, iron is transported across the luminal membrane by the transporter DMT1 (turquoise). Iron can then be stored as ferritin or transported outside the enterocyte through the transporter ferroportin (purple). At this point, it is oxidized back into  $\text{Fe}^{3+}$  by the multicopper oxidase Hephaestin (green). Iron can also be acquired through heme and

imported into the cell through the heme transporter (orange). Once outside the cell,  $\text{Fe}^{3+}$  binds to transferrin (dark grey) and is transported to cells that require iron.

### 1.3 Mammalian Multicopper oxidases

Three multicopper oxidases have been classified in humans: Ceruloplasmin, Hephaestin and Zyklopen. The function of Zyklopen is not known; however, both Hephaestin and Ceruloplasmin are known to function in cellular iron export. All three multicopper oxidases can oxidize iron and are found in different tissues such as the liver, intestine and placenta. The general belief is that vertebrate MCOs function on the cell surface by oxidizing iron ( $\text{Fe}^{2+}$  to  $\text{Fe}^{3+}$ ) to facilitate iron release from ferroportin.

#### 1.31. Ceruloplasmin

Ceruloplasmin is a 130-kDa, copper-containing plasma glycoprotein (non-membrane bound, serum protein) synthesized mainly in the liver [31-32]. The physiological function of ceruloplasmin ranges from copper transport, ferroxidase activity, coagulation and oxidative stress defense [31]. 95% of copper in the body is bound to Ceruloplasmin [33]. The ferroxidase function of Ceruloplasmin oxidizes  $\text{Fe}^{2+}$  to  $\text{Fe}^{3+}$  and aids in iron-binding to transferrin for iron transport [31]. Oxidation of iron to its ferric state operates as an antioxidant function against oxidative stress [31]. Disruption of Ceruloplasmin in 6–7-month-old mice results in an iron overload of the liver and spleen but lower iron levels in the serum compared to control animals [34]. Iron accumulation was also observed in the brains of 12-month-old Ceruloplasmin knockout mice, with iron accumulation gradually increasing as the mice age [35]. Indicating Ceruloplasmin may function in brain iron homeostasis [34]. The iron that accumulates in the brain and internal organs due to a homozygous mutation of the Ceruloplasmin gene causes aceruloplasminemia [36]. Patients with aceruloplasminemia develop symptoms such as muscle tone, memory, and speech anomalies [36].

#### 1.32. Hephaestin

Hephaestin is a homolog of Ceruloplasmin, with a 50% sequence identity in humans [37]. In contrast to Ceruloplasmin, Hephaestin is a membrane-bound protein present in the intestinal

epithelium (enterocytes), with a molecular weight of 130-kDa [32,37]. Hephaestin is responsible for oxidizing divalent iron for ferroportin, an intestinal iron exporter [37], and together they mediate iron outflow from enterocytes to the bloodstream [37]. Hephaestin is shown to be mainly expressed in the intestine. Still, studies have shown lower levels of expression in the brain, heart and pancreas, where it is believed that Hephaestin may play a role in protecting cells from oxidative stress caused by ferrous iron toxicity [37]. In contrast to Ceruloplasmin, Hephaestin knockout mice displayed earlier iron accumulation in the brain at 6-7 months of age [34]. Suggesting that both Hephaestin and Ceruloplasmin may function in brain iron homeostasis [34]. To date, Hephaestin has not been linked to any human disease. However, mice carrying a mutation in the *sla* (*sex-linked anemia*) gene (which encodes Hephaestin) can develop moderate to severe hypo-chronic anemia causing iron accumulation in enterocytes with no release into the bloodstream [37].

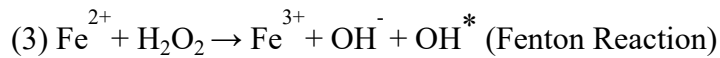
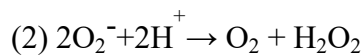
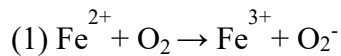
### 1.33. Zyklopen

Zyklopen is a more recent discovery than Hephaestin and Ceruloplasmin [38]. Zyklopen is predicted to be a membrane-bound protein with an overall molecular weight of 150-kDa [32]. Structurally Zyklopen bears similarity to Hephaestin, as both proteins contain a putative transmembrane domain at the C-terminus region [38]. The study in which Zyklopen was first identified found Zyklopen to be highly expressed in the placenta of mice [38]. The same study proposed Zyklopen's functional role in placental iron transport via transferrin from the mother to the fetus [38]. It was observed that in the presence of maternal anemia, the iron levels/status of the fetus remain unaffected [39]. Conversely, maternal copper deficiency causes the fetus to develop iron deficiency while placental iron levels remain unchanged [39]. However, a 2021 study published in the Journal of Nutrition determined that Zyklopen is not essential for mice's placental iron transport [40]. The study found no change in fetus iron levels when Zyklopen function was disrupted [40]. In addition, no difference of expression was observed for iron transport protein transferrin, transferrin 1 receptor and ferroportin due to Zyklopen disruption [40]. In conclusion, further studies into Zyklopen's exact role in iron transport need further clarification.

## 1.4 Iron Imbalance Generates Free Radical Species

Iron can donate and accept electrons; this property enables iron to be a versatile component of biochemical reactions. However, its capacity for electron transfer can also result in the generation of highly reactive oxygen radical species better known as ROS via the Fenton reaction. The Fenton reaction involves a ferrous iron reacting with hydrogen peroxide to produce a hydroxyl radical (OH<sup>\*</sup>) and a hydroxide ion (OH<sup>-</sup>) [41].

### **Fenton Reaction:**



Excess cellular iron generates hydroxyl radical, a ROS that is detrimental to cells and tissues [42]. Hydroxyl radicals contain an unpaired electron on the outer orbital and cause cell membrane damage by gaining an electron from the phospholipid bilayer [43]. This triggers a chain reaction of gaining an electron from the nearest molecule within the phospholipid bilayer [43]. In the process giving rise to new hydroxyl radicals [43]. This damages the membrane's structural integrity, results in free radical oxidative stress, and when unregulated, leads to apoptosis [44-45]. The peroxidation of lipids in the cell membrane by free radicals is known as lipid peroxidation [44-45]. The consequences of iron overloading can result in disorders such as hemochromatosis, liver fibrosis and cirrhosis [42]. Consequently, cellular iron must be tightly regulated to protect the cell against cellular damage.

## 1.5 Regulation of Intracellular Iron in Mammals

Iron levels are tightly regulated via Iron Regulatory Proteins (IRPs), which control the translation of specific target mRNAs. There are two forms of IRPs, an apo-form and a holo-form. The apo-form is active under low iron conditions. The apo-form binds to Iron Responsive Elements (IRE), located in mRNAs' 3'-UTR or 5'-UTR regions [24]. Depending on the location of the IRE-UTR region (3' or 5'), the apo-form will either stabilize or exert translational repression of the mRNA [24]. The apo-form exerts translational repression when binding to the 5'-UTR

region of mRNAs involved in decreasing cellular iron availability (ferritin, mitochondrial aconitase, and ferroportin transcripts) [15,24]. The mRNAs involved in cellular iron availability and trafficking (DMT1 and Transferrin Receptor-1 (TfR1) transcripts) contain a 3'-UTR region [15,24]. The binding of apo-form to the 3'UTR region stabilizes the mRNA and thereby increases the expression of the protein [15,24]. On the other hand, the holo-form is active when iron levels are normal. The holo-form contains an iron-sulfur (Fe-S) cluster in its catalyzing center and catalyzes the interconversion of citrate and isocitrate [46].

Two genes code for IRPs in vertebrates, *IRP1* and *IRP2* [47]. IRP1 can interconvert between the apo- and holo-form [48]. When iron levels are normal, IRP1 undergoes a conformational change to an aconitase form (holo-form) by incorporating a Fe-S cluster (Figure 2A) [46,48]. If iron levels are low, IRP1 undergoes a conformational change to its apo-form and binds to mRNA (Figure 2B). While IRP2 can only assume the apo-form and is degraded when iron levels are normal [24].

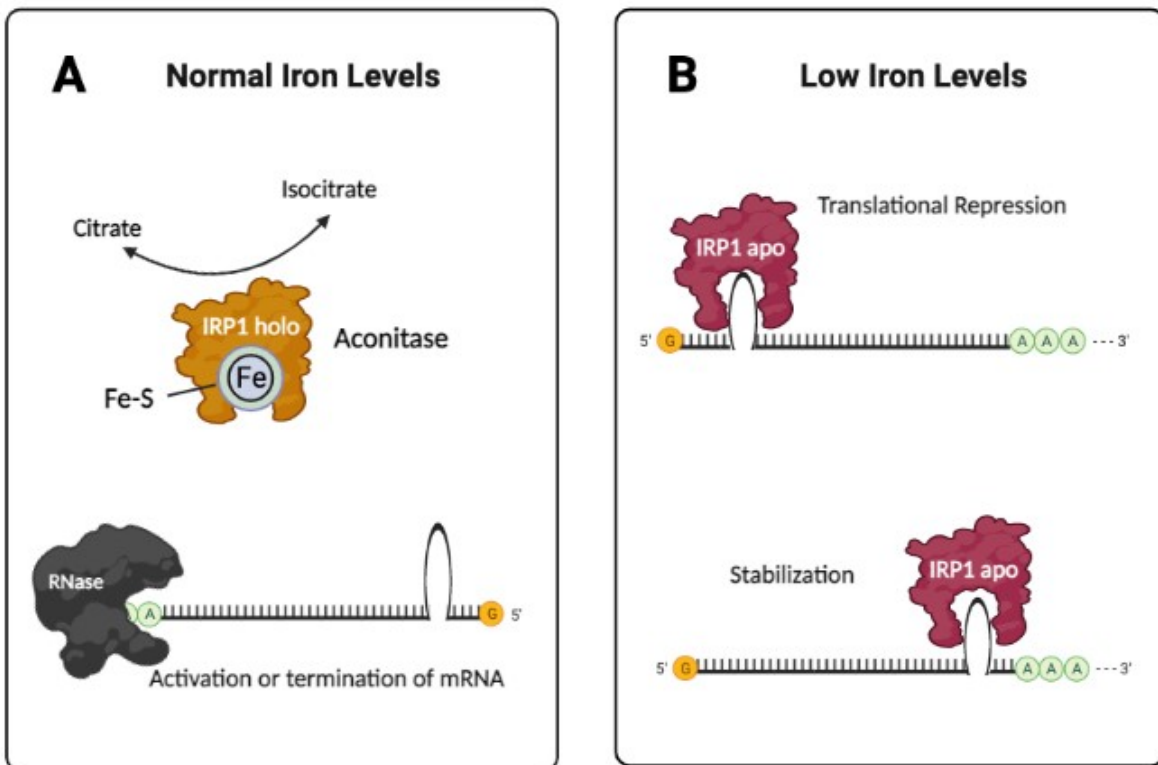


**Figure 2. Schematic representation of iron regulation in mammals.** There are two IRP genes in mammals, IRP1 and IRP2. However, only IRP1 can undergo a conformational change from its apo- to its holo-form. IRP2 only exists in apo-form and is degraded when iron levels are normal. **(A)** In the case of normal iron levels. IRP1 apo disassociates from the mRNA, and the released mRNA is now destabilized and degraded by RNase. The disassociated IRP1 undergoes a conformational change to its holo-form and binds to a 4Fe-4S cluster. Functioning as an aconitase by catalyzing the interconversion of citrate and isocitrate. **(B)** IRP1 will undergo a conformational change from its holo-form to its apo form and bind to the IRE site on the mRNA at the 3'-UTR or 5'-UTR region in low iron levels.

## 2.1 Iron Trafficking in Yeast

There are two iron uptake systems in yeast: Fet3p/Ftr1p and Fet4p. However, the Fet3p/Ftr1p system is highly specific to iron uptake, similar to transferrin's high affinity towards iron in vertebrates [17]. In comparison, Fet4p is a nonspecific divalent metal ion transporter that transports transition metals (zinc, copper, cadmium) along with iron across the plasma membrane, with no specific affinity towards iron [49]. Under iron-replete conditions, the low affinity iron transport system, Fet4p, is expressed [17]. While under low iron conditions, the Fet3p/Ftr1p system is induced because of its specificity and high affinity to iron [17, 50-51]. Both Fet3p and Ftr1p form a complex, where Fet3p, a ferroxidase with a single transmembrane domain, oxidizes ferrous iron to ferric iron [17, 50-51]. The complex acts as a high affinity iron transport system in conjunction with the Ftr1p protein, which is predicted to harbour seven transmembrane domains and transports the oxidized iron ( $\text{Fe}^{3+}$ ) across the membrane (Figure 3) [17]. Like humans, yeast also encodes two ferroxidases: Fet3p and Fet5p [17]. The given function of Fet5p is thought to be involved in iron transport from vacuolar stores in conjunction with the protein Fth1p [52].

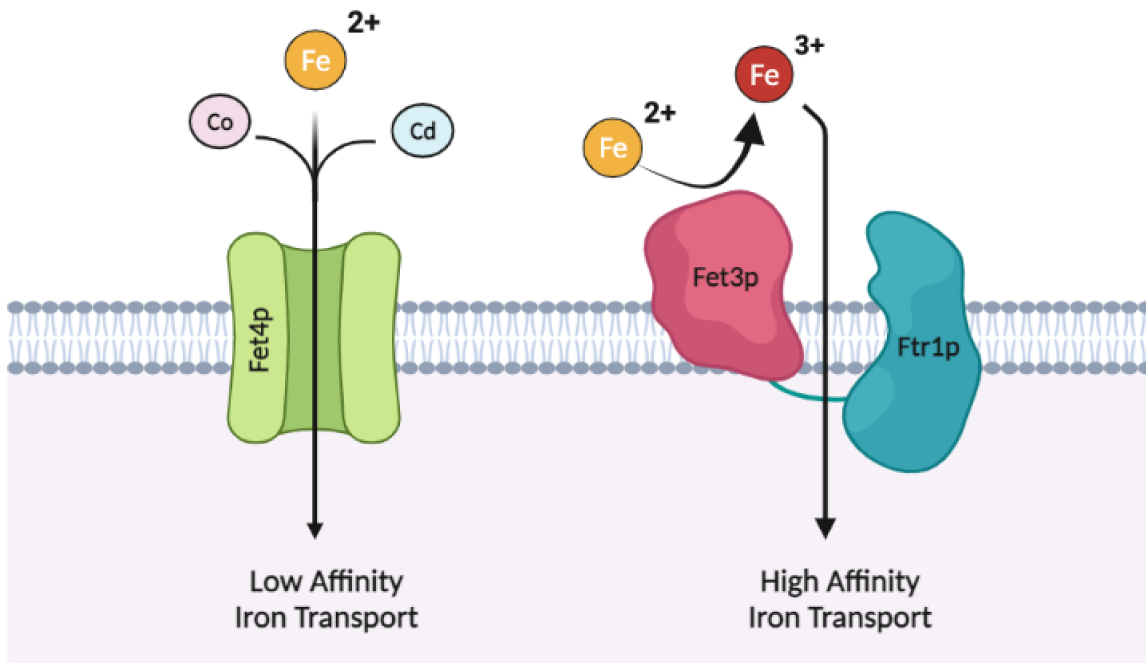


**Figure 3. Schematic representation of iron transport in yeast.** Yeast consists of two iron transport systems, one has low affinity, and the other has a high affinity for iron. The low affinity iron transport system, Fet4p, has no specificity to iron and transports both transitional metals zinc, copper, cadmium and iron across the membrane. The high affinity iron transport system, Fet3p/Ftr1p, specifically transports iron across the membrane under low iron conditions.

## 2.2 Regulation of iron in Yeast

Two mechanisms in yeast exist to regulate iron homeostasis. The first system involves iron regulation through transcription primarily by Aft1p [53]. Under iron-deprived conditions, Aft1p re-localizes from the cytosol into the nucleus to bind DNA and initiate transcription of genes involved in iron uptake [53]. Aft1p regulates 17 target genes involved in iron uptake and distribution [54]. Aft2p, a paralog of Aft1p, is a transcription factor that regulates a subset of Aft1p target genes [53,55], but its function is less clear compared to Aft1p [54]. The second system involves mRNA binding proteins, Cth1p and Cth2p [56]. In response to iron-deprived conditions, Cth1p and Cth2p target and bind to mRNAs encoding iron-dependent metabolic proteins, resulting in the degradation of the mRNA [56].

### 3.1 Iron Trafficking in *Drosophila*

As mentioned previously, both the systemic and cellular iron transport systems in *Drosophila* is less characterized compared to mammals and fungi. How iron is absorbed from the diet and transported across cells and tissues remains unknown. What is known about *Drosophila* is that there are no ferroportin, hepcidin, and transferrin receptor homologs encoded in the *Drosophila* genome [18]. However, *Drosophila* has a DMT1 homolog, *Malvolio* (*Mvl*), *Dcytb* homolog termed *CG1275*, three transferrin genes (*Tsf1*, *Tsf2* and *Tsf3*), three ferritin genes (*Fer1HCH*, *Fer2LCH* and *Fer3HCH*) and four genes encoding multicopper oxidases (*Mco1,3,4* and *straw*) [18,57].

Comparable to DMT1, *Malvolio* transports transition metals such as copper, zinc, cadmium and ferrous iron across the plasma membrane into the cell's cytosol [23]. Whether *Malvolio* requires a ferric reductase to reduce  $Fe^{3+}$  to  $Fe^{2+}$  similar to *Dcytb* in vertebrates for iron transport across the membrane is not clear [16]. *Malvolio* mutants display iron-deficient phenotypes and are predicted to function in iron import into the cell [58]. In contrast to mammals, fly ferritin is characterized as a secretory protein complex with a subcellular localization found in the ER and Golgi complex of the cell [18]. In mammals, only a small amount of ferritin is found in the blood serum [59]. Ferritin found in the hemolymph is loaded with iron, suggesting a possible transport function in *Drosophila* [59]. Alternatively, cytoplasmic ferritin may act merely as a sink for excess cellular iron. Iron transport via the secretory pathway (ER/Golgi) requires iron to be transported from the cytoplasm to the Golgi [59]. The zinc transporter *Zip13* is suggested to export iron from the cytosol into the secretory pathway compartments where iron can be incorporated into ferritin [60]. The function of *CG1275* is unknown, its specific role in iron homeostasis is ambiguous [18]. Transferrin in *Drosophila* is localized to the hemolymph, and its function in relation to trafficking iron is unclear [18]. As previously mentioned, there are three transferrin homologues in *Drosophila*. *Tsf1* is predicted to function similarly to transferrin in mammals as an iron transporter [61]. *Drosophila* *Tsf1* is mainly expressed in the fat body and abundantly found in the hemolymph [61]. *Tsf1* synthesized in the fat body is secreted into the hemolymph, where it's predicted to facilitate iron transport from the gut back to the fat body [61]. *Drosophila* *Tsf2*, also known as melanotransferrin, is an essential component of septate epithelial junctions, with no known iron transport involvement [62]. *Drosophila* *Tsf3* function is

uncharacterized but is suggested to be involved in the circadian rhythm regulation [63]. In place of a transferrin receptor to mediate iron transport between iron-bound transferrin and a cell, Malvolio and ferritin have been proposed as candidates for an alternative iron transport system [16]. Ferritin is predominantly found in the hemolymph and the secretory pathway. Ferritin is a heteropolymer that contains 24 subunits made up of two types, 12 *Fer1HCH* (Ferritin 1 Heavy Chain Homologue) and 12 *Fer2LCH* (Ferritin 2 Light Chain Homologue) [64]. *Fer1HCH* contains a ferroxidase domain, and *Fer2LCH* is essential for the stabilization/formation of the iron core [16,65]. *Fer3HCH* (Ferritin 3 Heavy Chain Homologue), also known as mitochondrial ferritin, is predicted to contain a ferroxidase domain functioning specifically in the mitochondria and has been linked to protecting the mitochondria from oxidative stress [16]. Ferritin is predicted to have two functions in *Drosophila*, iron storage akin to mammalian ferritin and possibly an iron transporter based on its localization [66]. Ferritin is thought to be exported into the hemolymph to transport iron to different parts of the body, comparable to mammalian transferrin function [66] (Table 1.0 -1.1. and Figure 4).

To summarize, gaps exist in our knowledge with *Drosophila* lacking key proteins involved in the mammalian iron transport [18]. How is iron transported with the presence of transferrin and no transferrin receptor [18]? The high concentration of ferritin in the hemolymph of *Drosophila* raises the question of whether ferritin is involved in systemic iron transport [18]. Lastly, with no ferroportin ortholog in *Drosophila*, how is iron exported outside of enterocytes? [18] Therefore how iron is imported, transported and exported is important for understanding *Drosophila* iron homeostasis.

**Table 1.0. Summary of potential candidates involved in *Drosophila* iron transport.**

Protein	Localization	Predicted movement
Transferrin (Tsf1)	Hemolymph and basal gut surface	Iron export, from the gut to tissues [61]
Malvolio	Apical plasma membrane of enterocytes	Transport iron across the apical plasma membrane into the cell [23]
Ferritin	Hemolymph and secretory pathway	Transport iron via secretory pathway outside the cell [60]

**Table 1.1.** Comparison of human and *Drosophila* genes involved in iron homeostasis.

Protein	Human gene	<i>Drosophila</i> gene (CG#)	Function of protein
Transferrin Melanotransferrin lactotransferrin	<i>TF</i>	<i>Tsf1</i> (CG6186) <i>Tsf2</i> (CG10620) <i>Tsf3</i> (CG3666)	Iron transport protein via blood plasma/hemolymph
Transferrin receptor 1	<i>TFRC</i>	-----	Cellular iron uptake via bound Fe <sup>3+</sup> to transferrin
Transferrin receptor 2	<i>TFR2</i>	-----	Iron sensor for bound Fe <sup>3+</sup> to transferrin
Divalent Metal Transporter 1 (DMT1)	<i>SLC11A2</i>	<i>Malvolio</i> (CG3671)	Fe <sup>2+</sup> iron transporter
Mitoferrin 1	<i>SLC25A37</i>	<i>dmfrn</i> (CG4963)	Mitochondrial iron importer
H-ferritin	<i>FTH1</i>	<i>Fer1HCH</i> (CG2216)	Ferritin subunit involved in iron storage
L-ferritin	<i>FTL</i>	<i>Fer2LCH</i> (CG1469)	Ferritin subunit involved in iron storage
Mitochondrial ferritin	<i>FTMT</i>	<i>Fer3HCH</i> (CG4349)	Mitochondrial iron storage
Ferroportin 1	<i>SLC40A1</i>	-----	Fe <sup>2+</sup> iron exporter
Duodenal cytochrome b (Dcytb)	<i>CYBRD1</i>	CG1275	Ferric iron reductase in intestine
Ceruloplasmin Hephaestin	<i>CP</i> <i>HEPH</i>	<i>Mco1</i> (CG3759) <i>Mco3</i> (CG5959) <i>Mco4</i> (CG32557)	Multicopper ferroxidase
IRP1	<i>ACO1</i>	<i>IRP1A</i> (CG4900) & <i>IRP1B</i> (CG6342)	Cellular Iron regulator
IRP2	<i>IREB2</i>	-----	Cellular Iron regulator
Hepcidin	<i>HAMP</i>	-----	Systemic Iron regulator

Information based on [18,16 &amp; 67].

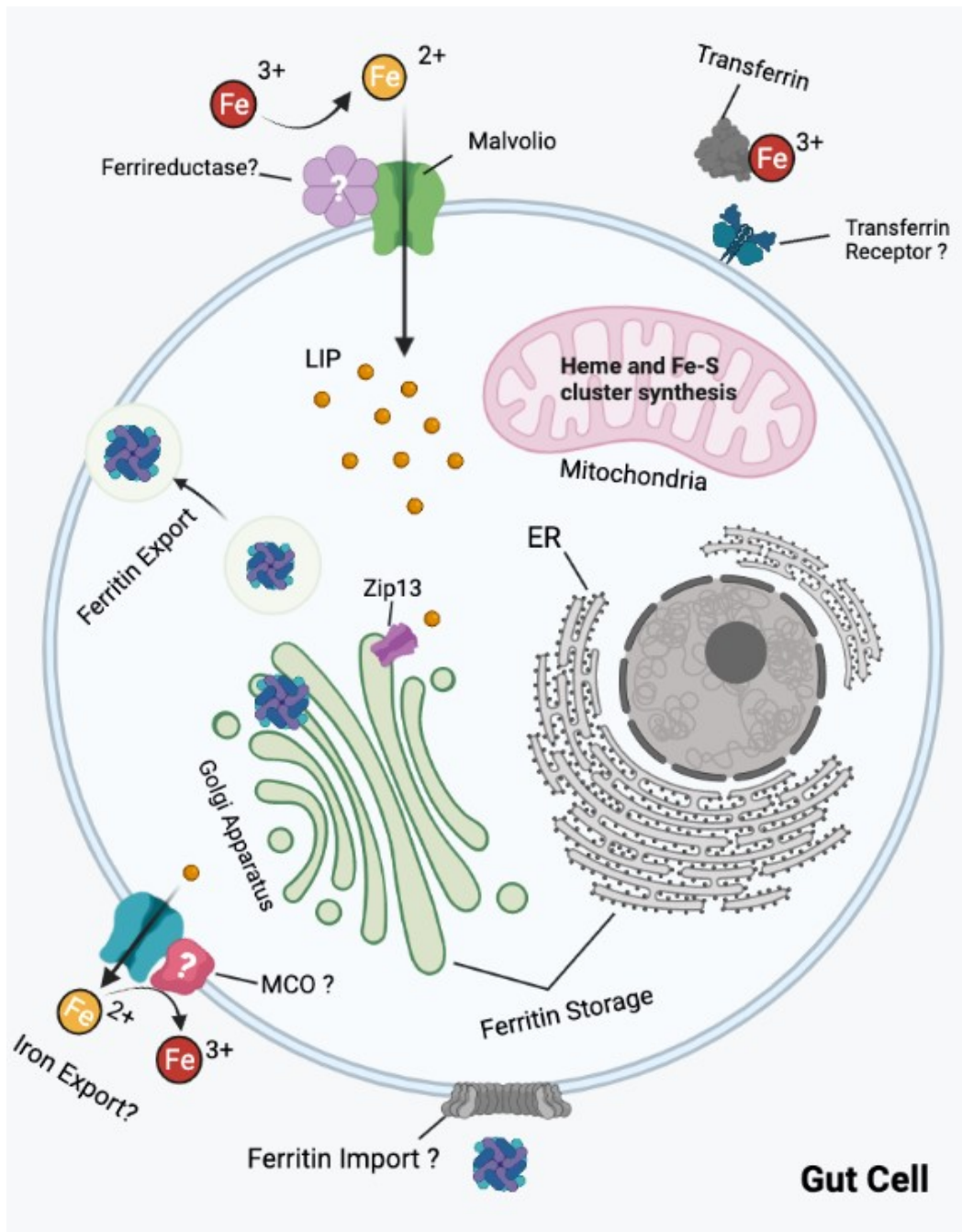


**Figure 4. Schematic representation of iron transport in *Drosophila*.** Iron is thought to be reduced to ferrous iron by an unknown ferrireductase and imported through the cell's plasma membrane by the Malvolio transporter. Once in the cell, iron is released into the labile iron pool, from which it can be transported into the mitochondria for heme and Fe-S cluster synthesis. Zip13. is predicted to export iron from the cytosol into the ER/Golgi for incorporation into ferritin. How iron is exported out of the cell is unknown, as there are no ferroportin homologs in *Drosophila*. Intracellular ferritin is localized in the ER

and Golgi apparatus of the cell and functions as a secretory protein, leading to high ferritin concentrations in the hemolymph. Whether ferritin is imported back into cells is unclear. *Drosophila* contains a transferrin homolog, but no transferrin receptor has been identified.

### 3.2 *Drosophila* Multicopper oxidases

Multicopper oxidases are ubiquitous copper-bound enzymes and function as ascorbate oxidase, ferroxidases and laccases [58]. In *Drosophila*, four genes encode multicopper oxidases: *Mco1*, *Mco2* (now named *straw*), *Mco3* & *Mco4*. Information regarding their roles in *Drosophila* is limited and relies heavily on predictions. Additionally, no solid evidence has been provided to indicate whether any of the four *Drosophila* MCOs function as ferroxidases in vivo.

#### 3.21 Multicopper oxidase 1

*Mco1* is primarily expressed in the intestine and Malpighian tubules [66]. *Mco1* is predicted to function as an intestinal ferroxidase and was found in a study to result in iron-depleted flies using RNAi-mediated knockdown [66]. Preliminary examination of *Mco1* identified a functional ferroxidase activity [66]. The knockdown of *Mco1* reduced iron abundance in the midgut region of the intestine and caused pupal lethality [66]. Given the localization of *Mco1* on the basal surface of midgut epithelial cells, correlated with the identified ferroxidase activity and the presence of a putative iron binding residue, *Mco1* was suggested to function similarly to mammalian Hephaestin [66]. The proposed function of *Mco1* is to oxidize ferrous iron to ferric iron, whereupon its release into the hemolymph binds to transferrin for transport to cells in need of iron [66].

#### 3.22 Multicopper oxidase 2 (*Straw*)

*Mco2* orthologues are commonly identified as laccases, a phenol-oxidizing enzyme conserved among insects [66]. *Straw* is predicted to function as laccase, and it is involved in the pigmentation of a newly synthesized cuticle [68-69]. The cuticle is the exoskeleton material of arthropods; phenol-oxidizing enzymes oxidize the ectodermal cells of the cuticle producing melanin in a process known as sclerotization [70]. RNAi-mediated knockdown of *straw* in the wings of *Drosophila* resulted in blockage of cuticle pigmentation, indicating *straw* functions in

cuticle melanin production [70]. It remains to be explored whether *straw* encodes a ferroxidase domain.

### 3.23 Multicopper oxidase 3

*Mco3* has no known ortholog outside *Drosophila* and encodes a putative iron-binding region, a putative signal peptide and a transmembrane domain [58,71]. Ferritin is the primary iron-storage protein present in the middle midgut region of the intestinal cells, and this region of the midgut is known as the iron storage region. *Malvolio* mutants affect iron accumulation in the iron storage region of the midgut [58]. However, *Mco3 / Malvolio double* mutants accumulate iron in the intestine midgut region, implicating that *Mco3* affects iron storage in the intestine midgut region [16,58]. Additionally, *Mco3* mutants accumulated copper, around 20% more than control flies [58]. Suggesting *Mco3* involvement in copper homeostasis [58]. Finally, the predicted function of *Mco3* is a ferroxidase however a ferroxidase activity assay still needs to be conducted to confirm this [69].

### 3.24 Multicopper oxidase 4

*Mco4* is the ortholog of the yeast cellular iron import protein Fet3p, a multicopper ferroxidase. With few studies into *Mco4* function in *Drosophila*, the current role of *Mco4* remains to be elucidated. This thesis examines whether *Mco4* is a ferroxidase candidate and whether it is involved in cellular iron uptake. Propositioning *Mco4* as a potential ferroxidase candidate involved in cellular iron import is based on, (i) It's an ortholog to the yeast high affinity iron importer (Fet3p), (ii) *Mco4* expression appeared significantly upregulated in three independent RNA-Seq experiments, each of which corresponded to iron-deprived conditions (accomplished by different means, as explained in chapter 3) and (iii) the recent finding in our lab suggests that the *Mco4* mRNA may harbour an IRE site and is thus regulated by IRP1A, which I will discuss in the next paragraph. Taken together, upregulation of *Mco4* levels in cells exposed to iron-deprived conditions indicates *Mco4* may participate in iron uptake via a high affinity iron import system when dietary iron is low. The possibility of *Mco4* functioning as a high affinity iron importer would be a paramount finding as no high affinity iron import system has ever been identified in higher eukaryotes.

### 3.3 Regulation of iron in *Drosophila*

Similar to vertebrates, *Drosophila* iron metabolism is also regulated by IRPs. In *Drosophila*, two genes encode IRPs, *IRP1A* and *IRP1B*. IRP1A can interchange between apo- and holo-form by incorporating a Fe-S cluster in its catalytic center [46]. While IRP1B is thought to maintain only the holo-form (which cannot bind RNA) [72]. In *Drosophila*, *SdhB* and *Fer1HCH* are the only known mRNAs that contain IREs [72]. However, using an RNA-Seq and RNA-immunoprecipitation (RIP)-qPCR candidate gene approach carried out by Dr. Nhan Huynh, a former Ph.D. student from the King-Jones lab, identified eight transcripts containing uncharacterized IREs [73]. Specifically, an RNA-Sequencing (RNA-Seq) experiment using PG-specific overexpression of IRP1A variants was used: IRP1A wildtype (*phm>IRP1A*), a version of IRP1A locked into the apo-form (*phm>IRP1A<sup>C450S</sup>*), and a version of IRP1A with abolished/strongly reduced RNA-binding (*phm>IRP1A<sup>3R3Q</sup>*) was performed [73]. The RNA-Seq results were analyzed by filtering for upregulated transcripts in *IRP1A<sup>C450S</sup>* samples but showed no or little upregulation in the *IRP1A* and *IRP1A<sup>3R3Q</sup>* lines [73]. This resulted in 23 upregulated transcripts. *Mco4* based on fold changes – ranked #2 in this cohort (Figure 12) [73]. The rationale was that the apo-IRP1A would stabilize transcripts harbouring novel IREs, while the other conditions should either show a lower degree of upregulation (IRP1A wildtype) or no upregulation (IRP1A<sup>3R3Q</sup>).

Following these results, Dr. Nhan Huynh performed an RNA-immunoprecipitation (RIP)-qPCR experiment using whole body larvae samples extracted from *tubulin>IRP1A<sup>C450S</sup>*, *tubulin>IRP1A* and *tubulin>IRP1A<sup>3R3Q</sup>* strains. *Tubulin>IRP1A<sup>3R3Q</sup>* was used as a negative control since this variant should display little or no IRE-binding. *SdhB* was used as a positive control since it harbours a documented canonical IRE [73]. Out of the 23 transcript candidates, only eight were co-immunoprecipitated in apo-IRP1A (aka IRP1A<sup>C450S</sup>) samples used. One of the identified transcripts was *Mco4* [73], suggesting the *Mco4* mRNA contains an unidentified IRE (Figure 5) [73]. Since attempts to identify the IRE in *Mco4* with SIREs, a software designed to identify such motifs, failed (Nhan Huynh, personal communication), I hypothesize that the presumptive *Mco4* IRE represents a novel type that lies outside the search parameters of SIREs [74]. These preliminary data are exciting since only two IRE-containing transcripts have been described in *Drosophila*, compared to nine in vertebrates [73]. Importantly, this finding suggests

that *Mco4* is post-transcriptionally regulated by IRP1A and strengthens the notion that *Mco4* participates in iron regulation and transport.

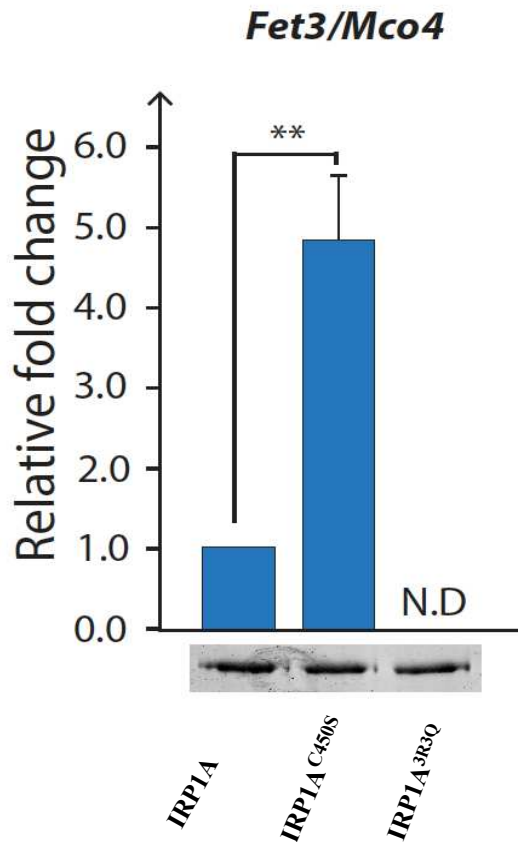


**Figure 5. RIP-qPCR results for IRP1A<sup>C450S</sup> show *Mco4* interaction.** IRP1A apo-form (IRP1A<sup>C450S</sup>) binds to putative IRE on *Mco4* mRNA under low iron conditions, while IRP1A holo-form (IRP1A<sup>3R3Q</sup>) did not immunoprecipitate *Mco4* mRNA. The samples were normalized to contain the same amount of IRP1A variant protein (IRP1A, IRP1A<sup>C450S</sup> and IRP1A<sup>3R3Q</sup>) as shown in the western blot panel below the graph. ND = not detected, \*\*p-value<0.01. From “Characterizing new players involved in iron homeostasis during *Drosophila* larval development: Shifting the classic paradigm of iron metabolism” by Nhan Huynh, 2020, Doctor of Philosophy Thesis, 140. Copyright (2020) by the University of Alberta. Reprinted with permission.

#### 4.1 The *Drosophila* Prothoracic Gland as a Model for Studying Iron Metabolism

The *Drosophila* life cycle consists of four main stages: egg, larva (L1, L2 & L3), pupa and adult [75]. Metamorphosis of larval to pupal development is mediated by steroid hormones [75]. Steroid hormones govern physiological changes and reproduction in multicellular organisms [76]. During *Drosophila* development, steroid hormones are typically released as precise pulses in a controlled timely manner by endocrine glands in response to a brain signal [77]. An important insect steroid hormone, ecdysone, is synthesized mainly in the prothoracic gland (PG) during development [77]. Ecdysone is essential for larval growth and development; it governs developmental transitions (moulting and metamorphosis) and behaviour [13,78]. Released ecdysone pulses serve as checkpoints for moults from larval to pupal stages, determining successful metamorphosis [13]. The Prothoracicotrophic hormone (PTTH) activates the Ras/Raf/ERK pathway, which is thought to regulate ecdysone secretion [78-79]. Ecdysone synthesis from cholesterol to 20-Hydroxecdysone (20E), the best-characterized biologically active form of ecdysone, necessitates proteins known as ‘Halloween enzymes’ [13]. Cholesterol is first converted to 7-dehydrocholesterol (7DC) by the enzyme Neverland which requires a Fe-S cluster cofactor, before undergoing a series of enzymatic steps involving Shroud, a short-chain dehydrogenase/reductase and six cytochrome P450 enzymes (Cyp6t3, Spook, Phantom, Disembodied, Shadow and Shade) to synthesize 20E [13]. All Halloween enzymes but shroud require heme or Fe-S clusters as a cofactor [13]. Both heme and Fe-S clusters need to incorporate iron atoms into their final structures to be functional. Therefore, iron is essential for ecdysone synthesis, making the PG an effective genetic model system to study iron metabolism because of its high iron requirements for metamorphosis and larval growth (Figure 6) [13].

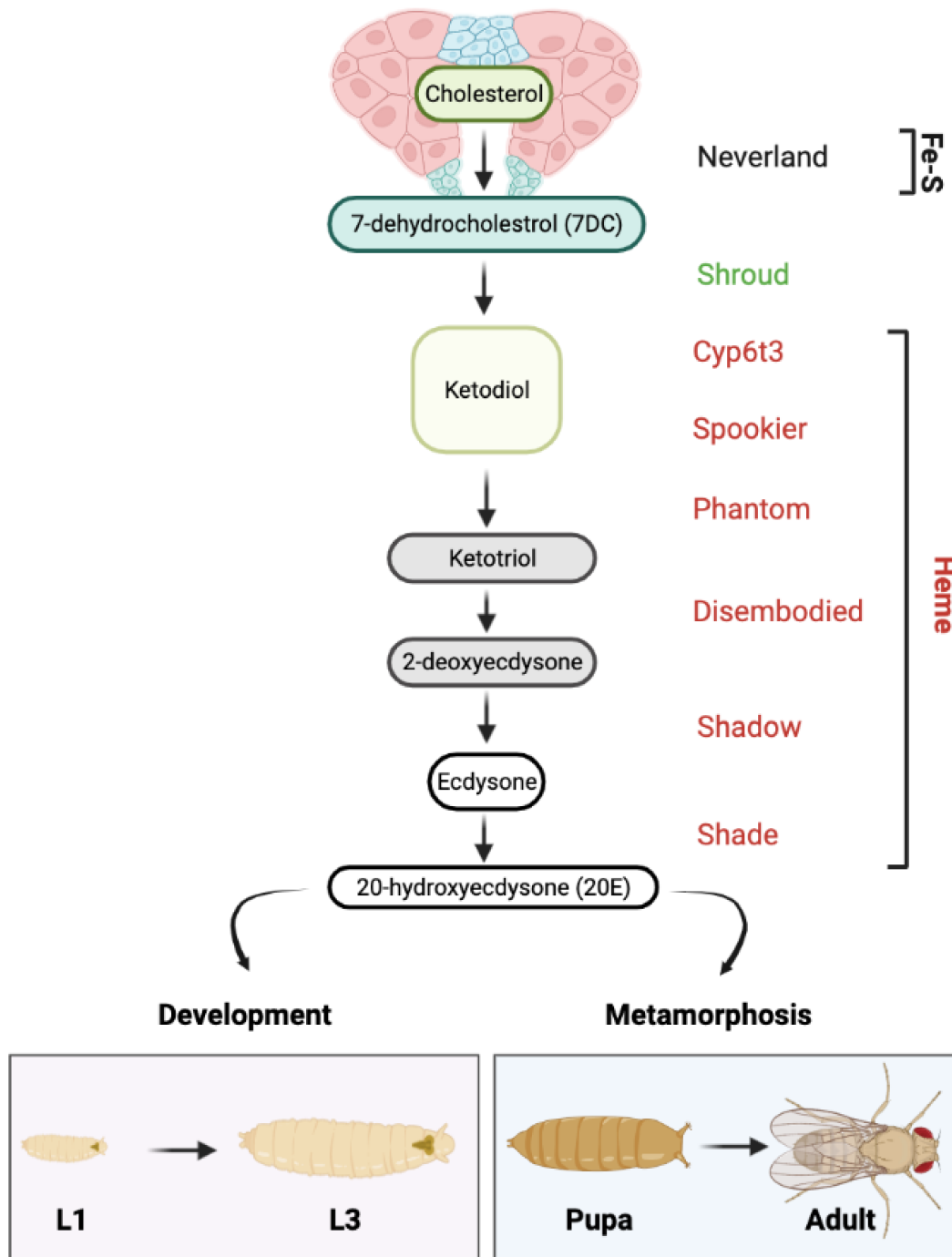


**Figure 6. Ecdysone biosynthesis in the PG.** Ecdysone is produced in the PG. The hormone coordinates developmental growth and metamorphosis in *Drosophila*. Ecdysone is synthesized from cholesterol and undergoes a series of enzymatic steps to form 20-hydroxyecdysone (20E), an ecdysone biologically active form. The enzymes involved in the ecdysone biosynthesis pathway are known as

Halloween enzymes, and all but one (Shroud, in green) require either Fe-S cluster (enzyme name in black) or heme (enzyme names in red) as co-factors.

## 4.2 Heme Synthesis

Free heme has the potential to be cytotoxic and is therefore tightly regulated. Heme is usually found bound to hemoproteins such as hemoglobin and myoglobin. Interestingly, both heme and Fe-S synthesis occur across the mitochondria and the cytosol. Heme synthesis is well characterized and highly conserved between *Drosophila* and humans [80]. Heme is synthesized from two precursors, glycine and succinyl-CoA. The first step occurs in the mitochondria, where the precursors are converted to aminolaevulinic acid (ALA) via the enzyme ALAS [80,81]. Once produced, ALA is exported to the cytosol, where two of its molecules are condensed to form monopyrrole porphobilinogen moieties catalyzed by aminolevulinate dehydratase (ALAD) [80]. Four monopyrrole porphobilinogen molecules are then utilized by the enzyme PBG deaminase (PBGD) to form tetrapyrrole hydroxymethylbilane [80,82]. This is then converted to uroporphyrinogen III by uroporphyrinogen synthase (UROS) [80,83]. The final cytoplasmic step consists of the synthesis of coproporphyrinogen III (CPgenIII), catalyzed by uroporphyrinogen decarboxylase (UROD) [80]. The following last three steps are carried out in the mitochondria, where protoporphyrinogen IX is synthesized by the enzyme coproporphyrinogen III oxidase (CPOX) [80]. Protoporphyrinogen IX is then oxidized to protoporphyrin IX (PPIX) by protoporphyrinogen oxidase (PPOX) [80,84]. The final step of the heme synthesis pathway is the incorporation of ferrous iron into the porphyrin ring to form heme, catalyzed by the enzyme ferrochelatase (FECH) (Summary in Figure 8) [80,85]. Heme concentrations are regulated through the protein levels of the enzyme ALAS (via transcriptional regulation of the *ALAS* gene), the first enzyme in the heme biosynthesis pathway [80]. I am highlighting the heme pathway because mutations in the enzyme genes *UROD*, *CPOX*, *PPOX* and *FECH* result in heme precursor accumulation. These aggregates result in a striking red autofluorescence in the presence of UV light, often accompanied by an enlargement of the PG (Figure 7A). Additionally, a red autofluorescence can also be observed in the gut of *PPOX* mutants under a brightfield setting (Figure 7B). This phenotype of heme precursor accumulation corresponds to a well-known disease in humans called porphyria [58].

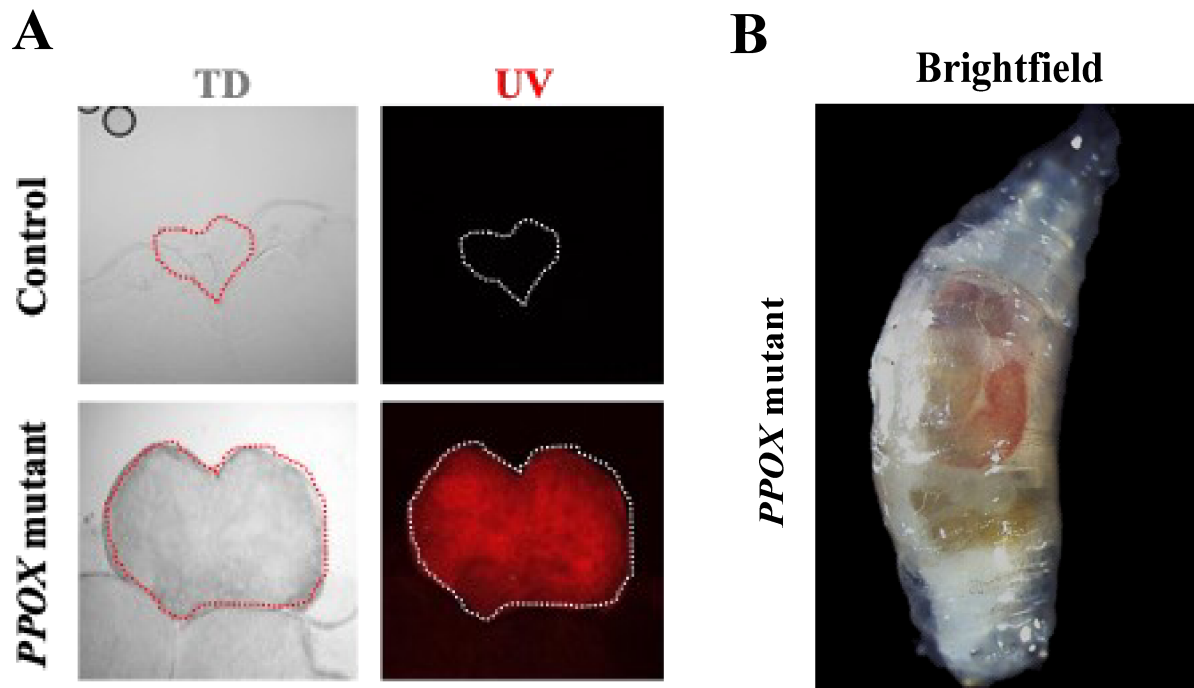


**Figure 7. Mutation in the *PPOX* gene (*PPOX*<sup>13702</sup> allele) results in a porphyria-like phenotype.** PPOX is an enzyme responsible for the oxidation of protoporphyrinogen IX to protoporphyrin IX (PPIX) in the heme biosynthetic pathway. When mutated (*PPOX*<sup>-/-</sup>), it results **(A)** in the enlargement of the PG and a strong red autofluorescence under UV light. **(B)** A red phenotype can be observed in the gut of third instar larvae under brightfield, magnification 4X LEICA DCF500 camera.

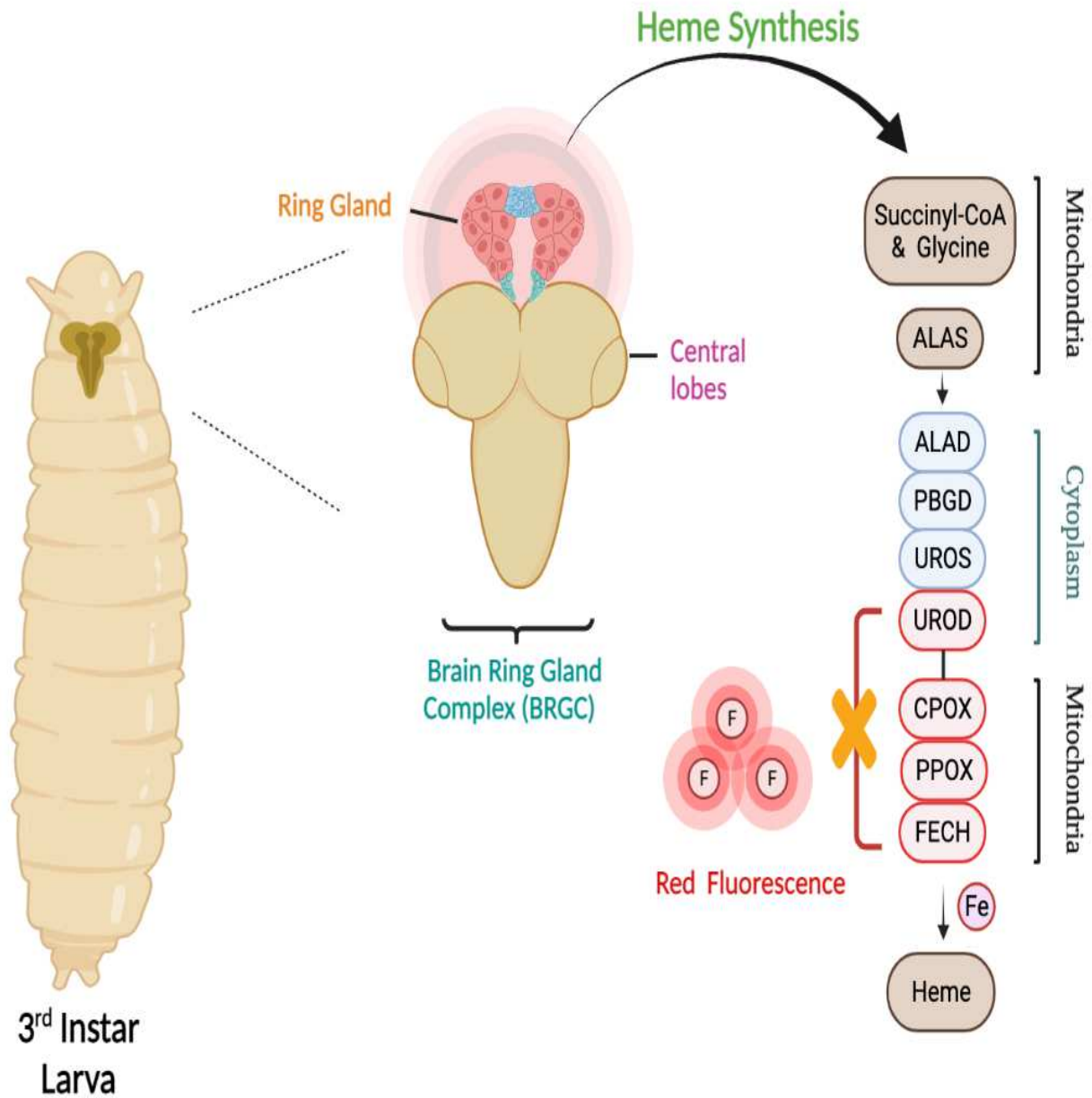


**Figure 8. Heme biosynthetic pathway.** Heme synthesis requires a series of eight enzymatic reactions, with the first step occurring in the mitochondria (ALAS), four steps occurring in the cytoplasm (ALAD, PBGD, UROS, UROD) and the last three steps occurring in the mitochondria (CPOX, PPOX, FECH). Loss-of-function mutations affecting enzymes shown in red results in heme precursor accumulation and a red autofluorescence phenotype observed in the prothoracic gland.

## 5.0 Overview of the Secretory Pathway Involving Membrane-bound Proteins

I hypothesize that Mco4 is a membrane-bound protein involved in high affinity iron import. Using the software PSIPRED, I identified a single putative transmembrane domain in the Mco4 protein sequence, and importantly, a signal peptide was also predicted (Discussed in Chapter 5 in further detail) <sup>[86]</sup>. For membrane proteins to be incorporated into the membrane, they must contain a signal peptide. The signal peptide is around 16-30 amino acids in length and direct proteins from the cytoplasm to the rough endoplasmic reticulum (RER) <sup>[87-88]</sup>. Proteins containing a signal peptide upon translation in the cytoplasm are recognized by a protein complex termed signal-recognition particle (SRP) <sup>[89-91]</sup>. Together with the synthesizing ribosome, they are directed to the RER <sup>[89-91]</sup>. SRP binds to the SRP receptor on the RER surface, forming a channel, translation continues and only the translated polypeptide chain is transported into the RER lumen <sup>[90,92-93]</sup>. The signal peptide is cleaved off by a signal peptidase, and translation is completed in the RER lumen <sup>[89,94-97]</sup>. The cleaved peptide is then released into the cytosol, where it may influence specific signal transduction pathways <sup>[98]</sup>. The newly synthesized protein is then incorporated into a transport vesicle by budding off the RER and transported to the *cis*-Golgi reticulum <sup>[89, 99-100]</sup>. The transport vesicle containing the synthesized protein fuses to the *cis*-Golgi. The protein begins its migration from the Golgi side nearest to the RER, *cis*-Golgi, to the Golgi positioned furthest from the RER, *trans*-Golgi <sup>[89, 99-100]</sup>. This process is known as cisternal migration <sup>[89]</sup>. Post-translational modification of the protein occurs as the protein is transported within the Golgi apparatus to produce a mature protein <sup>[89]</sup>. The mature protein is sorted and sent to its respective destination via transport vesicles that bud from the *trans*-Golgi <sup>[89]</sup>. There are five possible destinations; 1) the Lysosome, for synthesized degradative enzymes, 2) remain in the *trans*-Golgi apparatus, for Golgi function 3) return to the RER for RER function, 4) incorporation into the plasma membrane, where the transported vesicle fuses with the plasma membrane and the target membrane protein is embedded into the cell plasma membrane, and 5) secretion to the outside of the cell, the transported vesicle fuses with the plasma membrane and the vesicle contents are excreted outside the cell in a process known as exocytosis/secretion (example insulin) <sup>[88]</sup> (Figure 9).

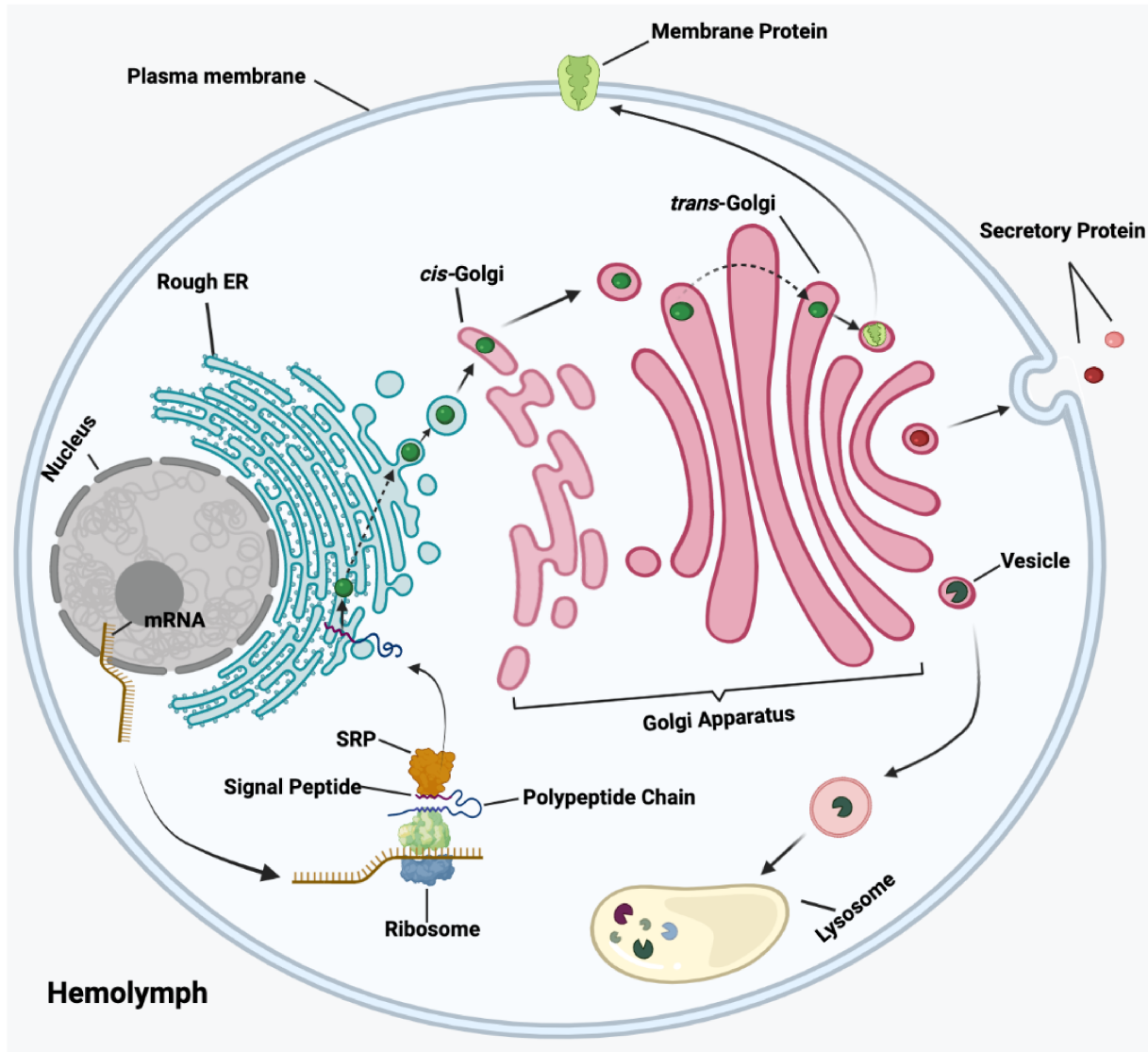


**Figure 9. Secretory pathway overview.** The signal-recognition particle (SRP) (orange) recognizes ribosomes synthesizing proteins containing a signal peptide. SRP binds to the signal peptide (purple) and guides the translating ribosome to the rough ER (blue). The polypeptide chain enters the rough ER lumen to complete translation. The synthesized protein (dark green) buds from the rough ER to form a transport vesicle and fuses with the cis-Golgi (light pink). The protein moves from the cis-Golgi to the trans-Golgi (dark pink). As this occurs, the protein is subjected to post-translational modifications to form a mature protein. Proteins can either remain in the trans-Golgi, return to the rough ER, be transported to lysosomes (yellow), secreted outside the cell, or be incorporated into the plasma membrane.

## 6.0 Research objectives

*Mco4*'s possible function in *Drosophila* is unclear and with no apparent role in *Drosophila* iron transport being reported. However, preliminary RNA-Seq data generated in our lab found *Mco4* to be highly upregulated under iron-deprived conditions. Suggesting *Mco4*'s potential role in iron homeostasis. The overall aim of this thesis was to investigate whether *Mco4* is involved in high affinity iron import. My thesis is divided into three main objectives, each representing a chapter (#).

4. To analyze the effects of RNAi-mediated *Mco4* knockdown using available tools.

**Rationale:** Iron in *Drosophila* is essential for heme and ecdysone synthesis. Therefore, I hypothesized that if *Mco4* were to be involved in iron import into the cell, then loss-of-function generated by RNAi-mediated knockdown of *Mco4* should result in either one or all of these phenotypes: PG porphyria-like phenotype, enlargement of the PG, developmental delays and possibly a decrease in the survival rate.

5. To determine the subcellular localization of *Mco4* within a cell.

**Rationale:** Visualizing the subcellular localization of *Mco4* within a cell provides insight into determining its function. To evaluate the localization of *Mco4*, an *ex vivo* construct for transfection into S2 cells, and a *UAS-Mco4* transgenic line was generated. I hypothesized that *Mco4*, similar to Fet3p yeast ortholog, is a membrane-bound protein.

6. To establish a *Mco4* null mutant model using CRISPR/Cas9.

**Rationale:** An efficient strategy to study the function of a gene is to create a complete null. It is essential to study *Mco4* null mutants to determine the impact a lack of *Mco4* has on *Drosophila* physiology and development. I hypothesized that the removal of *Mco4* could result in either one or all of the following phenotypes: PG porphyria-like phenotype, enlargement of the PG, developmental delays and possibly a decrease in the survival rate.

Addressing these objectives together in this thesis provides insight into understanding and characterizing the function of *Mco4*. This thesis provides the foundation for further investigations into the *Mco4* function.

## CHAPTER 2

### Materials and methods

#### 2.1 *Drosophila* husbandry and maintenance

All fly stocks were maintained on a standard cornmeal-based medium. The stocks were stored at 25°C in bottles (for experiments) or 18°C in vials (for fly stock maintenance). During experiments, Nutri-Fly food (Genesee Scientific, catalogue number: 66-113) was used unless stated otherwise and is referred to as “standard or normal food” throughout this thesis. The recipe was modified from the Bloomington *Drosophila* Stock Center (<https://bdsc.indiana.edu/information/recipes/bloomfood.html>) as follows; 17.8 grams of Nutri-Fly powder was measured and added to 100 mL autoclaved Mili-Q water. The mixture was placed on heat and allowed to simmer for around 5 minutes (min). The mixture was then allowed to cool down to room temperature (RT), and 450 µl of propionic acid was added and mixed well. The mixture was then dispensed into Petri dishes, vials or bottles and stored at 4°C for Petri dishes and 25°C for bottles/vials. This recipe was the base for all media used in the feeding experiments with the addition of certain compounds specific to the feeding experiment. The stocks used in this study are outlined in [Table 2.1](#).

#### 2.2 Preparation of embryo collection plates

This recipe was adapted and modified from Cold Spring Harbor Protocols (<http://cshprotocols.cshlp.org/content/2007/9/pdb.rec11113.full>). Three grams (g) of Bacto agar was added to 100 mL autoclaved Mili-Q water and autoclaved for 40 min. Once completed, 25 mL of any generic grape juice punch was added, and the mixed mixture was allowed to cool down to RT. In a 5 mL Eppendorf tube 0.125 g of methylparaben was added to 2.5 mL of ethanol and mixed. Once the grape juice mixture had cooled, the methylparaben/ethanol mixture was added and mixed thoroughly. The liquid was then dispensed into Petri dishes and stored at 4°C.

### 2.3 Iron-supplemented medium

The final concentration used for generating iron-enriched media was 1 mM of Ferric Ammonium Citrate (FAC). The 100X stock solution was prepared by adding 0.265 g of FAC (Sigma Aldrich #F5879) in 10 mL autoclaved Milli-Q water. 1 mL is then added to 100 mL of prepared Nutri-Fly food to achieve the final concentration.

### 2.4 Iron-chelated medium

The final concentration for generating iron-depleted media was 100  $\mu$ M of Bathophenanthrolinedisulfonic acid disodium salt hydrate (BPS). The 100X stock solution was prepared by adding 0.059 g of BPS (Sigma Aldrich #146617) in 10 mL autoclaved Milli-Q water. 1 mL was then added to 100 mL of prepared Nutri-Fly food to achieve the final concentration.

### 2.5 Survival study

100 virgin females were collected into a vial and allowed to age for five days to ensure the virginity of the flies. The aged female flies were then crossed to 50 males and placed into a cage containing grape-juice medium for two days in a 25°C incubation chamber. Following this, the grape juice medium was switched three times per hour to ensure the collection of newly fertilized eggs. Next, 50 embryos were collected per replicate (three replicates total) and placed in Petri dishes containing the appropriate medium. The following day hatched larvae were scored, and on the third day, L2 and L3 larvae were scored and placed in a vial containing the same medium. The number of pupae and the number of eclosed adults were counted and plotted in a graph for visualization. Throughout this process, the larvae were monitored regularly for any larval or pupal arrest and kept in a 25°C incubation chamber.

### 2.6 Staging, Dissection and Slide preparation

Staged L3 larvae were used for dissection and involved collecting embryos similarly to the survival rate study but instead with regular or supplemented Nutri-Fly food. The larvae were kept on the medium for around three days; following the 68–70-hour mark, L3 larvae were removed, leaving only L2 larvae. The remaining L2 larvae were staged, and every 2 hours, the newly transitioned L3 larvae were collected and placed in a petri dish containing the same

medium. After 44-48 hours, the L3 larvae were rinsed in water to remove any excess food stuck to the larvae and dissected in 1X PBS. The dissected tissues were fixed in 1X PBS 4% formaldehyde (ThermoFisher #28906) for 30 min at RT. This was followed by washing once in 1X PBS for 5 min. The samples were then added to a drop of mounting buffer (50% PBS | 50% glycerol) on a slide, covered with a coverslip and sealed with nail polish. The images were acquired using a confocal microscope (Nikon C2 Plus).

## 2.7 Tissue Immunostaining: BRGC & Gut samples

This protocol was modified from the Cell Signaling Technology immunostaining protocol (<https://www.cellsignal.com/learn-and-support/protocols/protocol-if>). The dissected tissues were fixed with 1X PBS 4% formaldehyde in a petri dish for 30 min at RT. Then rinsed once with 1X PBS for 5 min and blocked for 1 hour with 200  $\mu$ l of the Blocking Buffer (1X PBS | 5% normal goat serum (Abcam #ab7841) | 0.3% Triton<sup>TM</sup> X-100). The primary antibody, Myc-tag (9B11) mouse mAb#2276, was diluted as indicated in **Table 2.2** in an Antibody Dilution Buffer (1X PBS | 1%BSA | 0.3% Triton<sup>TM</sup> X-100). The blocking buffer was aspirated, and 200  $\mu$ l of the primary antibody was added and incubated for one hour at RT. The secondary antibody, goat anti-mouse IgG H&L (Alexa Fluor <sup>®</sup> 488), was diluted in an antibody dilution buffer as indicated in Table 2.2. The primary antibody solution was then aspirated, and samples were rinsed once with 1X PBS for 5 min. The sample was then incubated with 200  $\mu$ l of the secondary antibody for 2 hours in the dark. The sample was then rinsed once with 1X PBS and incubated with DAPI (Cell Signaling #4083) for 15 min. The immunolabelled tissues were mounted in a mounting buffer (50% PBS | 50% glycerol) on a prepared slide, covered with a coverslip and sealed with nail polish. The images were acquired using a Confocal microscope (Nikon C2 Plus).

## 2.8 DNA extraction from adult flies by DNAzol

To extract DNA from adult flies using the DNAzol reagent (Thermo Fisher Scientific, #10503027), 50 adult flies were added to a 1.5 mL tube and snap-frozen by liquid nitrogen. Pre-prepared pestles in liquid nitrogen were used to grind the frozen flies into a homogeneous powder. 200  $\mu$ l of DNAzol was added to the sample and mixed for around 15 seconds with a motorized pestle; this process was repeated three times. The final volume of DNAzol was added, 400  $\mu$ l, to a total of 1 mL of DNAzol. The sample was then vortexed for 15 seconds and left at

RT for 5 min. The sample was centrifuged at 13,000 rpm for 15 min at 4°C, and the green viscose phase was transferred into a new 1.5 mL Eppendorf tube. 600-800 µl of chloroform (1:1 ratio) was added into the tube and mixed thoroughly by inversion around 3-4 times. This was then centrifuged at 13,000 rpm for 2 min at 4°C, the upper phase (green viscose phase) was then transferred into a new 1.5 mL Eppendorf tube, and 500 µl of 100% ethanol was added and mixed by placing on a shaker for three min at RT. The sample was centrifuged for two min at 13,000 rpm and 4°C, allowing the DNA to form a pellet, and the supernatant was discarded. 800 µl of 70% ethanol was added and mixed by inversion 3-4 times. The solution was then centrifuged at 13,000 rpm for one min at 4°C, and the supernatant was discarded, leaving a pellet. The pellet was air-dried for three min at RT. 100 µl of nuclease-free water was added to dissolve the pellet using a pipette tip. 200 µl of chloroform was added and mixed by inverting the tube 3-4 times and centrifuged for two min at 13,000 rpm and 4°C. The upper phase was transferred into a new 1.5 mL Eppendorf tube, and 4 µl of 5 M NaCl was added and mixed by pipetting, then 500 µl of 100% ethanol was added and mixed by placing the tube on a shaker for three min at RT. Once completed, the sample was centrifuged for two minutes at 13,000 rpm and 4°C. The supernatant was removed, leaving behind the final DNA pellet. 800 µl of 70% ethanol was added to the tube and inverted 3-4 times to wash the pellet. The sample was centrifuged one last time at 13,000 rpm for one min at 4°C, and the supernatant was removed. The pellet was air-dried for three min at RT and dissolved with 200 µl of 8mM NaOH. The final DNA concentration was measured using a Nanodrop.

## 2.9 DNA extraction from a singly adult fly for transgenic insertion validation

This protocol was adapted from Georg Dietzl in Barry Dickson's Lab, IMP Vienna 12/2002(<https://www.rockefeller.edu/research/uploads/www.rockefeller.edu/sites/8/2018/10/SingleFlyGenomic.pdf>). To extract DNA from a single adult fly, freshly made squishing buffer was first made by adding 20 µl of 200 g/mL Proteinase K (Sigma AM2546) to the remaining squishing buffer components (10 mM Tris-HCl pH 8.0, 1 mM EDTA, 25 mM NaCl). The single fly was placed in an Eppendorf tube and mashed with a pipette tip, preferably a P10. Then, 50 µl of the squishing buffer was added and incubated at 37°C for 30 min. The sample was then heated to 95°C for 3 min to inactivate the Proteinase K and centrifuged for 30 seconds. The supernatant was removed into a new Eppendorf tube, and 1 µl was used for the PCR reaction.

## 2.10 RNA extraction from isolated PG and whole-body larval samples using TRIzol and the QIAGEN RNeasy® Mini Kit (cat.nos.74104)

Samples containing 50 dissected BRGC or six whole larvae were placed into 120 µl of ice-cold TRIzol reagent (Thermo Fisher Scientific, #15596026) and centrifuged. If a sample was not used immediately, it was flash-frozen in liquid nitrogen and stored at -80°C. Pre-prepared pestles in liquid nitrogen were used to homogenize the sample on ice, and 880 µl of cold TRIzol was added to a final volume of 1 mL and vortexed for 15 seconds. 200 µl of chloroform was then added and vortexed again for 15 seconds. The sample was then allowed to sit on ice for 1 min and centrifuged at 14,000 rpm for 15 min at 4°C. The top clear aqueous phase, around 500 µl, was transferred into an RNase-free Eppendorf tube, and an equal volume of 70% ethanol was added and mixed by pipetting. Then 700 µl of the solution was transferred to an RNeasy Mini spin column placed with a 2 mL collection tube. The sample was centrifuged at 12,000 rpm for 15 seconds, and the flow-through was discarded. This was repeated until the remaining solution was used. Then the mini spin column was washed by adding 700 µl of RW1 buffer and centrifuged for 15 seconds at 12,000 rpm. The flow-through was discarded, and 500 µl of the RPE buffer was added to the column and centrifuged for 15 seconds at 12,000 rpm. The flow-through was discarded, and 500 µl of RPE buffer was added to the column and centrifuged for 2 min at 12,000 rpm. The column was transferred into a new 2 mL collection tube and centrifuged for 1 min at 13,000 rpm, allowing the membrane to dry. The column was then placed in a new 1.5 mL Eppendorf tube, and 30 µl of RNase-free water was added to the membrane. This was then centrifuged for 1 min at 12,000 rpm, and the RNA was eluted out of the membrane. The final RNA concentration was verified using 2µl of the sample in Nanodrop (Thermo Scientific, Nanodrop 1000 Spectrophotometer) and stored at -20°C.

## 2.11 Gel extraction using the QIAquick® Gel Extraction kit (Qiagen, cat.nos.28704)

The DNA was excised from the agarose gel using a sterile scalpel and a UV imager. The excised gel piece was placed into a pre-weighed Eppendorf tube and weighed. To dissolve the gel, three 3 volumes of the QG buffer was added to 1 volume of the gel (100 mg ~ 100 µl). The sample was then incubated at 50°C for 10 min and vortexed every 2-3 min. Once the gel was dissolved completely, 1 gel volume of isopropanol was added to the sample, vortexed and

transferred to a QIAquick spin column with a 2 mL collection tube. The sample was centrifuged for 1 min, and the flow-through was discarded. An additional 500 µl QG buffer was added to the QIAquick column and centrifuged for 1 min to remove any excess agarose left behind, and the flow-through was discarded. 750 µl of PE buffer was added to the QIAquick column to wash the DNA and allowed to stand for 5 min followed by centrifugation for 1 min at 13,000 rpm. The QIAquick column was placed into a clean 1.5 mL Eppendorf tube, and the DNA was eluted by adding 30 µl of EB buffer and allowed to stand for 1 min. The Eppendorf was centrifuged for 1 min at 13,000 rpm, and the final DNA concentration was verified using Nanodrop.

#### 2.12 DNA extraction using the Thermo Scientific GeneJET Plasmid Miniprep Kit (#K0503)

The 5 mL bacterial culture was harvested at 8,000 rpm for 2 min at RT forming a pellet. 250 µl of the resuspension solution was added to the pelleted cells and vortexed, resuspending the cells. The cells were then lysed using 250 µl of the lysis solution, and the tube was inverted 4-6 times to mix. Next, 350 µl of the neutralization solution was added, and the tube was inverted 4-6 times to mix. The tube was then centrifuged for 5 min at 8,000 rpm, and the supernatant was transferred to the Thermo Scientific GeneJET spin column. The column was centrifuged for one min, and 500 µl of the wash solution was added and centrifuged for 60 seconds. The wash step was repeated twice, and the flow-through was discarded. The empty column was centrifuged for 1 min, and the column was transferred into a new Eppendorf tube. To elute the plasmid from the column, 50 µl of the elution buffer was added to the column and incubated for 2 min. The column was centrifuged for 2 min, and the flow-through was collected. The final plasmid concentration was verified using the Nanodrop.

#### 2.13 Midiprep using the QIAGEN® Plasmid Midi Kit (cat.nos.12145)

The 100 mL bacterial culture was harvested at 8,000 rpm for 15 min at 4°C, forming a pellet. 4 mL of the P1 Buffer was added to resuspend the pelleted cells, and 4 mL of the P2 Buffer was added to the cells and mixed slowly by inversion. The resulting viscous solution was incubated at RT for 5 min. 10 mL of the prechilled P3 Buffer was added to the viscous solution and inverted 6 times slowly, and incubated on ice for 15 min. The cell suspension was then centrifuged at 8,000 rpm for 30 min at 4°C. A 100 mL QIAGEN-tip was equilibrated with a 4 mL QBT Buffer and allowed to be emptied by gravity flow. The centrifuged cell suspension was

applied to the equilibrated QIAGEN-tip and allowed to be drained by gravity flow. The QIAGEN-tip was washed twice with the 10 mL QC Buffer and allowed to be drained by gravity flow. The DNA was then eluted with the 5 mL QF Buffer into a 15 mL falcon tube and precipitated by adding 3.5 mL RT isopropanol and mixed by inversion. The falcon tube was then centrifuged at 8,000 rpm for 30 min at 4°C, and the supernatant was discarded. The pellet was washed with 2 mL of RT 70% ethanol and centrifuged at 8,000 rpm for 10 min. The supernatant was discarded, and the pellet was air-dried for 10 min and dissolved in 50 µl TE buffer. The final plasmid concentration was verified using Nanodrop.

#### 2.14 Purification of PCR products

To 20 µl of PCR product, 200 µl of 100% cold ethanol was added in an Eppendorf tube and placed in a -20°C freezer for 30 min. The sample was centrifuged at 12,000 rpm for 10 min at 4°C, and the supernatant was discarded. The remaining pellet was washed with 500 µl of 75% ethanol and centrifuged for 1 min; this step was repeated twice. The supernatant was then discarded, and the pellet was dried for 10 min. The pellet was subsequently dissolved with 30 µl of nuclease-free water, and the final DNA concentration was verified using Nanodrop.

#### 2.15 Preparation of Competent cells

This protocol was modified from Cold Spring Harbor, Ultra-competent cells protocol (<http://cshprotocols.cshlp.org/content/2020/6/pdb.prot101196.full.pdf+html>). Preparation of competent cells following this protocol is a 3-day process. On the first day, 50 µl of competent *E. coli* DH5α cells were spread on an LB plate and incubated at 37°C for 16-20 hours. On the second day, a single colony from the incubated plate was aseptically picked and inoculated in a 5 mL LB medium (starter culture). The starter culture was then placed in an incubator shaker to incubate at 37°C for 8 hours. 2.5 mL of the starter culture was transferred to a beaker containing 1 L of LB and incubated at 18-22°C for 14 hours with moderate shaking. On the third day, an OD<sub>600</sub> measurement was taken using a spectrophotometer every 30 min until an OD reading of 0.55 was reached. The culture was then placed in an ice bath for 10 min. The cells were then harvested by centrifugation at 3900 rpm for 10 min at 2°C. The medium was then poured, leaving behind a pellet. The bottle containing the harvested cells was placed on a paper towel to dry. Once dry the cells were resuspended in 80 mL cold Inoue transformation buffer (55mM

MnCl<sub>2</sub>.4H<sub>2</sub>O | 15 mM CaCl<sub>2</sub>.2H<sub>2</sub>O | 250 mM KCl | 10 mM PIPES | H<sub>2</sub>O to 1L). The resuspended cells were harvested a second time by centrifugation at 3900 rpm for 10 min at 2°C. The medium was then poured, leaving behind a pellet and placed on a paper towel to dry for 2 min. Once dry the cells were resuspended in 20 mL cold Inoue transformation buffer (55mM MnCl<sub>2</sub>.4H<sub>2</sub>O | 15 mM CaCl<sub>2</sub>.2H<sub>2</sub>O | 250 mM KCl | 10 mM PIPES | H<sub>2</sub>O to 1L). The bacterial suspension was then transferred to a pre-chilled 50 mL canonical flask, and 1.5 mL of DMSO (Sigma -Aldrich #276855) was added. The bacterial suspension was gently swirled to mix the contents thoroughly and placed on ice for 10 min. The competent cells were then aliquoted into pre-chilled sterile 1.5 mL Eppendorf tubes, snap-frozen in liquid nitrogen and stored at 80°C.

## 2.16 Transformation

This protocol was modified from the NEB High Efficiency Transformation Protocol (<https://international.neb.com/protocols/0001/01/01/high-efficiency-transformation-protocol-c2987>). 50 µl of competent *E. coli* DH5α cells (see section 2.15) were thawed on ice for up to 10 min and mixed gently by flicking 3-4 times. Half of the Gibson assembly PCR reaction (see section 2.18) or 70 ng of the plasmid DNA was added to the competent cells and flicked 4 times to mix. The tube with the cell mixture was placed on ice for 30 min. Next, the tube was heat-shocked at 42°C for 45 seconds and subsequently placed on ice for 5 min to help the bacteria recover. 1,000 µl of RT LB was added to the mixture and gently rotated for 60 min at 37°C in a shaking incubator. The samples were then centrifuged at 5,000 rpm for 5 min, and the supernatant was discarded. 100 µl of LB was added to the tube containing the pellet and mixed by pipetting; the resulting mixture was spread on an Ampicillin selection plate (catalogue number 69-53-4) at a concentration of 1:1000 and incubated overnight at 37°C for 14-16 hours.

## 2.17 Colony PCR

In a PCR tube, a single isolated colony was suspended in 10 µl of nuclease-free water and mixed by pipetting. 1 µl of the mixed solution was used in the PCR reaction to screen positive transformants. Once identified, the remaining 9 µl of the suspension was added to 5 mL of LB with a selective antibiotic in preparation for DNA extraction.

## 2.18 Gibson Assembly Reaction

The Gibson Reaction concentrations used for the insert and backbone were calculated using the NEB website (<https://nebiocalculator.neb.com/#!/ligation>). The PCR fragment ratio (insert) to the backbone used throughout this thesis was a 3:1 ratio. Following the 3:1 ratio, 1  $\mu$ l of the PCR fragment (13 ng/ $\mu$ l), 1  $\mu$ l of the backbone (70 ng/ $\mu$ l) and 6  $\mu$ l of the 1.33XGibson master mix was added to a PCR tube. The reaction was incubated at 50°C for 4 hours in a PCR thermocycler.

## 2.19 Generation of constructs for S2 cell transfection

The S2-cell constructs were based on the Ac5-EGFP-C-4Myc plasmid containing the *Drosophila* Actin5c promoter and four C-terminal Myc-tags. The Ac5-EGFP-C-4Myc backbone was amplified into two fragments via PCR, removing the EGFP marker. The *Mco4* cDNA was amplified by PCR from the DGRC Indiana cDNA clone GOLD RE57944 to either contain or lack the signal peptide. The three fragments (2 backbone fragments + cDNA with or without the SP fragment) were gel-purified and combined using Gibson assembly reaction, resulting in two plasmids. The completed constructs were then transformed into DH5 $\alpha$  cells. The resulting colonies were screened using colony PCR (see section 2.17), and the final plasmids were sent for Sanger sequencing. The plasmids were individually transfected into S2 *Drosophila* cells (see section 2.22). These constructs are described in Chapter 5, and the primers used to construct these plasmids are mentioned in [Table.2.3](#). All generated constructs are listed in [Table 2.4](#).

## 2.20 Generation of a transgenic *UAS-Mco4* line

The *UAS-Mco4* line was generated using the pBID-UASC-GRM (#35203) plasmid <sup>[101]</sup>. I utilized the pBID-UASC-GRM (#35203) plasmid and the phiC31 integrase system ( $\Phi$ C31), coupled to an *attp40* insertion site for site-directed insertion into the second chromosome. The plasmid contains a UAS promoter and three C-terminal Myc-tags. The pBID-UASC-GRM backbone was amplified into two fragments via PCR, removing the *ccdB* sequence. The *Mco4* cDNA was amplified by PCR from the DGRC Indiana cDNA clone GOLD RE57944. The three fragments were gel-purified (see section 2.11) and combined using a Gibson assembly reaction. The completed construct was transformed into DH5 $\alpha$  cells, and the resulting colonies were screened using colony PCR (see section 2.17). The correct transformant was then cultured for

DNA extraction of the plasmid and sent for Sanger sequencing. This was then followed by midiprep, and the plasmid was then sent to GenetiVision for injection into the *yw nos-PhiC31; attP40* line. This construct is discussed in Chapter 5, and the primers used to generate this plasmid are listed in [Table.2.3](#). All generated constructs are listed in [Table 2.4](#).

### 2.21 Generation of the *Mco4* null mutant CRISPR line

Two guide RNA (gRNA) target sites were selected using the Harvard CRISPR gRNA tool (<http://www.flyrnai.org/crispr/>). The two target gRNA sites were confirmed via Sanger sequencing to verify the presence of the target gRNA site. The gRNA sites were then amplified by PCR and cloned into pCFD5 (#73914) pre-digested with BbsI (NEB R3539S) plasmid via the Gibson assembly reaction. The plasmid was transformed into DH5 $\alpha$  cells, and the resulting colonies were screened using colony PCR (see section 2.17). The correct transformant was then cultured for DNA extraction of the plasmid and sent for Sanger sequencing. Primers are listed in [Table.2.3](#).

The donor plasmid was constructed utilizing the pHD-DsRed-attP (#51019) plasmid <sup>[102]</sup>. Two 1 kb homology arms, left and right, were PCR-amplified and gel-purified (see section 2.11). The left homology arm was digested via *AarI* (Thermofisher #ER1581) and ligated to the pHD-DsRed-attP plasmid digested with *AarI*. The ligated plasmid was then transformed into DH5 $\alpha$  cells; the resulting colonies were screened using colony PCR. The resulting positive plasmid was digested with *SapI* (NEB #R0569S), and the *SapI*-treated right homology arm was ligated to the former. The ligated plasmid was then transformed into DH5 $\alpha$  cells; the resulting colonies were screened using colony PCR (see section 2.17). The correct transformant was then cultured for DNA extraction of the plasmid and sent for Sanger sequencing. The gRNA and target DNA plasmids were then sent to GenetiVision Production for combined injection into the *yw nos-Cas9/CyO* injection line. These constructs are discussed in Chapter 6, and the primers used to construct these plasmids are listed in [Table.2.3](#). All generated constructs are listed in [Table 2.4](#).

### 2.22 Transfection of S2 Cells

This protocol was adapted from the *Drosophila* Schneider (S2) Cells Protocol (Invitrogen #R690-07). The cells were grown on a sterile coverslip in a 6-well culture plate with Schneider

Insect medium (Sigma #S0146-500ML) supplemented with 10% heat-inactivated FBS; this is known as complete Schneider Insect medium. The cells were then incubated at 37°C for 14 hours. Afterwards, the cells were transiently transfected with a calcium phosphate mixture: Solution A (36 µl 2M CaCl<sub>2</sub> | X µl 19 µg construct | Tissue culture sterile water to a total of 300 µl) and Solution B (300 µl 2X HEPES-Buffered Saline) were added to one another dropwise with constant mixing to form the final transfection mixture. The transfection mixture was added to the cells dropwise and incubated for 24 hours at 37°C. The next day the cells were washed twice with the complete Schneider Insect medium and incubated in fresh complete Schneider Insect medium for 2 days at 37°C, before immunostaining.

### 2.23 Cell Immunodetection

Cell Immunostaining was performed following the Cell Signaling Technology immunostaining protocol (<https://www.cellsignal.com/learn-and-support/protocols/protocol-if>). The S2 Cells Schneider medium was aspirated from the wells containing a coverslip with the attached cells. The cells were fixed with 1X PBS 4% formaldehyde for 30 min at RT. The cells were rinsed once with 1X PBS for 5 min on a shaker and blocked with 200 µl Blocking Buffer for 1 hour. The primary antibody, Myc-tag (9B11) mouse mAb#2276, was diluted as indicated in **Table 2.2** in an antibody dilution buffer. The blocking buffer was aspirated, and 200 µl of the primary antibody was added and incubated for 1 hour at RT. The secondary antibody solution, goat anti-mouse IgG H&L (Alexa Fluor ® 488), was diluted in an antibody dilution buffer as indicated in Table 2.2. The primary antibody solution was aspirated and rinsed once with 1X PBS for 5 min. The cells were then incubated with 200 µl of the secondary antibody for 2 hours in the dark. The cells were then rinsed once with 1X PBS and incubated with DAPI for 15 min. The coverslip side with the attached cells was mounted downwards in a slide containing a drop of mounting buffer (50% PBS | 50% glycerol) and sealed with nail polish. The images were acquired using a confocal microscope (Nikon C2 Plus).

### 2.24 cDNA Synthesis

200 ng of RNA sample were reverse transcribed into cDNA using the ABI High-Capacity cDNA Synthesis Kit (Thermo Fisher Scientific #4368814). In a PCR tube, the reaction mixture was prepared as follows: X µl RNA sample (= 200 ng), X - 10 µl RNase-free water, 2.0

μl RT Buffer, 0.8 μl 25x dNTP Mix, 2.0 μl 10X random primers, 4.2 μl RNase-free water and 1 μl reverse transcriptase, to a final volume of 20 μl. The PCR conditions were 25°C for 10 min, 37°C for 120 min, 85°C for 5 seconds and 4°C Hold. The sample was diluted 1:10 with nuclease-free water and stored as 20 μl aliquots at –20°C.

## 2.25 Quantitative Real-Time PCR (qPCR)

### 2.25.1 Primer validation

Samples were serially diluted  $\frac{1}{4}$ ,  $\frac{1}{16}$ ,  $\frac{1}{64}$  and  $\frac{1}{1024}$  in a PCR tube by adding 20 μl of undiluted cDNA solution into 60 μl nuclease-free water. The serially diluted templates were added to a qPCR plate in triplicate. For one primer pair of validation, the Luna® universal qPCR Master Mix (Lot: 10111655) was prepared as follows for 13 reactions, an additional reaction accounting for any pipetting error: 65 μl of the Luna Master Mix and 32.5 μl of the primer that required validation (3.2 μM). 7.5 μl of the master mix was added to a qPCR plate in triplicate for each dilution, to a total of 12 wells. 2.5 μl of the serially diluted cDNA template was added to the plate in triplicates. The following qPCR program was run: 2 min – 95°C x1 cycle, 2 seconds – 95°C x 40 cycles and 20 seconds – 60°C x 40 cycles while choosing the Standard Curve setup and the 10 μl total reaction volume on the QuantStudio™ 6 Flex real-time PCR system (Applied Biosystems). The primer efficiency results were analyzed using a standard curve, and the  $r^2$  value was calculated. The primers used are listed in [Table.2.3](#).

### 2.25.2 qPCR protocol

Three biological repeats were used in triplicates for one qPCR sample being tested. One Luna® universal qPCR Master Mix reaction was prepared for each primer pair as follows: 5 μl of the Luna Master Mix and 2.5 μl of the 3.2μM primer. 7.5 μl of the master mix was added to a qPCR plate in triplicate for each biological repeat, to a total of 9 wells for one sample being tested. 2.5 μl of the diluted 1:10 cDNA template sample was added to the qPCR plate in triplicates. The following qPCR program was run: 2 min – 95°C x1 cycle, 2 seconds – 95°C x 40 cycles and 20 seconds – 60°C x 40 cycles while choosing the  $\Delta\Delta C_t$  quantification setup <sup>[103]</sup> and 10 μl total reaction volume on the QuantStudio™ 6 Flex real-time PCR system (Applied

Biosystems). The samples were normalized to *rp49* and analyzed using the  $\Delta\Delta\text{Ct}$  method <sup>[103]</sup>. The primers used are listed in [Table.2.3](#).

## 2.26 Statistics

Statistical significance of all quantifiable results was assessed using a two-tailed, paired t-test. Error bars represent a 95% confidence interval. Asterisks indicate levels of significance: \* $p < 0.05$ , \*\* $p < 0.01$ , and \*\*\* $p < 0.001$ .

## 2.27 Ferric iron staining

This protocol is modified from Xia et al., 2019 research article <sup>[104]</sup>. Wandering L3 larvae were dissected in 1X PBS, and the dissected gut was fixed with 1X PBS 4% formaldehyde in a petri dish for 30 min at RT. The tissue was permeabilized with 1X PBST (1X PBS | 0.3% Triton™ X-100) for 15 min. The 1X PBST was then aspirated from the sample and incubated for 1 hour in fresh Prussian blue staining solution (2%  $\text{K}_4\text{Fe}(\text{CN})_6$  + 2% HCl) at RT. Samples were then washed with 1X PBS and transferred into the mounting buffer (50% PBS | 50% glycerol) on a slide, covered with a coverslip and sealed with nail polish. The images were acquired using an epifluorescence camera (LEICA DFC500 Camera).

## 2.28 Centrifuge

The different centrifuges used in this chapter are listed below:  
Eppendorf centrifuge 5415 D was used for RT spins using Eppendorf tubes (0.5 - 2 mL).  
Eppendorf centrifuge 5424 R was used for 4°C spins using Eppendorf tubes (0.5 - 2 mL).  
Eppendorf centrifuge 5810 R was used for RT or 4°C spins using Falcon tubes (5 - 50 mL).

## 2.0 Tables

**Table 2.1 List of *Drosophila* stocks**

The commercially obtained fly lines were ordered from the Bloomington *Drosophila* stock center (BDSC) or the Vienna *Drosophila* research center (VDRC). We also received some lines as a gift from Michael O'Connor's lab. The embryo injection lines used by GenetiVision Production (<https://www.genetivision.com>) are also mentioned in this table. The balancers used to generate the stable homozygous transgenic lines were a kind gift from Anna Phan's lab. Finally, I used one fly line generated by Nhan Huynh (KKJ Lab).

Genotype	Description	Source	Stock #
<i>w<sup>1118</sup></i>	Wildtype	BDSC	3605
<i>phm22-Gal4</i>	PG-specific driver	Michael O'Connor's lab	-----
<i>w: tubulin-Gal4/TM3, GFP</i>	Whole-body driver	BDSC	5138
<i>w<sup>1118</sup>; P{GD5109} v15602</i>	<i>Mco1</i> -RNAi	VDRC	15602
<i>w<sup>1118</sup>; P{GD12744} v22959</i>	<i>Mco2</i> -RNAi	VDRC	22959
<i>w<sup>1118</sup>; P{GD6275} v43288</i>	<i>Mco3</i> -RNAi	VDRC	43288
<i>w<sup>1118</sup>; P{GD12310} v22606/TM3</i>	<i>Mco4</i> -RNAi (1)	VDRC	22606
<i>y1 v1; P {TRiP.HMJ23531} attP40</i>	<i>Mco4</i> -RNAi (2)	Bloomington	61947
<i>w<sup>1118</sup>; UAS-IRP1A<sup>C450S</sup> (II)</i>	IRP1A apo-form only transgenic expression	KKJ Lab	-----
<i>UAS-AGBE<sup>IRI</sup></i>	<i>AGBE</i> -RNAi	VDRC	108087
<i>yw; nos-Cas9/CyO</i>	<i>Mco4</i> null mutant CRISPR line	GenetiVision	-----
<i>yw nos-PhiC31; attP40</i>	<i>UAS-Mco4</i> line	GenetiVision	-----
<i>Fm7a</i>	Balancer: CRISPR line	Anna Phan's lab	-----
<i>w; CyO/Sco; TM2/TM6</i>	Balancer: <i>UAS-Mco4</i> line	Anna Phan's lab	-----

<b>Table 2.2 Immunostaining antibodies and staining reagent concentrations</b>			
<b>Antibody/Stain</b>	<b>Source</b>	<b>Experiment</b>	<b>Dilution</b>
DAPI	Cell Signaling #4083	S2 Cells & Tissue	1:50,000
Myc-tag (9B11) mouse	Cell Signaling #2276	S2 Cells	1:8000
Myc-tag (9B11) mouse	Cell Signaling #2276	Tissue	1:1000
Goat Anti-Mouse IgG H&L (Alexa Fluor® 488)	Abcam #1500777	S2 Cells & Tissue	1:500

<b>Table 2.3 List of primers</b>		
<b>Primer name</b>	<b>Sequence: 5' – 3'</b>	<b>Uses</b>
<b>Primers used to screen the genome sequence and colony PCR</b>		
gRNA 1 FP	CGGCATCCTCTGTTCTTCCC	Verify CRISPR gRNA sequence
gRNA 1 RP	CATTTTCCAAGTGGCTCGC	
gRNA 2 FP	GCATCCCATCCACCTGCACG	
gRNA 2 RP	GTGCACGATGGTTGGAAGTCC	
attB1- <i>Mco4</i> FP <sup>R</sup>	CAAGTTTGTACAAAAAAGCAGGCTATGAA ATTCAATTTGGTGCAG	C.PCR <i>UAS-Mco4</i> line
Myc PBID BB C.PCR RP	GCAGACAATTTGATGTTGCAATCGCAGTTC C	
Ac5-seq FP	GCCAGCAGTCGTCTAATCCA	C.PCR S2 Constructs
Ac5-seq RP	CTCCCCCTGAACCTGAAACAT	
pCFD5 seq FP	GACTCAGTTCGTATATATAGACC	C.PCR gRNA plasmid
pCFD5 seq RP	GCACAATTGTCTAGAATGCATAC	
pHD-BB-1 FP	ACGAAAGGCTCAGTCGAAAG	C.PCR donor construct
pHD-HSP70 RP <sup>R</sup>	CGGTCGAGGGTTCGAAATCGATAAG	
pHD-SV40 FP <sup>R</sup>	GGCCGCGACTCTAGATCATAATC	
pHD-BB-2 RP	TGATATCAAATTATACATGTCAACG	
<b>Primers used to verify transgenic lines through PCR and Sequencing</b>		
DSCP FP	CGTGCCGCTGCCTTCGTT	<i>UAS-Mco4</i> line
SV40 pA RP	CCTTAGAGCTTTAAATCTCTGTAGG	
pHD-SV40 FP <sup>R</sup>	GGCCGCGACTCTAGATCATAATC	<i>Mco4</i> null mutant line
Right-Genomic-RP	CCACAAGTTTGGTTGCATTCGG	
Left Arm FP <sup>R</sup>	AAATCACCTGCTTTATCGCACCACCCACAA ACGCACACAC	
pHD-HSP70 RP <sup>R</sup>	CGGTCGAGGGTTCGAAATCGATAAG	
<b>Primers used to generate constructs</b>		
Left Arm FP <sup>R</sup>	AAATCACCTGCTTTATCGCACCACCCACAA ACGCACACAC	donor plasmid

Left Arm RP	CCAGCACCTGCTTCGCTACAGTGGGCTTCC GTCATCGCTTAC	2 PCR reactions
Right Arm FP	CCGCGCTCTTCGTATCCTGGGTCCCGAAGT TATCAC	
Right Arm RP	CCGTGCTCTTCTGACACTGGAACACTTTGT CGTGG	
pCFD5 FP	TTCGATTCCCGGCCGATGCACTGACAGTA ACATTTGGCCGTTTTAGAGCTAGAAATAG C	gRNA- CRISPR Plasmid 1 PCR reaction
pCFD5 RP	CTATTTCTAGCTCTAAAACAGGAACCCAC TAGGCCACCTGCACCAGCCGGGAATCGAA C	
attB1- <i>Mco4</i> FP <sup>R</sup>	CAAGTTTGTACAAAAAAGCAGGCTATGAA ATTCAATTTGGTGCAG	<i>UAS-Mco4</i> construct  3 PCR reactions
attB2- <i>Mco4</i> RP	CTTGACAGCTCGTCCATCCACTTTGTACA AGAAAGCTGGGTGGCCACCGAACTGCACA G	
GRM BB FP	GCCTCCTTCTCTGTCCACAG	
attB1 GRM RP	CTGCTTTTTTGTACAAACTTGTGATATCGA GCTCTCCCGGGAATT	
attB2 GRM FP	ATGGACGAGCTGTACAAGTCTAGA	
GRM BB RP	CTGTGGACAGAGAAGGAGGC	
<i>Mco4</i> (Ac5) FP	TCCAGTGTGGTGGAAATTCGCCACCATGGC CATGAAATTCAATTTGGTGCAG	Insert: <i>Mco4</i> Ac5 plasmid
S.P Del <i>Mco4</i> (Ac5) FP	TCCAGTGTGGTGGAAATTCGCCACCATGGC CATGATTCAAGATGCCAGTGGCAAG	Insert: delete putative SP <i>Mco4</i>
<i>Mco4</i> (Ac5) RP	TGGCGGAGCTTCTGATGGCCACCGAACTG CACAGAC	RP for inserts
C-Myc-BB 1-FP	ATCAGAAGCTCCGCCACCATG	

C-Myc-BB 1-RP	TCAGAGTTGATGCCATTCATG	Ac5 plasmid BB (S2 Cells) 3 PCR reactions (Insert + BB)
C-Myc- BB 2-FP	CATGAATGGCATCAACTCTGA	
C-Myc- BB 2-RP	GAATTCCACCACACTGGAC	
<b>qPCR Primers</b>		
<i>rp49</i> FP	TTCCTTGACGTGCCAAAAC	Normalization of qPCR sample
<i>rp49</i> RP	AATGATCTATAACAAAATCCCCTGA	
<i>Mco4</i> FP	CAGCCGATGACCTGCTACTA	Measure <i>Mco4</i> transcript levels
<i>Mco4</i> RP	AAGCGGAATTTGGACTGGA	

BB: Vector Backbone

FP: Forward Primer

RP: Reverse Primer

SP: Putative Signal Peptide

<sup>R</sup>: Primer used twice in different PCR reactions

**Table 2.4** List of generated constructs

Name of Construct	Plasmid used	Expression	Description
<i>Ac5-Mco4-C-4Myc</i>	<i>Ac5-EGFP-C-4Myc</i>	S2 Cells	<i>Mco4</i> Myc-tag
<i>Ac5-Mco4-ΔSP-C-4Myc</i>	<i>Ac5-EGFP-C-4Myc</i>	S2 Cells	<i>Mco4</i> SP deletion Myc-tag
<i>pBID-UASC-GRM-Mco4</i>	<i>pBID-UASC-GRM</i>	<i>In vivo</i>	<i>UAS-Mco4</i> line
DsRed Donor Plasmid	PhD-DsRed-attp	<i>In vivo</i>	<i>Mco4</i> <sup>-/-</sup> null mutant CRISPR line
<i>Mco4</i> gRNA's plasmid	pCFD5		

## CHAPTER 3

### *Preliminary data generated in our lab suggests Mco4 may act as a high affinity iron importer*

RNA-Sequencing is a powerful technique used to detect differential gene expression in the sample. Three recent independent RNA-Seq experiments completed by two former Ph.D. students from the King-Jones lab, Dr. Nhan Huynh and Dr. Sattar Soltani, revealed significant upregulation of *Mco4* under iron-deprived conditions in brain ring gland samples.

The first independent RNA-Seq data that identified elevated *Mco4* transcript levels was completed by Sattar Soltani (manuscript in preparation). The high throughput RNA-Seq was completed using RNA samples from wildtype (*w<sup>1118</sup>*) flies reared on a dietary iron-chelated food (100  $\mu$ M Bathophenanthroline Sulfate; BPS) for five generations. It takes five generations for populations reared under iron-deprived conditions to experience a ~50% lethality. After the fifth generation, the animals were transferred to a dietary iron-enriched media or remained on iron-chelated food (1 mM Ferric Ammonium Citrate; FAC). This method allows for identifying transcriptional responses to changes in dietary iron concentrations, for which we used *w<sup>1118</sup>* animals. Two biological samples were collected, each containing RNA prepared from 50 brain ring gland complex (BRGC) tissues at 12 hours post-L3 instar moult. The analysis of the RNA-Seq dataset revealed 57 differentially expressed genes in response to dietary iron changes. Of these, *Mco4* ranked 12/57 upregulated transcripts and resulted in a 42-fold upregulation (Figure 10).

The 1,4-Alpha-Glucan Branching Enzyme (*AGBE*) gene belongs to the glycosyl hydrolase 13 family and is involved in glycogen synthesis [15]. A paper published by Dr. Nhan Huynh revealed *AGBE* to be a regulator of iron homeostasis that interacts physically with the IRP1A holo-form to repair its Fe-S clusters from oxidative damage, ensuring holo-IRP1A function [15]. The same study also found that genetic manipulation of *AGBE* via PG-specific RNAi or PG-specific gene disruption (*phm22>AGBE<sup>RNAi</sup>* and *phm22>AGBE<sup>FCF</sup>*) impaired iron

metabolism, essentially mimicking iron-deprived conditions. The resultant iron-deprived conditions are due to two possible scenarios 1) iron levels are indeed depleted or 2) iron levels remain the same or higher but are inaccessible (Synchrotron data of IRP1A RNAi showed lower iron levels in the PG) [15]. These conditions resulted in an L3 arrest and enlargement of the ring gland with an observable red autofluorescence under UV light (Figure 11A), similar to what is observed in a *PPOX* mutant (*PPOX*<sup>-/-</sup>) [15]. The red autofluorescence indicates heme precursor accumulation owing to the disruption of the heme biosynthesis pathway. Taken together, this signifies *AGBE*'s involvement in cellular iron homeostasis and is further supported by *phm22>AGBE*<sup>FCF</sup> rescue through iron supplementation [15].

The following RNA-Seq experiments (second, third and fourth) were all completed by Nhan Huynh. For the second and third RNA-Seq experiments, *phm22>AGBE*<sup>RNAi</sup> and *phm22>AGBE*<sup>FCF</sup> fly lines were used. Animals were reared on Nutri-Fly food, and the extracted RNA was prepared from 50 ring glands at 40 hrs post-L2/L3 moult for one replicate. Three biological samples were collected for each independent cross. This method allows for identifying transcriptional responses to genetically induced iron deprivation changes through loss of *AGBE* function. The RNA-Seq experiments performed under genetic iron deprivation conditions resulted in an increase of *Mco4* expression levels of 114- and 73-fold, in *phm22>AGBE*<sup>RNAi</sup> and *phm22>AGBE*<sup>FCF</sup> respectively (Figure 11B). The high *Mco4* transcript levels under genetically induced iron deprivation were consistent with the upregulated *Mco4* expression in control larvae reared on iron-depleted media. The two independent RNA-Seq datasets identify *Mco4* transcriptional response to a state of iron deprivation using two different approaches, dietary and genetic manipulation to iron levels in the PG.

As explained in Chapter 1 section 3.3, the fourth RNA-Seq dataset completed by Nhan Huynh was performed using PG-specific overexpression of IRP1A variants: IRP1A wildtype (*phm22>IRP1A*), a version of IRP1A locked into the apo-form (*phm22>IRP1A*<sup>C450S</sup>), and a version of IRP1A with impaired RNA-binding (*phm22>IRP1A*<sup>3R3Q</sup>) [73]. Transcripts that were upregulated in *phm22>IRP1A*<sup>C450S</sup> but not mis-regulated in *phm22>IRP1A* and *phm22>IRP1A*<sup>3R3Q</sup> were filtered [73]. The RNA-Seq results displayed 23 upregulated transcripts, with *Mco4* ranking 2/23 based on fold change and a ~165-fold upregulation (Figure 12) [73]. Summary of the

four *Drosophila* Multicopper oxidases fold changes in all three independent RNA-Seq experiments can be found in [Table 3.1](#).

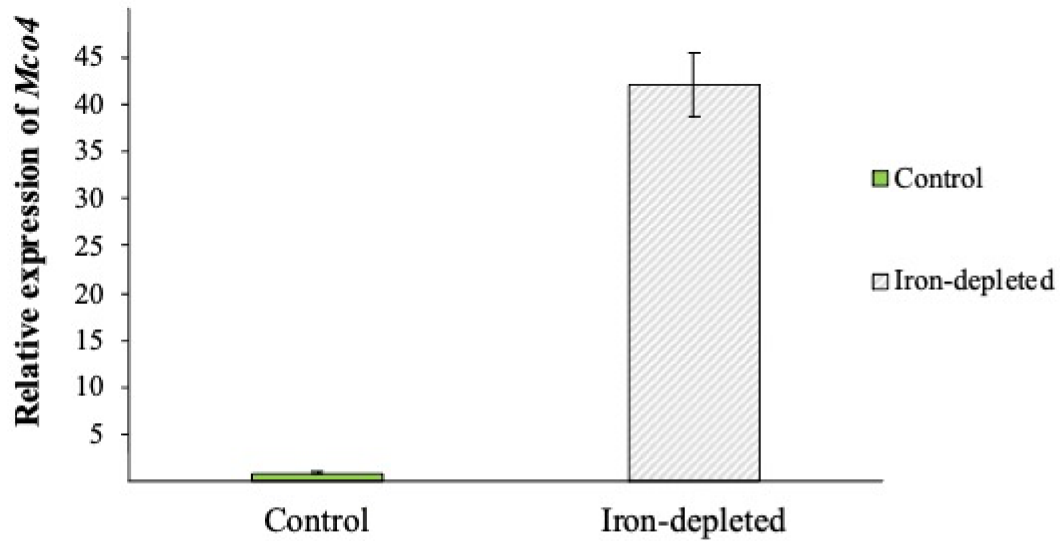
Mco4 is the ortholog of a yeast protein, Fet3p, which functions as a high affinity iron importer ([Table 3.2](#)) <sup>[17, 105-106]</sup>. Fet3p works in partnership with another protein named Ftr1p, which has no ortholog in *Drosophila*. Fet3p acts as a ferroxidase and oxidizes Fe<sup>2+</sup> to Fe<sup>3+</sup> in preparation for its transport across the membrane through the channel protein Ftr1p <sup>[17]</sup>. Collectively, these findings provide a solid basis for modulating Mco4's possible function. The strong upregulation of *Mco4* under iron-deprived conditions suggests that Mco4 is an integral part of *Drosophila's* biological response to iron deprivation. This finding is consistent with the idea that Mco4 is only needed when iron levels are critically low and supports a model where iron uptake under normal conditions is conducted by other metal transporters. Phrased differently, I hypothesize that Mco4 and an uncharacterized partner protein are transcriptionally induced to mediate high affinity iron transport across the membrane under iron-deprived conditions. To test this hypothesis and understand the role of *Mco4* in response to low iron conditions, I conducted experiments using *Mco4* knockdown animals and generated null mutant animals under standard and iron-chelated conditions. I also characterized the localization of Mco4 in the cell, the results of which I describe throughout this thesis.

**Table 3.1** Summary of *Drosophila* MCOs fold changes in all three independent RNA-Seq experiments.

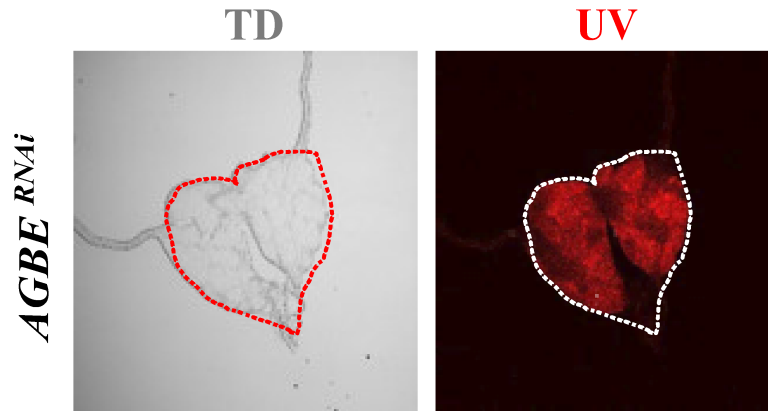
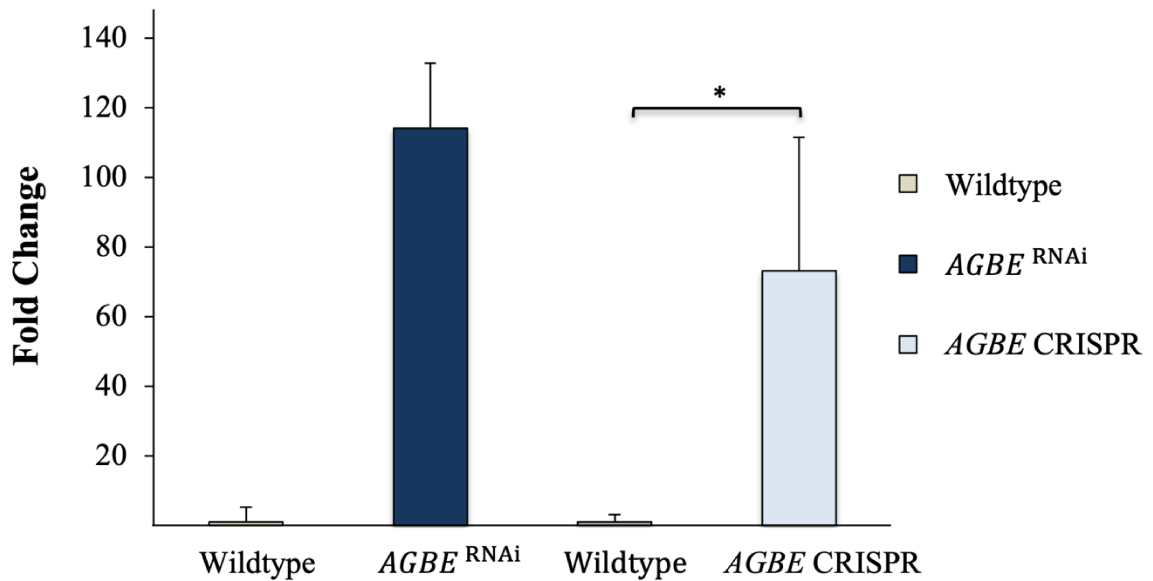
Gene	Dietary Iron	<i>AGBE</i> <sup>RNAi</sup>	<i>AGBE</i> <sup>CRISPR</sup>	<i>IRPIA</i> <sup>C450S</sup>
<i>Mco1</i>	-10	0.40	0.02	4.20
<i>Straw</i>	4	0.67	0.95	2.00
<i>Mco3</i>	-10	0.43	0.11	-1.08
<i>Mco4</i>	42	114.17	73.06	164.46

**Table 3.2** Protein alignment of *Drosophila* MCOs with yeast Fet3p using BLASTP <sup>[105-106]</sup>.

Protein	Sequence Identity	Sequence Similarity	Query Cover	Length
<i>Mco1</i> Isoform B	37%	(293-450) 54% (775-886) 49%	41%	959
<i>Straw</i> Isoform G	25%	41%	72%	784
<i>Mco3</i>	25%	42%	72%	677
<i>Mco4</i>	25%	42%	73%	645



**Figure 10.** RNA-Seq experiment revealed upregulation of *Mco4* under dietary iron changes in Brain-Ring Gland Complex samples. *w<sup>1118</sup>* flies were first reared on an iron-depleted diet for five generations. In the sixth generation, flies were reared under iron-depleted conditions or iron-enriched diets. Larvae were collected at 12 hours post-L3 instar moult, and the Brain-Ring Gland Complex (BRGC) tissue was dissected for RNA-Seq analysis. The RNA-Seq experiment was completed by Sattar Soltani, error bars represent 95% confidence interval and n= 2 replicates per sample.

**A****B**

**Figure 11. PG-specific disruptions of *AGBE* results in a porphyria-like phenotype and high *Mco4* upregulation.** (A) Under UV light, the PG isolated from *AGBE* RNAi larvae (*phm22>AGBE*<sup>RNAi</sup>) reared on Nutri-Fly food displayed red autofluorescence. (B) L3 instar larvae were reared on Nutri-Fly food, and the ring glands were dissected and collected for RNA-Seq analysis (*phm22>AGBE*<sup>RNAi</sup> and *phm22>AGBE*<sup>FCF</sup> (CRISPR)). The RNA-Seq experiments were completed by Nhan Huynh, error bars represent 95% confidence interval, \**p* < 0.05 and n= 2 replicates per sample.

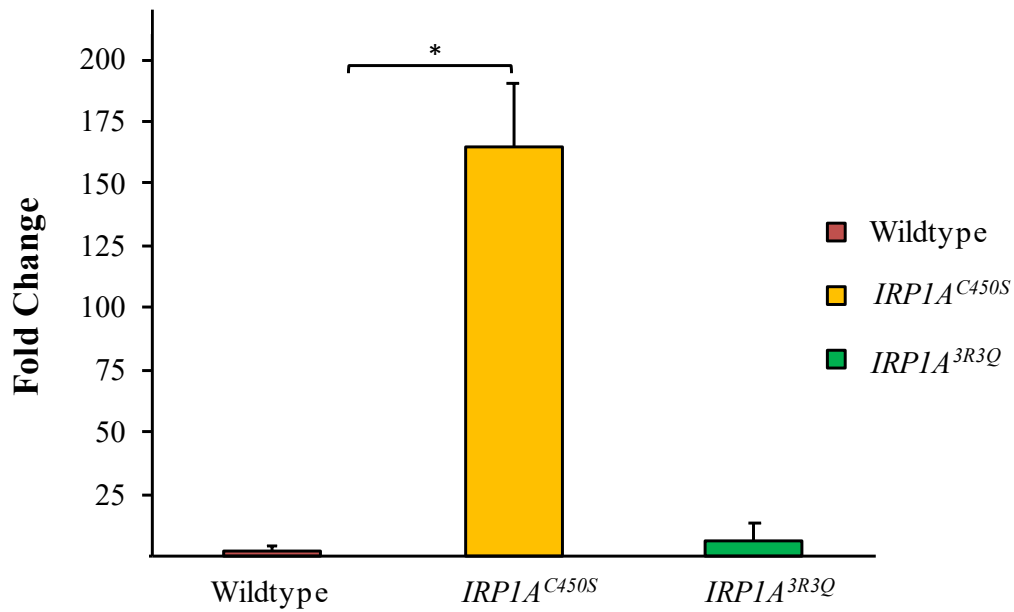


**Figure 12. Transgenic expression of apo-IRP1A in the PG results in elevated *Mco4* expression.** Depicts RNA-Seq experiment completed by Nhan Huynh using *phm22>IRP1A*, IRP1A apo-form (*phm22>IRP1A<sup>C450S</sup>*) and the non-RNA-binding form (*phm22>IRP1A<sup>3R3Q</sup>*) PG-specific transgenic expression line. Fifty L3 instar larvae were dissected, and the ring glands were collected for RNA-Seq analysis. Error bars represent 95% confidence interval, \* $p < 0.05$  and  $n = 2$  replicates per sample.

## CHAPTER 4

### *Characterizing Mco4 function in Drosophila*

#### *4.1 Individually analyzing the PG-specific knockdown of all four Drosophila multicopper oxidases using RNAi.*

Although iron metabolism in *Drosophila* has been widely studied, little is understood of the components involved in iron import, export and trafficking. A critical aspect of mammalian iron absorption is the enzymes that catalyze iron's oxidation and reduction states. Ferric iron (III) is first reduced to ferrous iron (II) by Dcytb when absorbed by the small intestine. It is then oxidized upon its export across the basolateral membrane by Hephaestin, a multicopper ferroxidase enzyme<sup>[18]</sup>. This raises the question of whether *Drosophila* iron absorption also requires the oxidation of iron via a ferroxidase enzyme<sup>[58]</sup>. Multicopper oxidases are versatile enzymes found in plants, animals, yeasts and insects. The multicopper oxidase (MCO) family in *Drosophila* consists of four enzymes, *Mco1*, *straw*, *Mco3*, and *Mco4*.

The first step in this project was to identify which of the four *Drosophila* multicopper oxidase enzymes is a likely insect ferroxidase candidate involved in cellular iron uptake into the cell. I evaluated this by knocking down the gene expression of all four MCO's using RNA interference (RNAi) mediated knockdown and analyzing the resulting phenotypes. RNAi is a biological process that silences a gene's expression at the transcriptional level<sup>[107-108]</sup>. Over the years, RNAi has become an established tool used in *Drosophila* research to study a gene's function by manipulating its expression in all tissues or a tissue-specific manner using the UAS-Gal4 system. For this experiment, the UAS-RNAi fly lines were crossed to a *phantom22-Gal4* (*phm22>*) driver using the Gal4-upstream activation sequence (UAS) system to specifically knockdown the function of the targeted mRNA in the PG. The PG is a great model to study iron metabolism because the PG requires high iron levels for ecdysone production and heme synthesis<sup>[15]</sup>. Consequently, iron-depleted conditions in the PG affect ecdysone production, delaying larval development. A strong red autofluorescence phenotype can also be observed in

the PG under UV light when the heme synthesis pathway is impaired. Causing heme precursor accumulation due to a non-functional enzyme in the heme pathway or insufficient iron levels. Taken together, this makes the PG a valuable model for characterizing genes with a potential function in iron homeostasis.

The experiments were carried out in Nutri-Fly food. Nutri-Fly food follows a standard recipe from the BDSC and provides *Drosophila* with its nutrient requirements. The contribution of the knockdown of four genes was examined by testing the survival rate of the first generation, the lethality, and the occurrence of organismal developmental delays such as larval arrest or delayed pupariation. *w<sup>1118</sup>* flies were used as a negative control for both experiments, survival rate percentage quantification and ring gland phenotype.

## Results

Prothoracic gland-specific knockdown lines targeting *Mco1*, *straw*, *Mco3* and *Mco4* were generated by crossing the *phm-22-Gal4* driver to the corresponding UAS-RNAi lines (Figure 13). The PG-specific knockdowns of *Mco1* (*phm22>Mco1<sup>RNAi</sup>*), *straw* (*phm22>straw<sup>RNAi</sup>*), *Mco3* (*phm22>Mco3<sup>RNAi</sup>*), and *Mco4* (*phm22>Mco4<sup>RNAi-1</sup>*) showed no larval arrest. *Mco3* (*phm22>Mco3<sup>RNAi</sup>*) knockdown showed a relative drop of 33% in pupal formation and adult eclosion compared to the control. In contrast, *Mco1* knockdown (*phm>Mco1<sup>RNAi</sup>*) resulted in nearly two-thirds of the population (64%) failing to reach adulthood relative to the control animals (*t*-test, *p*<0.001). Both *straw* (*phm22>straw<sup>RNAi</sup>*) and *Mco4* (*phm22>Mco4<sup>RNAi-1</sup>*) showed no significant reduction in the survival rate.

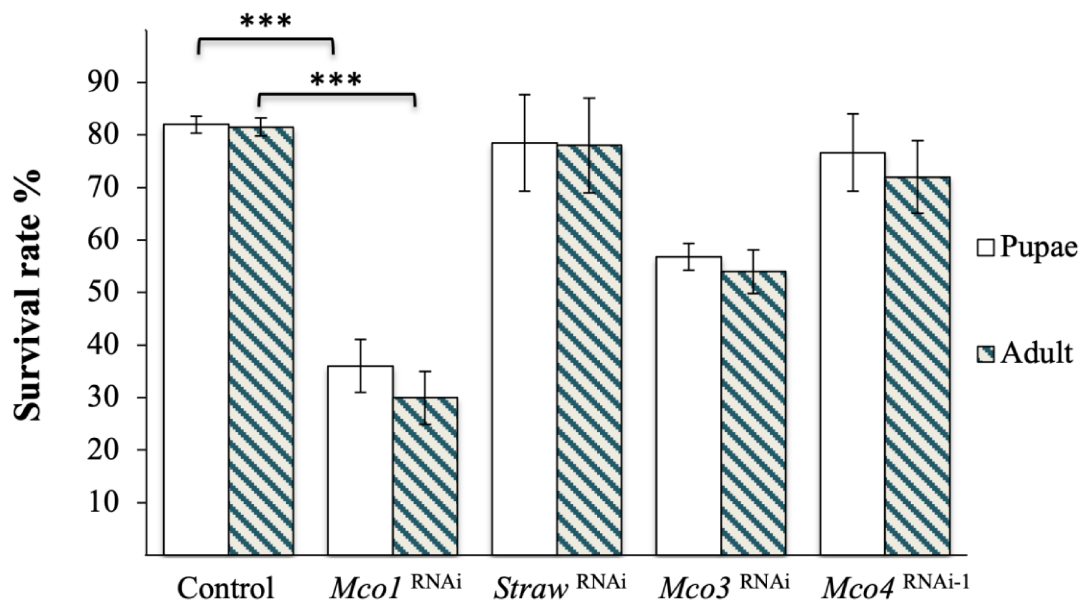


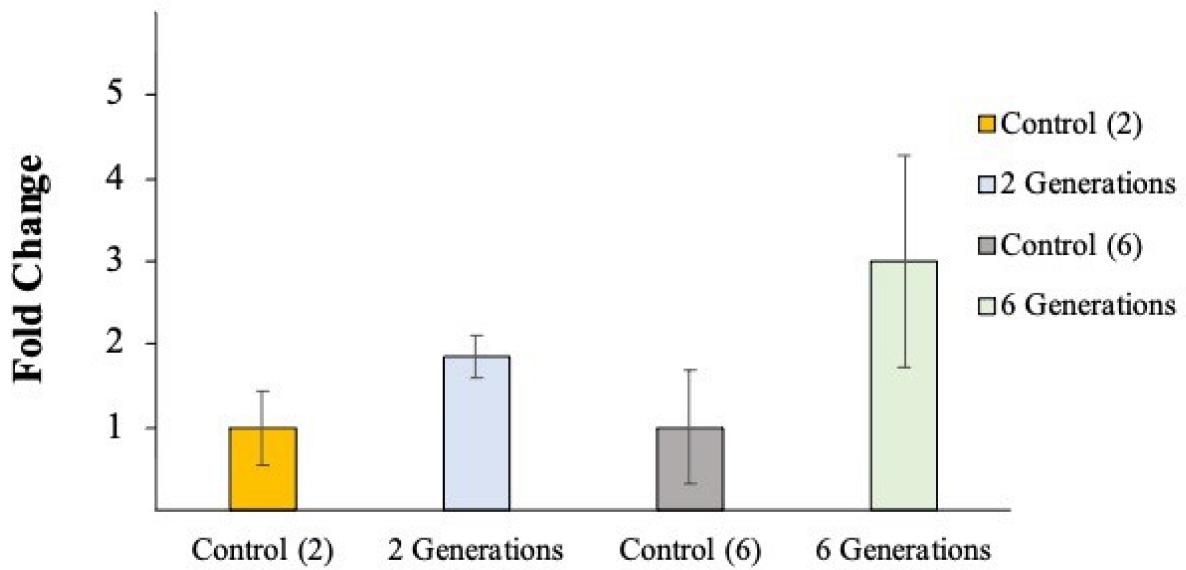
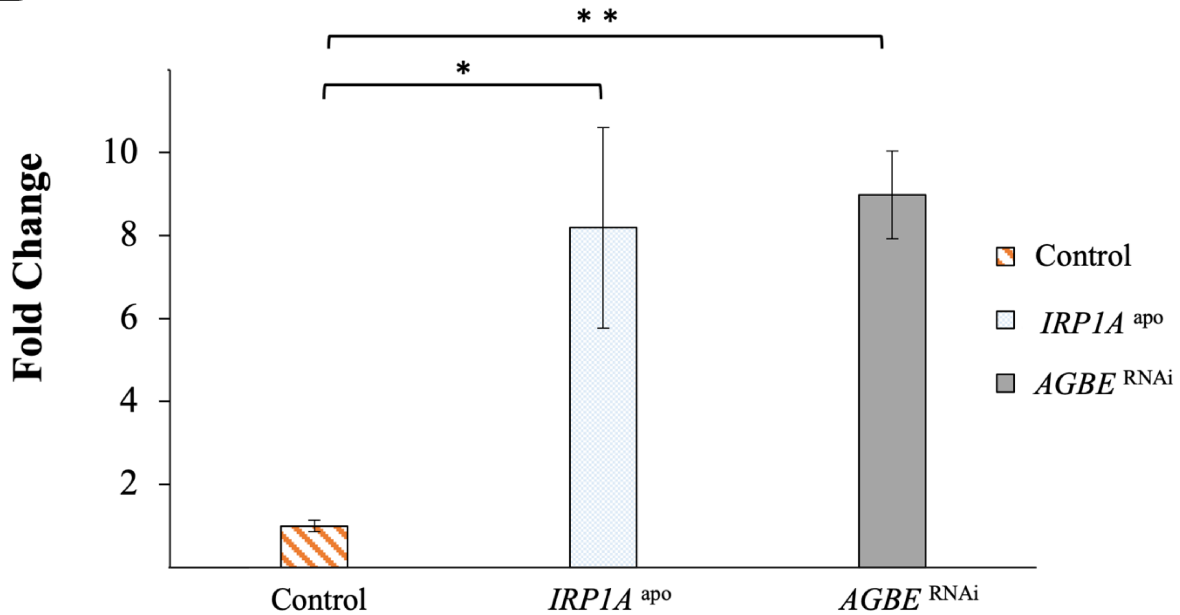
**Figure 13. Survival analysis of animals with PG-specific *Drosophila* multicopper oxidase (1-4) knockdown using RNAi.** Fifty eggs for one replicate were collected and reared on Nutri-Fly food or an iron-supplemented diet. The number of pupae and adult flies were counted to assess the survival rates. Flies were reared on Nutri-Fly food; *Mco1* (*phm22>Mco1*<sup>RNAi</sup>), *straw* (*phm22>straw*<sup>RNAi</sup>), *Mco3* (*phm22>Mco3*<sup>RNAi</sup>) and *Mco4* (*phm22>Mco4*<sup>RNAi-1</sup>). Error bars represent 95% confidence interval, \*\*\*p-value<0.001 and n= 3 replicates per sample.

#### 4.21 RT-qPCR evaluation of RNA-Sequencing data.

My proposed hypothesis, arising from the RNA-Seq data provided by Nhan and Sattar, is that *Mco4* encodes a high affinity iron importer, analogous to yeast Fet3p, which is functionally vital under low-iron conditions. The generated RNA-Seq requires additional testing using an independent assay. The rationale is that if the results through two independent transcriptome analyses can result in the same data, the generated RNA-Seq data is likely reliable. RT-qPCR is a simple and popular method researchers use to confirm RNA-Seq data. To evaluate the RNA-Seq data, I performed four independent RT-qPCR experiments under similar test conditions. The target gene *Mco4* was normalized to Ribosomal protein 49 (*rp49*) transcripts. *Rp49* is a standard

housekeeping gene used for stable and reproducible expression [109]. The first RT-qPCR experiment I completed was to test the RNA-Seq data conducted by Sattar Soltani. The RT-qPCR experimental workflow used BRGC samples from *w<sup>1118</sup>* L3 larvae reared on iron-chelated food (100  $\mu$ M BPS) for five generations. After the fifth generation, the animals were transferred to either iron-chelated food (100  $\mu$ M BPS) or dietary iron-enriched media (1 mM FAC). The L3 larvae were dissected, and 50 BRGC samples were collected for three replicates. I found that *Mco4* transcripts were roughly 3-fold more abundant than the control (Figure 14A). Knowing that *Mco4* transcript levels are elevated after five generations of iron deprivation, I wanted to compare iron deprivation after only two generations on iron-chelated food (100  $\mu$ M BPS). I carried out RT-qPCR following the same experimental workflow as the five-generation RT-qPCR. The analysis revealed that the *Mco4* expression level is increased 2-fold, indicating one generation under iron-deprived conditions is enough to induce *Mco4* gene expression (Figure 14A). However, both results were statistically determined not to be significant.

The next RT-iron-deprived experiment I completed was the RNA-Seq experiment using PG-specific *AGBE<sup>RNAi</sup>* and the apo-IRP1A transgenic expression line (*phm22>IRP1A<sup>C450S</sup>*). Both RT-qPCR samples were prepared the same way; 50 BRGC samples for three replicates were collected from *phm>w<sup>1118</sup>*, *phm22>AGBE<sup>RNAi</sup>* and *phm22>IRP1A<sup>C450S</sup>* L3 larvae reared on Nutri-Fly food. In the *phm22>AGBE<sup>RNAi</sup>* and *phm22>IRP1A<sup>C450S</sup>* larvae, expression of *Mco4* displayed a significant increase of 9- and 8-fold (*t*-test *p*-value < 0.01 & *p*-value < 0.05) respectively when the larval-pupal transition occurs (Figure 14B).

**A****B**

**Figure 14.** RT-qPCR evaluations of high *Mco4* expression levels found in RNA-Seq data.

(A) *w*<sup>1118</sup> flies were reared on iron-depleted media for one or five generations. On the second and sixth-generation, flies either remained on an iron-depleted diet or switched to an iron-supplemented diet.

Third instar larvae were dissected, and fifty BRGC samples were collected for three replicates. *Mco4* expression levels under iron-depleted conditions were assessed after two and six generations. The *Mco4* expression levels were calculated relative to *Mco4* expression levels in FAC using the  $\Delta\Delta\text{Ct}$  method and *rp49* as a reference gene for normalization. **(B)** *phm22>AGBE<sup>RNAi</sup>* and *phm22>IRP1A<sup>C450S</sup>* larvae were reared on Nutri-Fly food. Brain Ring Gland Complex samples were dissected from L3 larvae. *Mco4* expression levels were calculated relative to *w<sup>1118</sup>* using the  $\Delta\Delta\text{Ct}$  method and *rpP49* as a reference gene for normalization. Error bars represent 95% confidence interval, \*p-value<0.05, \*\*p-value<0.01 and n= 3 replicates per sample.

#### 4.22 Analysing the effects of PG-specific *Mco4* knockdown

To determine whether *Mco4* is involved in the PG response to low iron conditions, I knocked down *Mco4* in the PG under normal and low iron conditions (100  $\mu\text{M}$  BPS) using RNAi. RNAi is a valuable tool for studying gene function by knocking down its expression [108,110]. However, RNAi can lead to off-target effects with genes containing a similar sequence [110]. In this context, it's important when using RNAi-mediated knockdown to use more than one independent RNAi line to validate an RNAi phenotype. Therefore, to knock down *Mco4*, I used two independent RNAi lines targeting distinct regions of the *Mco4* transcript (*Mco4<sup>RNAi-1</sup>* and *Mco4<sup>RNAi-2</sup>*) expressed under the control of a *phm22-Gal4* driver (*phm22>Mco4<sup>RNAi-1</sup>* and *phm22>Mco4<sup>RNAi-2</sup>*). Using these two independent RNAi lines ensures any induced RNAi-mediated knockdown phenotype is attributed to *Mco4* knockdown and not off-target effects [108].

For each cross, I assessed the survival rate and PG phenotypes. By dissecting third instar larvae and using confocal microscopy, I evaluated the enlargement of the PG and red autofluorescence phenotypes indicative of heme precursor accumulation (“porphyria-like” phenotype). Disruptions in the heme synthesis pathway result in observable phenotypes, a strong red autofluorescence and enlargement of the PG (Figure 7). The red autofluorescence and enlarged ring gland phenotypes observed in *PPOX* mutants (*PPOX<sup>-/-</sup>*) served as a positive control for heme synthesis disruption.

## Results

The *Mco4* RNAi knockdown caused no noticeable reduction in the survival rate under normal food conditions (Figure 15), and the PG did not exhibit any porphyria-like phenotypes when larvae were reared on the standard diet (Figure 16A) and low iron food (Figure 16B).

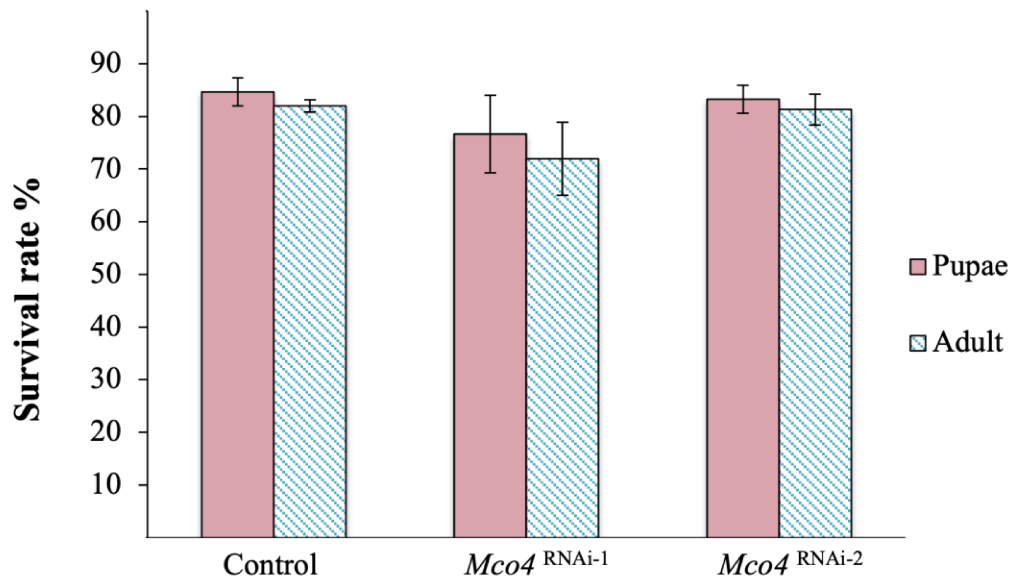


**Figure 15.** The survival rate of *Mco4* prothoracic knockdown flies reared on Nutri-Fly food. Fifty eggs for one replicate were collected and reared on Nutri-Fly food, the number of pupae and adult flies was counted to estimate the survival rate. Adult and pupae percent survival of *phm22>Mco4*<sup>RNAi-1</sup> and *phm22>Mco4*<sup>RNAi-2</sup> lines were analyzed. Error bars represent 95% confidence interval and n= 3 replicates per sample.

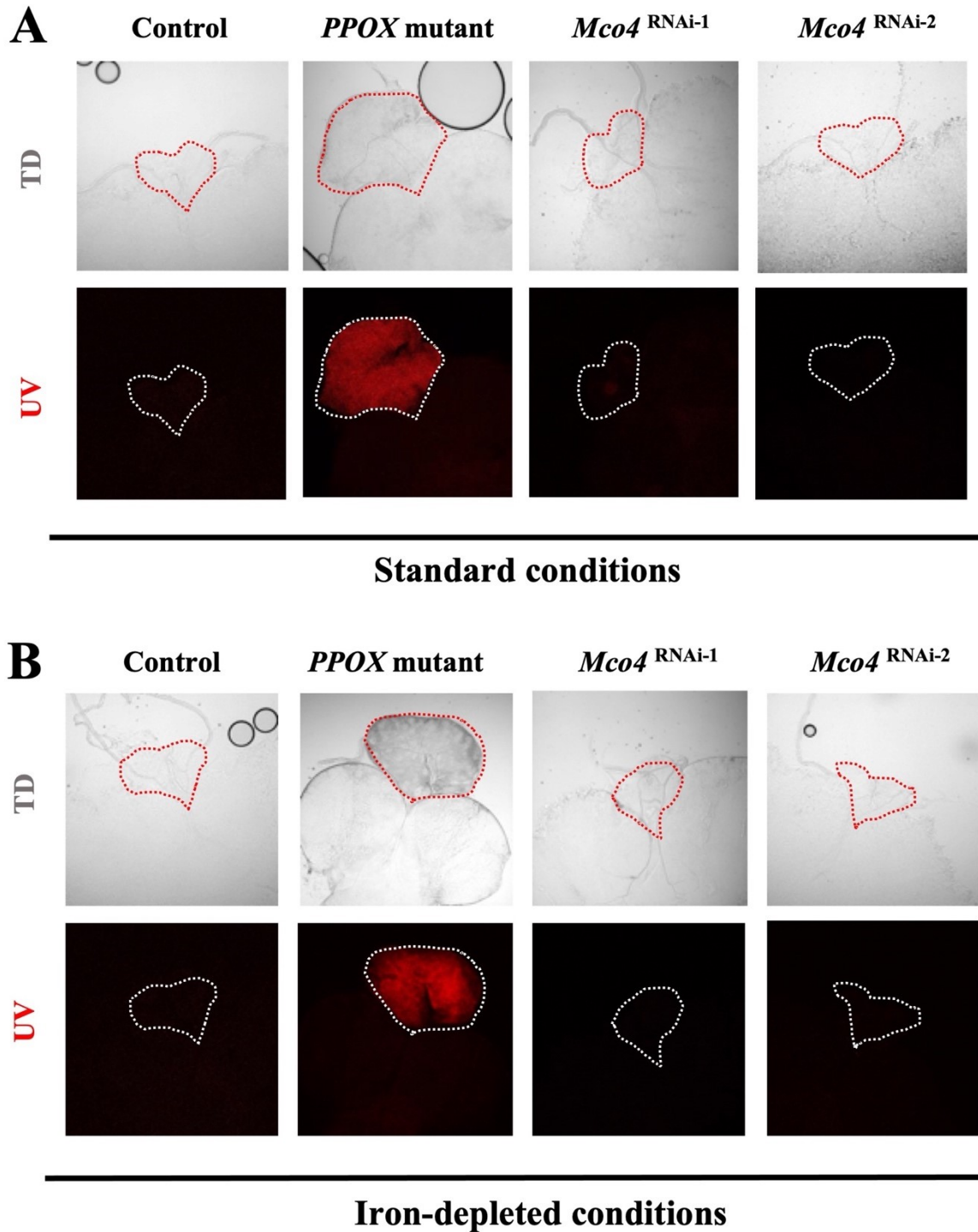


**Figure 16. Impairment of Mco4 function in the PG.** Third instar larvae BRGC were dissected and assessed for porphyria-like phenotypes, enlarged ring gland and red autofluorescence. Fluorescent images were captured using a Nikon C2 confocal microscope; the magnification used was 20X. The

transmitted detector (TD) channel corresponds to the transmitted light channel (first row of panels), and the UV channel corresponds to the red channel (second row of panels). **(A)** *Mco4* (*phm22>Mco4<sup>RNAi-1</sup>* and *phm22>Mco4<sup>RNAi-2</sup>*) knockdown under standard conditions were assessed for porphyria phenotypes. **(B)** *Mco4* (*phm22>Mco4<sup>RNAi-1</sup>* and *phm22>Mco4<sup>RNAi-2</sup>*) knockdown under iron-depleted conditions were assessed for porphyria-like phenotypes.

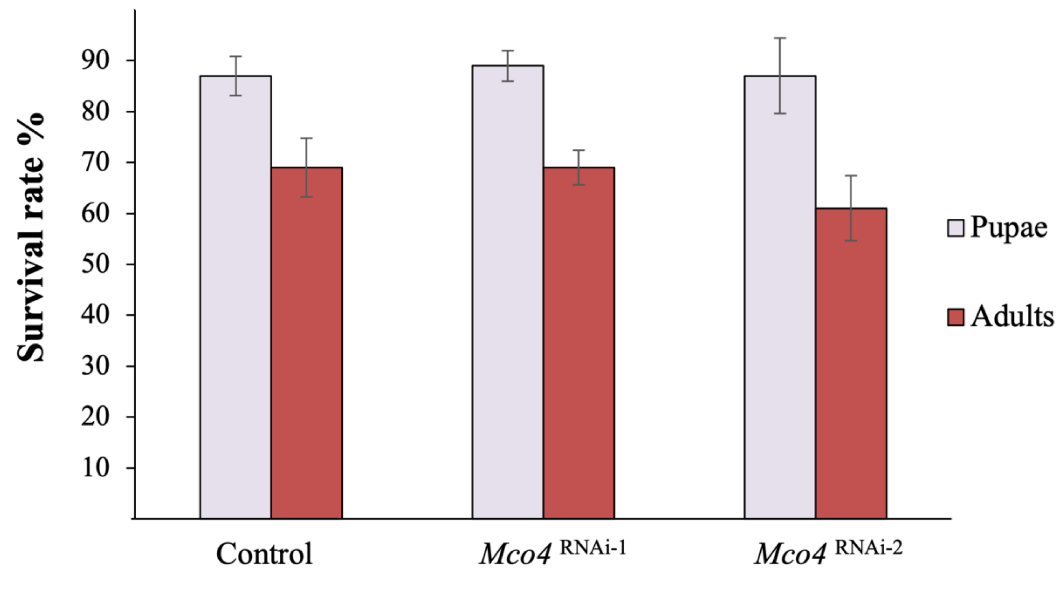
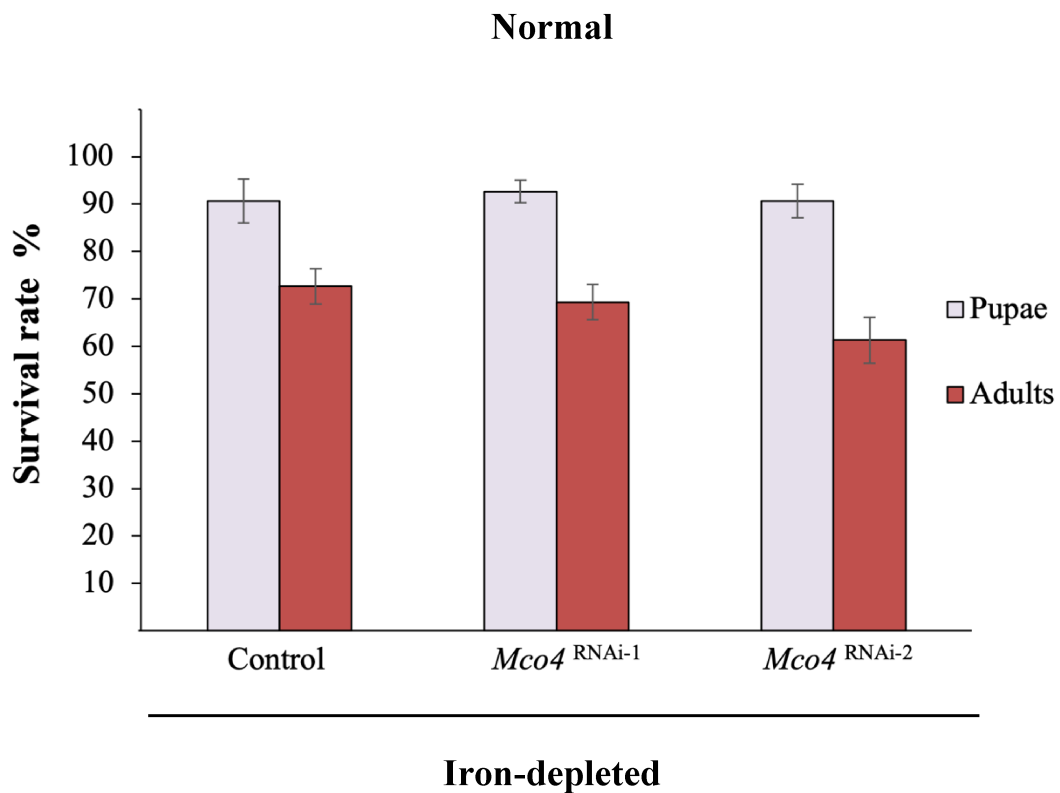
#### 4.23 Analysing the effects of ubiquitously knocking down *Mco4* function

In *Drosophila*, iron absorption occurs in the intestinal epithelial cells. However, the storage and transport of iron across cells are not fully understood. Many unanswered questions are relevant to understanding iron trafficking in *Drosophila*. For example, how is iron imported into the gut? Is it required for iron to be reduced to  $\text{Fe}^{2+}$  similarly to its mammalian counterpart, or is it necessary for iron to be oxidized to  $\text{Fe}^{3+}$  like in yeast by a ferroxidase enzyme? Based on Flybase.org [111], *Mco4* is moderately expressed in the midgut region of adult and third instar larvae. Therefore, I wanted to knockdown *Mco4* in the gut to observe whether *Mco4* plays a significant role in *Drosophila* iron absorption. *Mco4* is predicted to function as a ferroxidase, and as such, a *Mco4* knockdown should cause a reduction in iron oxidation. Consequently, I would expect that this impairs iron transport across the membrane (by affecting the function of a hitherto uncharacterized channel). The loss-of-*Mco4*-function in the gut should cause iron depletion phenotypes. To study whether *Mco4* knockdown triggers a heme deficiency phenotype in the gut, I used a ubiquitous driver, *tubulin-Gal4* crossed with two *UAS-Mco4* RNAi lines, *tubulin>Mco4<sup>RNAi-1</sup>* and *tubulin>Mco4<sup>RNAi-2</sup>*. I conducted both a survival rate analysis and analysis of the midgut under normal and low iron conditions (100  $\mu\text{M}$  BPS). As controls, I used *w<sup>1118</sup>* flies (*tubulin>w<sup>1118</sup>*) as a negative control and *PPOX* mutants as a positive control only in the confocal analysis of the midgut.

## Results

On both standard and low iron diets, a ubiquitous knockdown of *Mco4* neither produced developmental arrest nor decreased survival rates compared to controls (Figure 17A & 17B). *PPOX* mutants result in heme precursor accumulation in the gut and can be observed under a

brightfield setting (Figure 7B) and a confocal setting (Figure 18). Knockdown of *Mco4* using RNAi did not result in red autofluorescence in the gut under normal (Figure 18A) and low dietary iron supplementation (Figure 18B) for both RNAi lines, compared to the positive control *PPOX* mutants. Taken together, the observed data suggests *Mco4* function might not be associated with iron absorption in the gut since no iron deficiency phenotype was detected. However, more experiments are needed to address whether *Mco4* is involved in iron absorption in the gut. In support of the observed results, a future experiment could be carried out to validate both RNAi lines at the transcriptional and translational level to show they are indeed effective in silencing *Mco4* expression.

**A****B**

**Figure 17. The effect of a ubiquitous knockdown of *Mco4* on survival.** Fifty eggs for one replicate were collected and reared on Nutri-Fly food and iron-depleted media. The number of pupae and adult flies were counted to estimate survival rates. **(A)** *Mco4* (*tubulin*>*Mco4*<sup>RNAi-1</sup> and *tubulin*>*Mco4*<sup>RNAi-2</sup>)

knockdown under normal conditions does not affect the survival rate. **(B)** *Mco4* (*tubulin>Mco4<sup>RNAi-1</sup>* and *tubulin>Mco4<sup>RNAi-2</sup>*) knockdown under iron-depleted conditions also does not influence the survival rate. Error bars represent 95% confidence interval, and n= 3 replicates per sample.

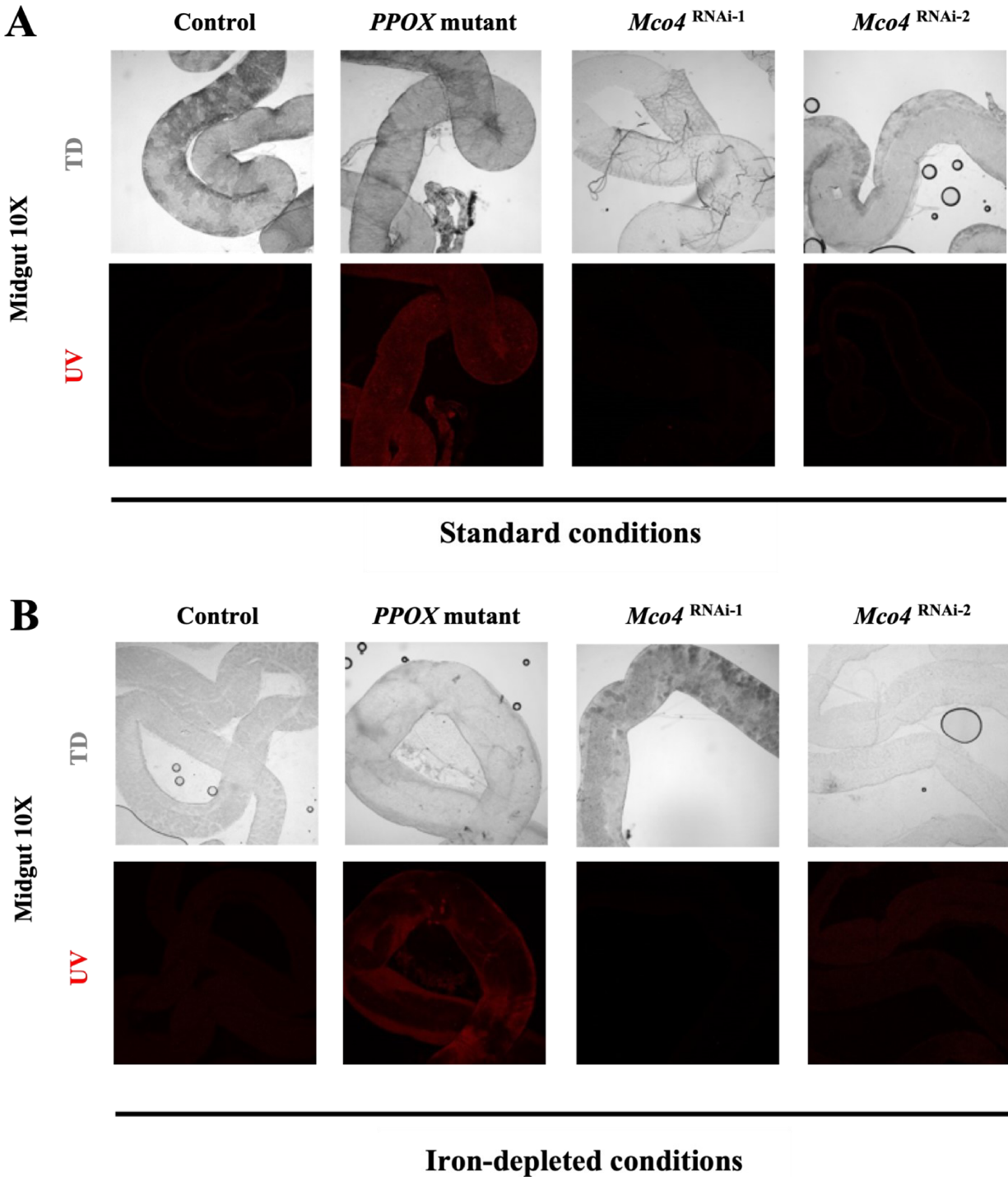


**Figure 18. Dissected midgut regions isolated from ubiquitous *Mco4* knockdown larvae reared on normal and iron-depleted conditions.** Third instar larvae guts were dissected, and the midgut region was assessed for red autofluorescence. Confocal microscopy was used to capture fluorescent images. The magnification used is 10X. The transmitted detector (TD) channel corresponds to the transmitted light channel (first row of panels), and the UV channel corresponds to the red channel (second row of panels). **(A)** Ubiquitous *Mco4* (*tubulin>Mco4<sup>RNAi-1</sup>* and *tubulin>Mco4<sup>RNAi-2</sup>*) knockdown under normal conditions does not result in a red autofluorescence. **(B)** Ubiquitous *Mco4* (*tubulin>Mco4<sup>RNAi-1</sup>* and *tubulin>Mco4<sup>RNAi-2</sup>*) knockdown under iron-depleted conditions also does not result in a red autofluorescence.

#### 4.24 Intestinal iron staining of *tubulin>Mco4<sup>RNAi-1</sup>* gut using Perl's Prussian Blue stain

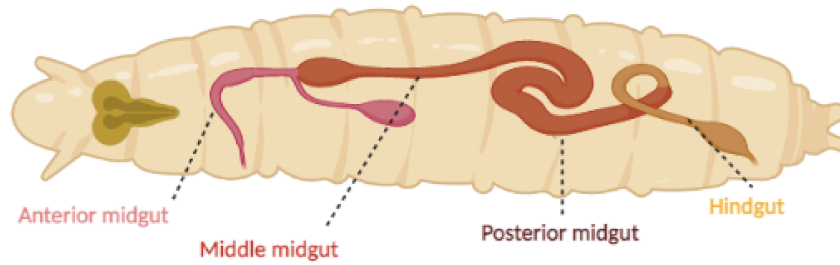
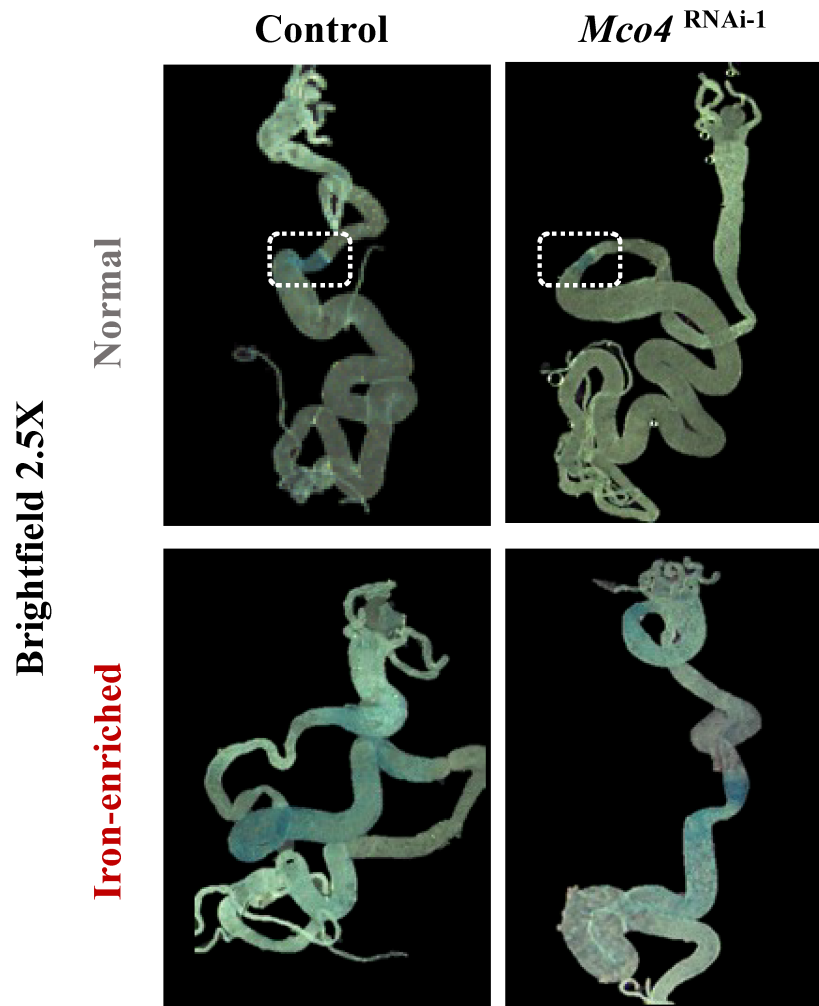
Although knockdown of *Mco4* (*tubulin>Mco4<sup>RNAi-1</sup>* and *tubulin>Mco4<sup>RNAi-2</sup>*) did not result in the characteristic red autofluorescence phenotype in the gut, one can still observe whether the iron import is impaired by visualizing ferritin. Ferritin is the primary iron-storage protein present in the intestinal cells, enterocytes. When cellular iron levels are high, ferritin stores ferric iron ( $\text{Fe}^{3+}$ ), preventing iron's release into circulation [112]. Iron is primarily stored in the midgut region of the gut. In *Drosophila*, the midgut is divided into the anterior midgut, middle midgut, and posterior midgut region (Figure 19A). An earlier study showed that when enterocytes experience a dietary iron overload, an accumulation of iron occurs in the anterior midgut region of the gut and moves through the gut to the posterior midgut [112]. I used Perl's Prussian Blue to stain the whole gut. In the presence of iron accumulation, the gut stains dark blue forming the pigment Prussian blue [113]. The larvae I used were reared on a regular and an iron-loaded diet (1 mM FAC). The flies were crossed with a ubiquitous driver, *tubulin-Gal4* and dissected at the L3 stage. *w<sup>1118</sup>* flies, *tubulin>w<sup>1118</sup>*, were used as a negative control and *Mco4<sup>RNAi-1</sup>*, *tubulin>Mco4<sup>RNAi-1</sup>* was used for the knockdown of *Mco4*.

## Results

When comparing iron absorption of third instar larvae from *tubulin>Mco4<sup>RNAi-1</sup>* and *tubulin>w<sup>1118</sup>*, I detected no visual difference in iron staining when reared on both a regular and an iron-loaded diet (Figure 19B). I observed iron accumulation in the anterior midgut of larvae that were reared on a normal diet and that of larvae were reared on an iron-loaded diet. Larvae reared on an iron-loaded diet showed a dark Prussian blue pigment in the middle of the midgut region and a lighter Prussian blue pigment in the anterior region of the gut, similar to the distribution I observed for the control *w<sup>1118</sup>*. Overall, iron accumulation observed with *Mco4*-RNAi knockdown displayed the same stain intensity in the gut as in the *w<sup>1118</sup>* control. This result is consistent with the previous results observed with *tubulin>Mco4*-RNAi knockdown, which showed no red autofluorescence in the gut under iron-chelated or normal conditions (Figure 18A & 18B). Therefore, knocking down *Mco4* does not appear to impact iron (ferritin) absorption in the gut. Thus, it seems that *Mco4* may not be involved in iron gut absorption. However, the issue could also lie with the RNAi lines used for these past experiments not working as expected or not mediating sufficient knockdown to observe any phenotypes. In support of this, I tested the efficiency of both RNAi lines (*tubulin>Mco4<sup>RNAi-1</sup>* and *tubulin>Mco4<sup>RNAi-2</sup>*) using RT-qPCR in the following paragraph.

**A**

Third Instar Larva

**B**

**Figure 19. Prussian blue larval gut staining of *tubulin>Mco4*<sup>RNAi-1</sup> larvae. (A)** Schematic representation of the different larval gut sections; Midgut (anterior, middle, posterior) and hindgut. **(B)** Larvae were reared on both a standard and iron-supplemented diet. Third instar larvae were dissected and stained with Perl's Prussian blue stain. *Mco4* (*tubulin>Mco4*<sup>RNAi-1</sup>) knockdown displays the same stain

intensity in the anterior and midgut region compared to the  $w^{1118}$  control. The images were acquired using an epifluorescence camera (LEICA DFC500 Camera) under brightfield, and the magnification used was 2.5X.

#### 4.25 Validating RNAi lines using RT-qPCR

$phm22>Mco4^{RNAi-1}$ ,  $phm22>Mco4^{RNAi-2}$ ,  $tubulin>Mco4^{RNAi-1}$ , and  $tubulin>Mco4^{RNAi-2}$  did not display any developmental delays, no decrease in the survival rates, nor any porphyria-like phenotypes. These data can be interpreted as one of three possible scenarios, the first being that *Mco4*-loss-of-function has no obvious phenotype with respect to development and iron metabolism. The second, *Mco4* is not involved in *Drosophila* iron import, and the third scenario is that the two *Mco4*-RNAi lines I have used do not work. To examine the third scenario and test whether the RNAi lines were functional, I performed RT-qPCR experiments to analyze *Mco4* levels in these lines. A ubiquitous driver, *tubulin*, was used to cross with  $w^{1118}$  flies ( $tubulin>w^{1118}$ ) and the two *Mco4* RNAi lines,  $tubulin>Mco4^{RNAi-1}$  and  $tubulin>Mco4^{RNAi-2}$ . A total of six L3 larvae reared on Nutri-Fly food were collected for one of three replicates. Samples were normalized to *rp49* gene expression levels.

## Results

The quantitative RT-qPCR showed that *Mco4* mRNA levels were significantly reduced in whole-body samples representing the  $tubulin>Mco4^{RNAi-1}$  and  $tubulin>Mco4^{RNAi-2}$  lines.  $Mco4^{RNAi-1}$  displayed a significant 3.5-fold reduction, and  $Mco4^{RNAi-2}$  showed a 2.5-fold downregulation compared to the control ( $t$ -test,  $p$ -value<0.01) (Figure 20), indicating that both RNAi lines are functional. That being said, although the RNAi-mediated knockdown of *Mco4* did reduce *Mco4* gene expression, it is possible that the observed reduction in *Mco4* transcript levels may not be sufficient enough to elicit an observable phenotype. Consequently, to address this issue, I generated a presumptive *Mco4* null mutant line using CRISPR/Cas9 to examine whether *Mco4* function is required for iron absorption in the PG and gut tissues of *Drosophila*, which I will cover in detail in chapter 6 of this thesis.

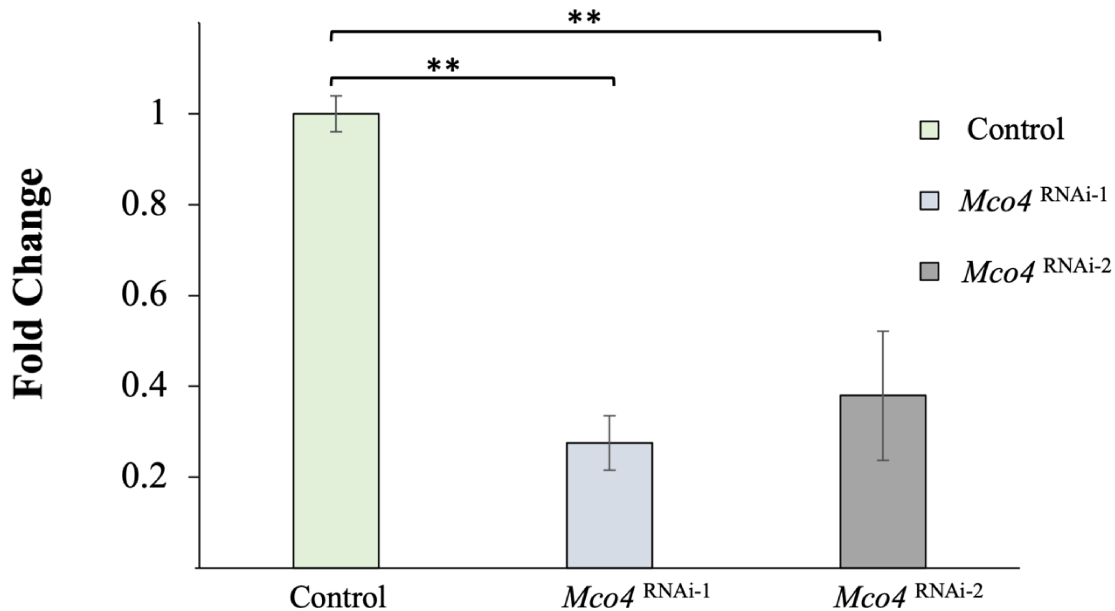


**Figure 20. RT-qPCR validation of *Mco4* RNAi lines.** Six L3 larvae reared on Nutri-Fly food were collected for RT-qPCR analysis. *Mco4* RNAi lines result in significant *Mco4* knockdown (*tubulin*>*Mco4*<sup>RNAi-1</sup> and *tubulin*>*Mco4*<sup>RNAi-2</sup>). *Mco4* expression levels were calculated relative to *w*<sup>1118</sup> using the  $\Delta\Delta C_t$  method. *rp49* was used as a reference gene for normalization. Error bars represent 95% confidence intervals, \*\*p-value < 0.01 and n= 3 replicates per sample.

## DISCUSSION

In terms of the correlation between the differential *Mco4* expression levels observed in the RT-qPCR and the RNA-Seq results, both showed upregulated *Mco4* expression levels under iron-depleted conditions. However, the RT-qPCR results showed a lower expression difference compared to the RNA-Seq data. The *Mco4* expression levels using RNA-Seq showed an increase of 114-fold & 164-fold for PG-specific *AGBE*<sup>RNAi</sup> and *phm22*>*IRP1A*<sup>C450S</sup> versus 9-fold and 8-fold respectively in the RT-qPCR. The factors that could alter the RT-qPCR outcome and affect the results are the RNA extraction technique I used, the 260/230 ratio of the RNA sample and the qPCR primer design I used to amplify the newly *Mco4* synthesized cDNA strands (Troy Locke, personal communication). To address these parameters, the reagent I used to extract RNA from

the sample was TRIzol, followed by a QIAGEN RNeasy kit for RNA purification. The TRIzol reagent is traditionally used for its simplicity in RNA extraction. However, it does have its drawbacks since phenol contamination can be an issue, greatly affecting the 260/230 ratio. This could have resulted in relatively low-quality RNA samples. Another aspect of RT-qPCR is that reference genes are used to normalize and calculate our experimental sample's expression levels. Most significantly, although both methods are used to measure gene expression levels, RT-qPCR measures Ct values with relative quantification to the used housekeeping gene and RNA-Seq is expressed as Reads Per Kilobase of transcript per Million reads mapped (RPKM) and represents absolute quantification.

Regarding publications, RNA-Seq data in relation to RT-qPCR shows a strong correlation <sup>[114]</sup>. However, inconsistencies with fold changes can be observed between the two data sets, especially in lowly expressed genes <sup>[114]</sup>. RNA-Seq is pointed to accurately measure lowly expressed genes, with high reproducibility, and has a greater dynamic range <sup>[114-115]</sup>. That being said, both RT-qPCR and RNA-Seq data show upregulated *Mco4* levels, hinting at *Mco4*'s possible function in the PG response to low iron conditions.

The collective data on *Mco4* knockdown in this chapter indicate that the survival rate of these knockdown animals on an iron-depleted diet and a standard diet is normal (Figure 15 & 17). The knockdown also did not result in iron-depletion or porphyria phenotypes (Figure 16 & 18). Additionally, I did not observe lower iron absorption than the control with the *Mco4* RNAi knockdown using Prussian blue staining (Figure 19). Combined, the results remain consistent with *Mco4* knockdown displaying no iron depletion phenotypes. In principle, if *Mco4* functioned as a high affinity iron importer by catalyzing the oxidation of iron and facilitating iron transport across the membrane, then upon *Mco4* knockdown under iron-depleted conditions, larvae should experience inadequate iron availability in tissues with high iron usage, such as the PG. This would hinder critical pathways that require iron, such as the heme pathway and consequently the ecdysone pathway responsible for appropriate growth and development. Therefore, I decided to generate constructs that can help build on this study and uncover *Mco4* gene function. For this purpose, I generated two *ex vivo* and two transgenic lines; to help understand the *Mco4* function

(Table 2.4). To this end, I will describe these transgenic lines and their uses in further detail in this thesis's fifth and sixth chapters.

## CHAPTER 5

### *Determining the subcellular localization of Mco4 in the cell*

In the case of Mco4, the prior investigation into its localization has not been studied. To study Mco4's proposed role in facilitating iron uptake/transport, it is essential to determine its subcellular localization within the cell [116]. Knowledge of a protein's localization can aid in identifying protein interactions and shed light on its function [117]. This chapter focuses on determining the subcellular localization of Mco4 using an *ex vivo* construct and a transgenic line. A first step towards identifying a protein's localization is using protein prediction tools. These algorithms analyze the protein sequence and predict the protein's structure and location. PSIPRED is simple software used to predict the transmembrane domain and orientation of a protein [86]. By running Mco4's protein sequence through PSIPRED, the software predicted a single putative transmembrane domain. Notably, a signal putative peptide was also detected on the N-terminal sequence. I then analyzed the signal peptide in further detail using the bioinformatics software SignalP5.0 [118]. The analysis predicted a likely signal sequence, with a Sec/SPI score of 0.9253 out of 1.0 and a cleavage site predicted to be positioned between the 22<sup>nd</sup> and 23<sup>rd</sup> amino acid (Figure 21A & 21B). Signal peptides are around 16-30 amino acids in length, present in newly synthesized secretory and membrane proteins [87]. Signal peptides on the N-terminal sequence guide membrane proteins to the endoplasmic reticulum, where it undergoes post-translational protein modifications before being incorporated into the cell plasma membrane [98]. The signal peptide is cleaved by a signal peptidase at the designated cleavage site [98].

Like its yeast ortholog, *Fet3*, *Mco4* is predicted to encode a signal peptide and a single transmembrane domain (Figure 22). Taken together, these findings point towards Mco4 predictably functioning as a transmembrane protein. To test this hypothesis, the most widely used method to determine protein localization is using a technique referred to as epitope tagging. The protein of interest is fused to an epitope tag recognizable by a specific antibody [119]. The epitope tag characterizes a protein's subcellular localization by tracking its course throughout the cell [120]. The procedure involves using indirect immunofluorescence to bind the protein (fused to

an epitope tag) to a primary and secondary antibody. The secondary antibody is labelled with a fluorescent dye, and the subcellular localization of the protein is imaged using a confocal microscope. The approach I took to study the subcellular localization involves creating tagged *Mco4* cDNA constructs to either transfect into S2 cells or generate a transgenic line through microinjection into embryos. It is essential when attempting to design the construct to consider the location of the epitope. When choosing between a C-terminal or an N-terminal tag, it is necessary to choose a C-terminal tag if the protein of interest contains a predicted signal peptide at the N-terminus, which are usually cleaved off <sup>[121]</sup>. The reason is that if the epitope is attached at the N-terminus, then upon cleavage/processing of the protein sequence would result in the removal of the epitope from the protein of interest. For this reason, all the tagged *Mco4* constructs I generated contain a C-terminal Myc-tag. Furthermore, I chose the route of conditionally overexpressing the cDNA of interest rather than tagging the endogenous gene in hopes of avoiding disrupting its expression or destabilizing the protein, which could affect its localization <sup>[122]</sup>. Arguably, producing additional protein from a transgene can, in some cases, affect the growth of the cell by overburdening its resources <sup>[123-124]</sup>. In other scenarios, overexpression of proteins can surpass the critical threshold of a protein and result in a mutant phenotype <sup>[123-124]</sup>.



```

Mco4      MKFNLVQTLVFTLCLISVQIYGIQDASGKRIVSKYERIMQY PQLSSGAGESSQWRAAEKD
Fet3p     -----MTNALLSIAVL-----LFSML-SLAQAETHTFNWTGWDY

Mco4      NQRHPCRRDCADKQPMTCYYM VVHYDDTMAETCKRYLQSKFRFKLSGKEYIDGIALATQL
Fet3p     RN-----

Mco4      AANDDCKYADGL-ESEVMV VNGQLPGMNIEVCYGD TVVADVINSMHET-TTIIHWGHMQRL
Fet3p     -----VDGLKSRPVITCNGQFPWPDITV NKGDRVQIYLTNGMNNNTNTSMHFHGLFQNG

Mco4      TPFMDGVPHVTQYPIEAGQAFRYRFEVDH-GGTNWWHSHEHQRAFGLAGPLVVRMPPKLN
Fet3p     TASMDGVPF LTQCP IAPGSTMLYNFTVDY NVGTYWYHSHTDGGQYEDGMKGLFIIKDDSF--

Mco4      PHAHL YDFDMSEHVIMI QDWVHNFV-----ESVAENILINGRGRNLKKGV
Fet3p     PY--DYD---EELSLSLSEWYHDLVTDLT KSFMSVYNPTGAEP I PQNLIVNNTMNLT----

Mco4      KAAKPTLYAHFPVVRGGRYRFRVI FNGVSNCPISFSIDKHDLVVIASDGN DIEPVEVQRIM
Fet3p     -----WEVQPDTTYLLRIV-NVGGFVSQYFWIEDHEMTVVEIDGITTEKNVTDMLY

Mco4      FHGAERFDFVLHANQE-VSNY WIRVKG----YSFCAKNQLHQE-AVLHYRDADTRALDHT
Fet3p     ITVAQRYTVLVHTKNDTDKNFAIMQKFDDTMLDVIPSDLQLNATSYMVYNKTAALPTQNYV

Mco4      LSYAYDAPGKTLNELGDDASGARAGNSISLANLNAQRPEPEVAPSVTFYTSMNAFEVRQGE
Fet3p     DS-----IDNFLDD-----FYLQPYEKEAIYGEPDHVITVDVVM D--NLKNGV

Mco4      GFRFQMDDISFSMPKMSLLQTRNLGVGQFFCNRSQQADLGFNCRQRHCQCSNVIQVPANQQ
Fet3p     NYAF-FNNITYTAPKVPTLMTV-LSSGD---QANNSEIYGSN-----THTFILEKDEI

Mco4      VEFVISSLSQTPHPIHLHG YTFRVVGMGVLGEQKIGQIEQIDKKTPLPRRAKGAPLKDSVQ
Fet3p     VEIVLNNQDTGTHPFHLHG HAFQTIQRDRTYDDALGEVPHSFDPDNHPAFPEYPMRRDTLY

Mco4      VPAFGY TILRFYSNSPGYWMFHCHISPHSENGMAAVV-----
Fet3p     VRPQSNFVIRFKADNPGVWFFHCHIEWLLQGLGLV LVEDPFGIQDAHSQQLSENHLEVCQ

Mco4      -----RVGEDVEMKMCVSN-----CGLCSSVA-----
Fet3p     SCSVATEGNAAANTLDLTDLTGENVQHAFIPTGFTKKGI IAMTFSCFAGILGIITIAIYGM

Mco4      -----
Fet3p     -----
MDMEDATEKVIRDLHVDPEVLLNEVDENEERQV NEDRHSTEKHQFLTKAKRFF

;
END;

```

**Figure 22. Sequence alignment of Mco4 and Fet3p.** Alignment of *Drosophila* Mco4 (Mco4, the top) and yeast Fet3p (Fet3p, the bottom) protein sequences. Amino acid sequence for Mco4 was obtained from Flybase.org and Fet3p from UniProt. They were aligned by Clustal Omega software. Pink boxes indicate potential signal peptide, and yellow indicates potential transmembrane domain.

## 5.1 Determining Mco4 localization ex vivo using S2 cells

When first examining the subcellular localization of Mco4, I utilized *Drosophila* Schneider 2 cells as a model system, commonly referred to as S2 cells. S2 cells are a great model when conducting localization studies for their simplicity and ability to readily take up DNA upon transfection [122]. To assess the subcellular localization of Mco4 in S2 cells, I generated two constructs based on the vector backbone of Ac5-EGFP-C-4Myc plasmid, which contains the *Drosophila* Actin5c promoter. To detect proteins, the first generated construct contained the complete *Mco4* cDNA sequence in frame with a sequence encoding four tandem Myc epitope tags to produce a tag at the C-terminus (Ac5-*Mco4*-C-4Myc). This construct was used to analyze Mco4 localization in S2 cells. In the second construct, the putative N-terminal signal peptide was deleted from the cDNA sequence, and the remaining *Mco4* sequence was tagged with four Myc-tags fused to the C-terminus (Ac5-*Mco4*- $\Delta$ SP-C-4Myc). The second construct was used to analyze the functional importance of the predicted signal peptide. Both constructs used are shown in Figure 23. The signal peptide is required for the secretion of proteins and the incorporation of proteins into the plasma membrane (Figure 9). Theoretically, deleting the signal peptide should impact the localization of the protein, resulting in the protein remaining in the cytosol [125]. In summary, I would expect to observe that Myc-tagged Mco4 localizes to the plasma membrane, and removing the signal peptide would result in cytosolic distribution. Additionally, the Ac5-EGFP-C-4Myc plasmid was used as a positive control, which expresses GFP in the whole cell.

### Results

Based on the results demonstrated in Figure 24, S2 cells transiently transfected with the Ac5-*Mco4*-C-4Myc construct showed Mco4 localization to the plasma membrane of the cells. However, cells transfected with the Ac5-*Mco4*- $\Delta$ SP-C-4Myc construct detected Mco4 localization almost exclusively in the cytosol, similar to that of the positive control Ac5-EGFP-C-4Myc. This indicates that the deletion of the signal peptide affected the translocation of Mco4 into the plasma membrane. Demonstrating the need for an existing signal peptide in Mco4 for its successful incorporation into the plasma membrane.

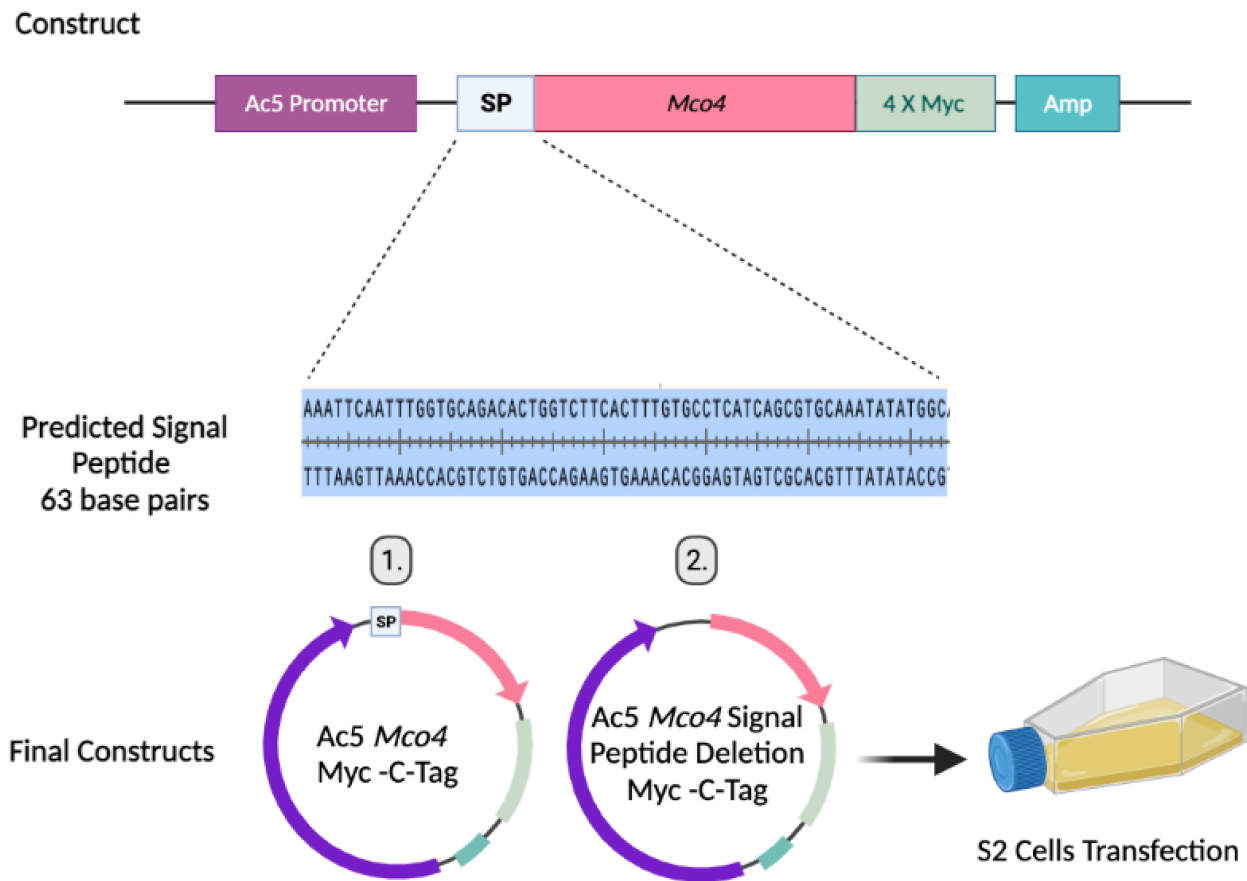


**Figure 23. Plasmid constructs generated to study Mco4 subcellular localization *ex vivo*.**

Schematic representation of the S2 cells constructs used in this study. The final Ac5-*Mco4*-C-4Myc and Ac5-*Mco4*- $\Delta$ SP-C-4Myc constructs include a *Drosophila* Actin5c promoter indicated as a purple box, *Mco4* cDNA (including or excluding the signal peptide) indicated as a pink box, four tandem Myc epitope tags indicated as a light green box and an ampicillin resistance gene indicated as a dark turquoise box. The highlighted box in blue indicates the predicted N-terminal signal peptide base-pair length. The number above the generated constructs refers order in which they were described in **(1)** Myc-tagged *Mco4* expression vector (Ac5-*Mco4*-C-4Myc) **(2)** Signal peptide *Mco4* deletion expression vector (Ac5-*Mco4*- $\Delta$ SP-C-4Myc). Both constructs were transiently transfected into S2 cells, and the results were imaged using a confocal microscope.

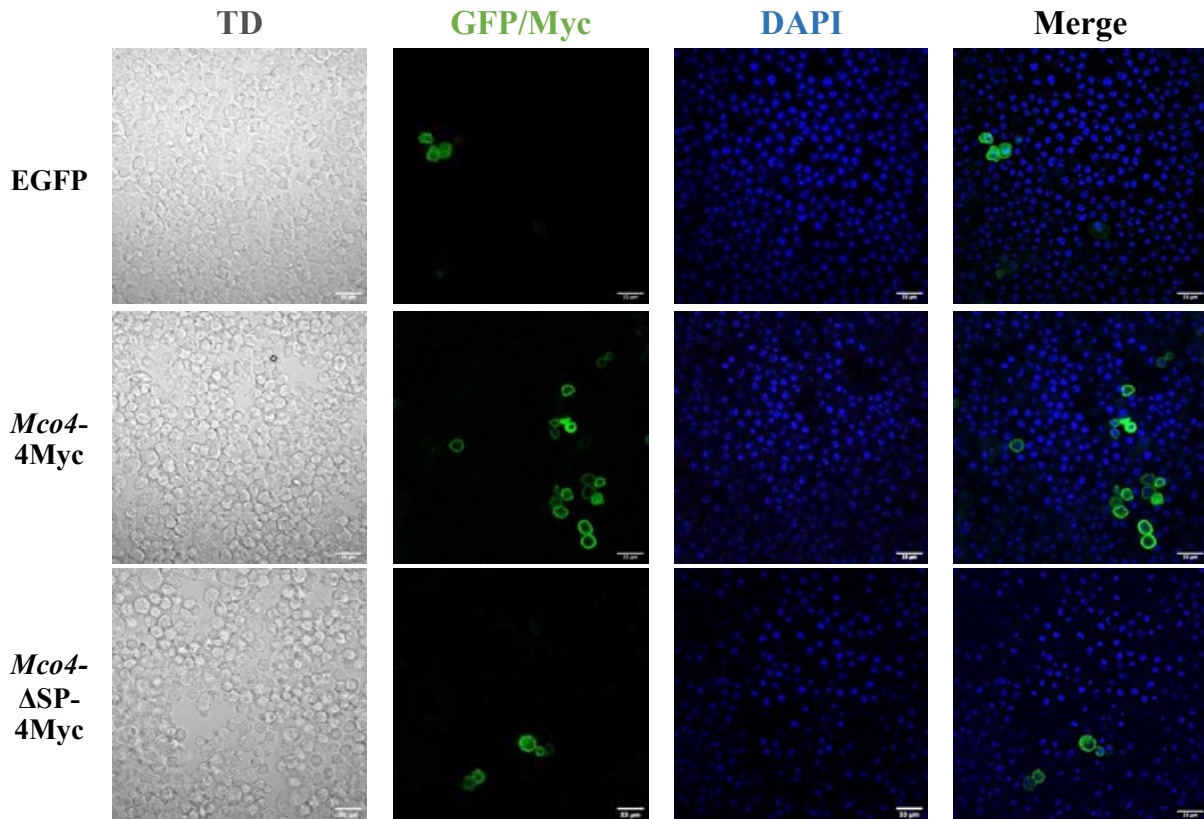


**Figure 24. Subcellular localization of Mco4 in S2 cells.** S2 cells were transiently transfected with the constructs Ac5-EGFP-C-4Myc, *Mco4*-4Myc and *Mco4* signal peptide deletion-4Myc expression vector. Cells are stained with anti-Myc antibody and DAPI. Confocal microscopy was used to capture the fluorescent images. The transmitted detector (TD) channel corresponds to the transmitted light channel (first panel), GFP/Myc signals the subcellular localization of the constructs (the green channel, second panel) and DAPI autofluorescence is used as a nuclear stain to visualize DNA (the blue channel, third panel). The second and third channels were computer-overlaid to show the last panel. The magnification used is 60X, and the scale bar represents 33  $\mu$ m.

## 5.2 Determine *Mco4* localization using a transgenic line.

Because the experiments with S2 cells only addressed *Mco4* localization *ex vivo*, it is important to validate the results using a transgenic line to attempt to replicate the physiological

conditions found in a living organism [126]. I generated a *UAS-Mco4* line (*UAS-Mco4-3Myc*). The Gateway destination vector pBID-UASC-GRM (#35203) was constructed to include an *attB* site and the *Mco4* cDNA sequence upstream of three Myc C-terminal epitope tags, expressed under the control of a *Drosophila* Synthetic Core Promoter (DSCP) [101]. Additionally, ten Upstream Activation Sequences (UAS) for Gal4 were included in the pBID vectors backbone to compensate for the promoter's low activity [101]. This addition of UAS sequences allows for spatiotemporal control over the expression of a given transgene [101]. The transgene-containing vector is injected into the germline of *Drosophila* embryos and is integrated into the *Drosophila* genome via the phiC31 integrase system ( $\Phi$ C31) at the *attP40* heterozygous landing site on the second chromosome. The phage attachment site (*attP*) functions as a docking site for plasmids containing a bacterial attachment site (*attB*) [127]. This technology provides a site-directed insertion into the genome and allows for more reproducible results since position effects are avoided, a common issue with traditional P-elements [101]. The resulting transgenic flies are then outcrossed to be made homozygous for the insertion. The workflow for generating this transgenic line is schematically shown in **Figure 25**. In terms of protein localization, it is essential to study the subcellular pattern in different tissues. Identifying the localization of a protein in a specific tissue provides a better understanding of its possible function [128]. To examine the subcellular distribution of Mco4 in various tissues, I crossed the *UAS-Mco4-3Myc* line to *tubulin-Gal4*. I studied the localization of Mco4 in different *Drosophila* tissues in third instar larvae reared on Nutri-Fly food, for which I used immunofluorescence detection. I used three types of tissues for this analysis: the midgut, salivary glands (SG), and the PG. Principally, iron is primarily stored in the midgut region of the gut, PG requires intensive iron amounts during larval development, and the SG is presumed to play a role in iron efflux via endosomal vacuoles [129].

## Results

Confocal analysis of the transgenically derived Myc-tagged Mco4 protein clearly showed localization in the outer plasma membrane of the larval midgut enterocytes. From the SG and PG results, I can conclude that Mco4 localization is not nuclear (**Figure 26**). Overall, at least in the case of the midgut cells, the obtained results using the *tubulin >UAS-Mco4-3Myc* cross are consistent with the observed plasma membrane localization of Mco4 in S2 cells transiently

transfected with the *Ac5-Mco4-C-4Myc* construct. The observed plasma membrane localization of Mco4 strengthens the hypothesis that Mco4 might function similarly to its yeast ortholog, Fet3p. Like Fet3p, Mco4 both contained a predicted transmembrane domain, signal peptide and localization in the plasma membrane (Figure 21-22).

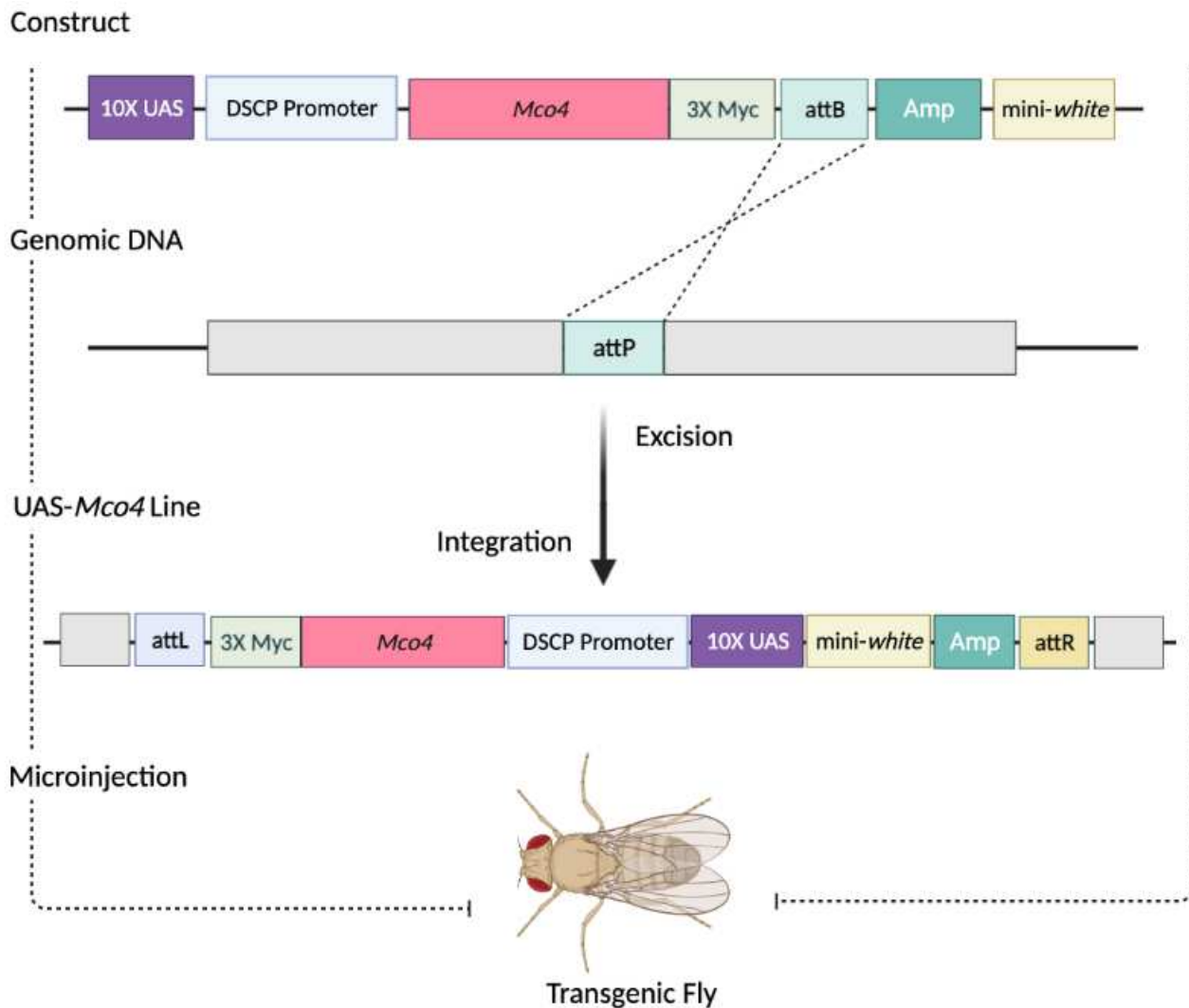


**Figure 25. Transgenic line generated to study Mco4 subcellular localization.** Schematic representation of the *UAS-Mco4* construct used to generate transgenic animals employing the  $\Phi$ C31 transgenesis method [101]. The final pBID-UASC-GRM-*Mco4* construct includes ten binding Upstream Activation sites (UAS) indicated as a purple box. A *Drosophila* Synthetic Core Promoter (DSCP) is indicated as a light blue box. A *Mco4* cDNA is indicated as a pink box. Three Myc-tags indicated as a light green box.

A  $\Phi$ C31 integrase *attB* sequence indicated as a light turquoise box. An ampicillin resistance gene indicated as a dark turquoise box and a mini-*white* gene indicated as a pale-yellow box. The construct is introduced into *Drosophila* embryos through microinjection. Integration into the genome occurs at the *attP* docking site by the enzyme phic31 integrase [101]. The resulting progeny are scored for positive transformants carrying the mini-*white* marker, identified by their orange eye colour phenotype when present in a *white* mutant background.

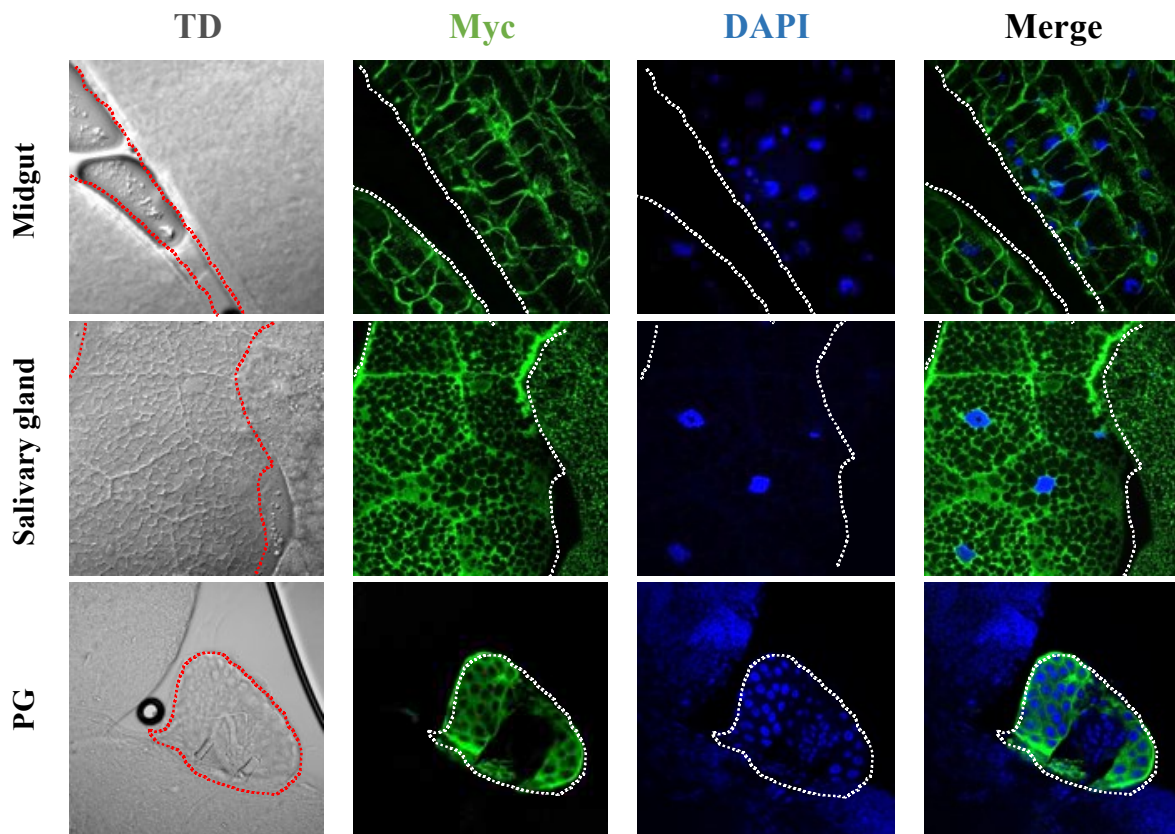


**Figure 26. Subcellular localization of Mco4 in three different tissues.** *Drosophila* embryos were injected with the pBID-UASC-GRM-*Mco4* expression vector, and the balanced offspring were crossed with a tubulin driver (*tubulin >UAS-Mco4-3Myc*). The following tissues were examined in the midgut, SG, and PG. Tissues dissected from third instar larvae were stained with anti-Myc antibody and DAPI. Confocal microscopy was used to capture the fluorescent images. The transmitted detector (TD) channel corresponds to the transmitted light channel (first panel). Myc signals the subcellular localization of the construct (the green channel, second panel) and to distinguish between the nucleus and the cytoplasm;

the tissues were stained with DAPI (the blue channel, third panel) to visualize DNA. The second and third channels were computer-overlaid to show the last panel. The magnification used is 60X.

## DISCUSSION

Determining *Drosophila melanogaster* multicopper oxidase 4 significance in iron transport requires understanding its distribution in different cells [130]. Utilizing bioinformatic tools, PSIPRED and SignalP 5.0. aided in gaining insight into Mco4's potential localization inside cells [86,118]. Analysis of the dataset retrieved from these prediction tools revealed that Mco4 is similar to its yeast counterpart in the number of domains, signal peptide presence and localization. The existence of a cleavable signal peptide is essential for Mco4 to function as a predicted membrane protein. This was highlighted in the results obtained following the signal peptide deletion in S2 cells, demonstrating the functionality of the predicted signal peptide. A protein bound for the secretory pathway is first processed in the RER before being transported to the plasma membrane [131]. Membrane-bound proteins are incorporated into the membrane, and secretory proteins are secreted outside the cell [131]. Experimentally, S2 cells transiently transfected with the Ac5-*Mco4*- $\Delta$ SP-C-4Myc construct with an absent putative signal peptide observed the confinement of Mco4 within the cytosol and its prevention from reaching the membrane. Accordingly, deletion of the signal peptide significantly compromised the ability of Mco4 to localize to the plasma membrane. When expressed in *ex vivo* (Ac5-*Mco4*-C-4Myc) and midgut cells (*tubulin* >UAS-*Mco4*-3Myc), Mco4 displayed membrane-bound localization. Comparison of the two model systems suggests Mco4 localization is consistent with its yeast ortholog, Fet3p.

Overexpression is a way to characterize the localization of a protein if the endogenous gene is lowly expressed, like Mco4. However, there are limitations to using overexpression as a genetic tool. Overexpression of a transgene can drain the cell's resources, consequently burdening the cell's protein assembly machinery and transport system [132]. The transport system can be divided into three parts: the modification of signal peptide, transportation and the removal of mis-localized proteins [133]. High-level expression of transported proteins like Mco4 can

potentially induce the ER stress response and lead to the misfolding of the protein and its mis-localization <sup>[133]</sup>. This may be a factor in the observed cytoplasmic localization of Mco4 in SG and PG tissues using the *tubulin>UAS-Mco4-Myc* cross. Additionally, overloading the protein assembly can hamper the synthesis of essential proteins affecting the condition of the cells and becoming toxic to a cell by materializing up to 15% of its total protein content <sup>[132]</sup>.

Finally, a *UAS-Mco4* line can prove to be helpful in future applications. Specifically in identifying protein-protein interactions in *in vivo* experiments using co-Immunoprecipitation (co-IP) approaches. The rationale behind this approach is that *Mco4*, like its ortholog *Fet3*, has only one predicted transmembrane domain and would likely need to interact with another transmembrane protein, likely a permease containing multiple transmembrane domains to facilitate iron transport through the plasma membrane. Yeast multicopper ferroxidase Fet3p is involved in high affinity iron import by working together with the permease protein Ftr1p, which is predicted to harbour seven transmembrane domains <sup>[17]</sup>. Iron is first oxidized from Fe<sup>2+</sup> to Fe<sup>3+</sup> state by Fet3p and is imported into the cell through Ftr1p <sup>[17]</sup>. This is because Fet3p requires Ftr1p, a symporter and because MCOs are not known to act as importers on their own. However, no fly ortholog of Ftr1p has been identified by any of the established ortholog prediction tools <sup>[57]</sup>. If Mco4 supposedly functions similarly to Fet3p, then co-IP experiments that use tagged Mco4 as bait can provide a list of possible candidate proteins that interact with Mco4 *in vivo* and may be involved in iron transport. Moreover, *UAS-Mco4* transgenic line can be used in experiments further to analyze its function through qualitative and quantitative analysis.

## CHAPTER 6

### *Generating an $Mco4^{-/-}$ null mutation via CRISPR/Cas9*

Despite the generated data in this thesis so far,  $Mco4$ 's possible function remains unclear. Given that  $Mco4$  shows similar characteristics to its yeast ortholog, it is not known what impact a lack of  $Mco4$  has on the development of a fly and whether the primary function of  $Mco4$  is related to iron import. In summary, to analyze the physiological function of  $Mco4$ , it is essential to study  $Mco4$  null mutants. However, to the best of my knowledge, no loss-of- $Mco4$ -function animals have been described in the literature so far. To address this problem, I generated a loss of function line using CRISPR/Cas9. CRISPR/Cas9 is a great tool for altering spatial and temporal control of a given gene [134]. This chapter will discuss the generated  $Mco4$  null mutant line ( $Mco4^{-/-}$ ) and its characterization in *Drosophila*. To clarify, when using the term ‘null mutant’, I am referring to the complete ubiquitous deletion of the  $Mco4$  gene in the genome.

The CRISPR/Cas9 system utilizes a gRNA to direct the Cas9 nuclease towards a target gene to induce a double-strand break (DSB) upstream a protospacer adjacent motif (PAM) sequence [71]. This reaction prompts repair pathways resulting in either a non-homologous end joining (NHEJ) or homology-directed repair (HDR) of the cleaved DNA [71], which depends on whether a repair template (i.e., normally a replicated chromosome) is available. NHEJ is regarded as the primary repair pathway; the outcome of this pathway is generally error-prone, generating INDELS in the process [71]. The HDR pathway is commonly activated during meiotic division and naturally occurs only in the presence of a sister chromatid (replicated chromosome) [71,135]. This pathway utilizes the replicated chromosome as a template to repair the damage or DSB within the chromosome, ensuring a successful outcome [71].

The established  $Mco4^{-/-}$  transgenic line was created using a CRISPR/Cas9 HDR-mediated approach. This technique requires a DNA donor construct (pHD-DsRed-attp #51019) and a gRNA vector (pCFD5 #73914) to successfully target and replace the endogenous target gene. The DNA donor construct was designed to contain a DsRed fluorescent selection marker

driven by the 3xP3 promoter. The transformation marker, 3xP3-DsRed, results in transgenic offspring with a spatiotemporal expression pattern of the red fluorescent marker (DsRed) in the eyes, central lobes of the brain (CNS), hindgut and the anal plates of larvae throughout all three larval stages<sup>[136]</sup>. The use of 3xP3-DsRed is a great advantage in selecting successful transformants. Positive transformants were selected based on the presence of red fluorescent eyes, expressing the red fluorescent protein DsRed<sup>[136]</sup>.

The DsRed marker gene was flanked with two homology arm sequences on each side (left and right). Each homology arm was approximately 1000 bp long and identical to the region flanking the target gene (*Mco4* in this case). The gRNA vector was designed to contain two gRNA sequences aimed to cleave the DNA as close as possible to the endogenous start and stop codons of the *Mco4* transcription unit. Taken together, the gRNA's aid the Cas9 nuclease in catalyzing two DSB's at the targeted genome. Following the double-strand DNA cleavage, HDR is promoted in the presence of the DNA donor construct. HDR requires the DNA donor plasmid as a template for the repair and replaces the entire excised gene with a region encoding the DsRed fluorescent selection marker. This process is shown in [Figure 27](#).

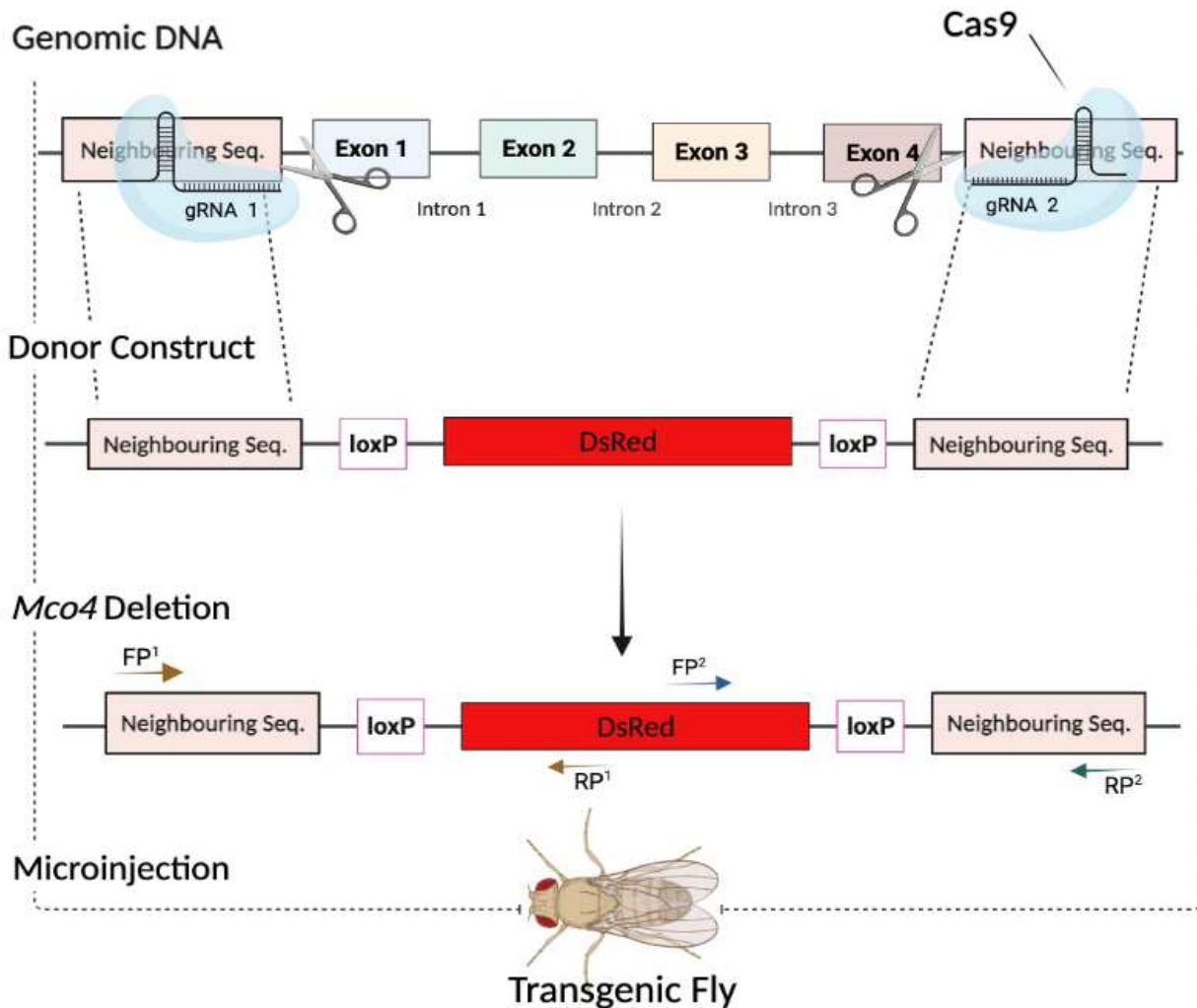


**Figure 27. Schematic overview of CRISPR/Cas9 HDR-mediated *Mco4*<sup>-/-</sup> line.** Schematic representation of the *Mco4*<sup>-/-</sup> transgenic animal created using the CRISPR/Cas9 HDR approach. The donor construct (pHD-DsRed-attP) includes two homology arms (left and right) indicated as a beige box, two loxP sites indicated as a light white box with a pink outline, and a DsRed cDNA sequence indicated as a red box. This construct and a gRNA construct (pCFD5 #73914) not shown in this diagram for simplification purposes are introduced into *Drosophila* embryos together through microinjection. The gRNAs cleave the endogenous target gene three bp from the PAM site, inducing the cell's repair pathway. In the presence of the donor construct, the HDR pathway is activated using the donor DNA as a template for repair. The resulting progeny are scored for positive transformants carrying the fluorescent selection marker DsRed, identified by their red fluorescent eye colour phenotype under a UV light. The DsRed marker can be excised from the genome using a Cre-loxP system since the DsRed cDNA was flanked with loxP sites. FP<sup>1</sup>,

FP<sup>2</sup>, RP<sup>1</sup> and RP<sup>2</sup> represent the primers and genomic amplification region used to validate the null mutant line (Primers listed in [Table 2.3](#)).

### 6.1 Validating *Mco4*<sup>-/-</sup> line through RT-qPCR

I successfully generated a homozygous deletion of the *Mco4* gene (*Mco4*<sup>-/-</sup>), which I first validated using PCR and sequencing to certify *Mco4*'s complete removal from the genome (Primers listed in [Table 2.3](#)). The genomic amplification region is shown in [Figure 27](#). This was followed by validation through sequencing cDNAs derived from *Mco4* mutants via RT-qPCR. Since *Mco4* is moderately expressed in the gut compared to other tissues, I used six samples of whole guts from the *Mco4*<sup>-/-</sup> mutant line and the control *w*<sup>1118</sup> for the RT-qPCR analysis. *rp49* was used as a reference gene for normalization.

## Results

RT-qPCR confirmed the deletion of *Mco4* in the mutant line as no expression was detectable of *Mco4* ([Figure 28](#)). In conclusion, the qPCR analysis confirms the deletion of *Mco4* on an RNA/transcriptional level, also supported by the genomic PCR and sequencing results. Taken together, the constructed line appears to be a complete *Mco4* null mutant line. However, to further ensure *Mco4*'s complete deletion, a corresponding western blot experiment is needed to monitor *Mco4* protein levels to confirm the validity of the results as mentioned above.

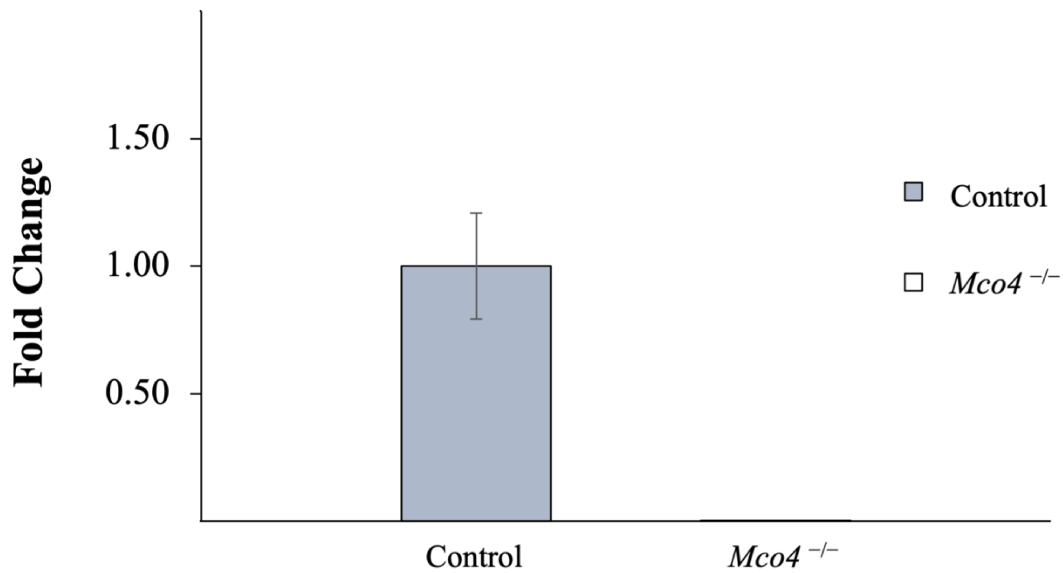


**Figure 28. Validation of *Mco4*<sup>-/-</sup> line using RT-qPCR.** Six L3 larvae whole gut samples were collected for RT-qPCR analysis for the experimental and control groups in triplicates. The *Mco4* expression levels were calculated relative to *w*<sup>1118</sup> using the  $\Delta\Delta C_t$  method. *rp49* was used as a reference gene for normalization. Error bars represent 95% confidence interval and n= 3 replicates per sample.

## 6.2 Examining the survival rates of *Mco4*<sup>-/-</sup> populations

*Mco4*<sup>-/-</sup> flies are homozygous viable. I quantified the survival rate of *Mco4*<sup>-/-</sup> flies under normal and iron-depleted conditions (100  $\mu$ M BPS). *Mco4*<sup>-/-</sup> flies showed a significant decrease in the pupal and adult survival rates compared to the control *w*<sup>1118</sup> flies on both diets (t-test, p-value < 0.01 & p-value < 0.001), as shown in **Figure 29**. Additionally, *Mco4*<sup>-/-</sup> flies on both diets showed no detectable effect on the larval arrest, pupal formation and adult eclosion rates compared to the control animals. Collectively, these data indicate a decrease in the survival rate of *Mco4*<sup>-/-</sup> flies. However, the development of *Mco4*<sup>-/-</sup> animals seems to be normal.

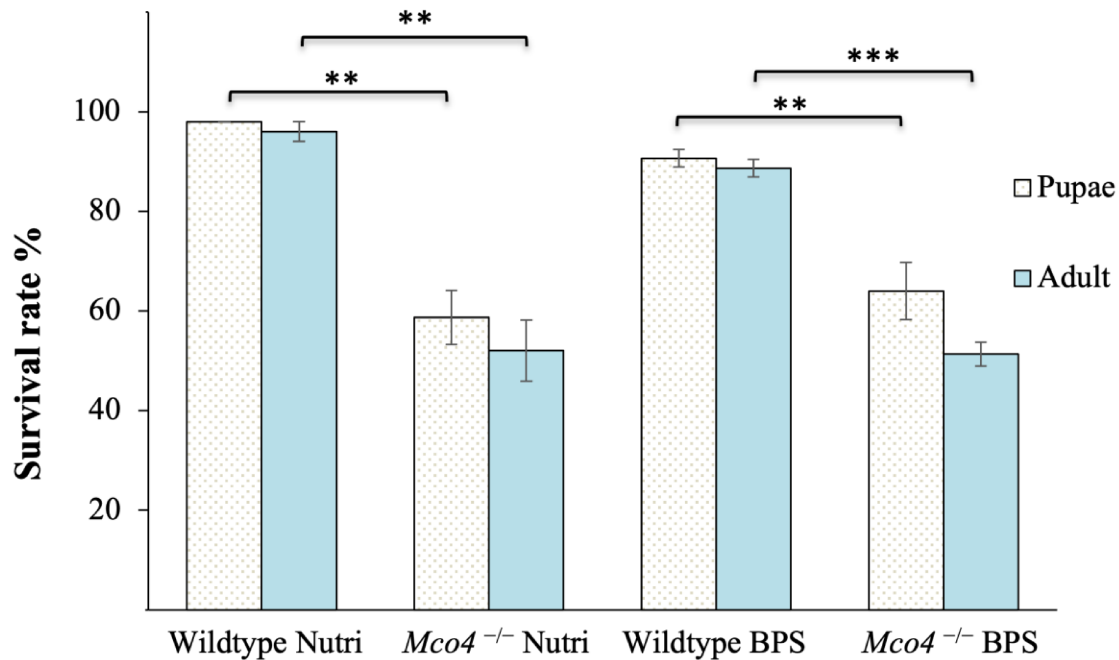


**Figure 29. The survival rate of *Mco4*<sup>-/-</sup> flies on standard and iron-depleted food.** Fifty eggs for one replicate were collected and reared on either Nutri-Fly food or iron-depleted media. The number of pupae and adult flies was counted to estimate the survival rate. Error bars represent 95% confidence interval and n= 3 replicates per sample.

### 6.3 Examining whether *Mco4*<sup>-/-</sup> flies display red autofluorescence

To determine whether *Mco4*<sup>-/-</sup> results in a porphyria-like phenotype in the PG and midgut, *Mco4*<sup>-/-</sup> larvae were reared on a regular and low iron diet (100  $\mu$ M BPS). Third instar larvae were dissected and evaluated using confocal to assess the enlargement of the PG and red autofluorescence phenotypes, indicating a heme precursor accumulation in the PG and midgut region. *w*<sup>1118</sup> flies served as a negative control.

## Results

*Mco4*<sup>-/-</sup> larvae displayed no associated porphyria phenotypes under both diets in the ring gland tissue but displayed a red fluorescence in the CNS (Figure 30). *Mco4*<sup>-/-</sup> larvae midgut region showed no red fluorescence in either diet, similar to the control (Figure 31). Additionally, the hindgut of *Mco4*<sup>-/-</sup> larvae reared on both diets displayed an observable red phenotype under brightfield and confocal settings, as shown in Figure 32A & 32B. The observed red fluorescence in the CNS and hindgut of the larvae corresponds with the expected spatiotemporal expression pattern of the 3xP3-DsRed transformation marker [136].

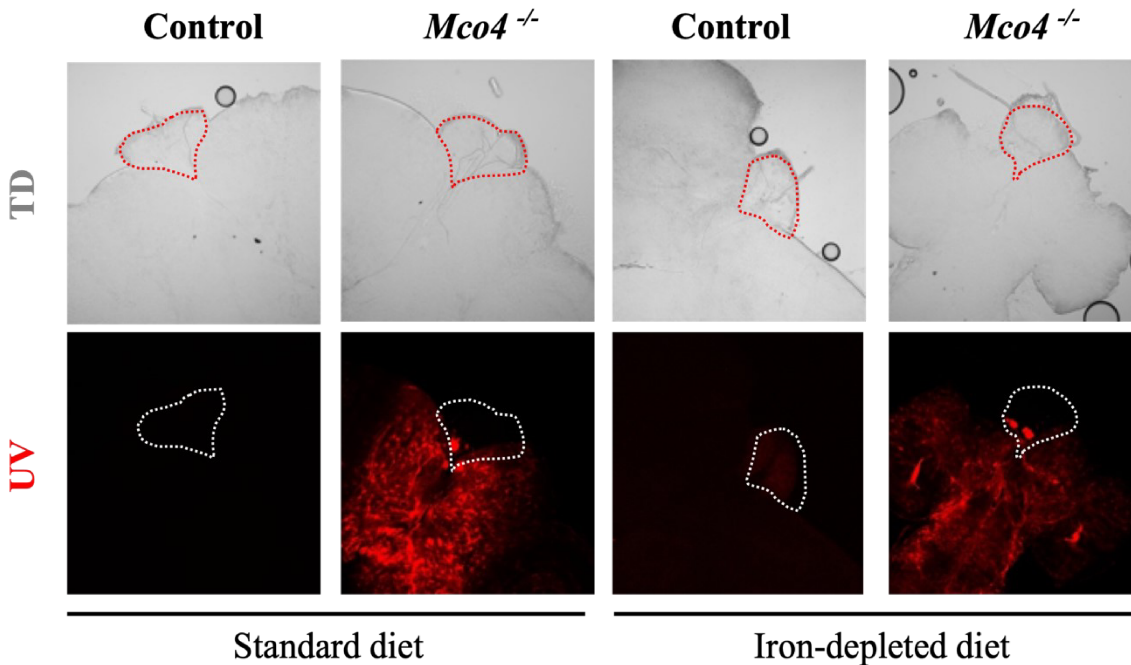


**Figure 30. Dissected PGs isolated from *Mco4*<sup>-/-</sup> larvae reared on standard, and iron-depleted diets.** Third instar larvae BRGC were dissected and assessed for porphyria phenotypes, enlarged ring gland and red autofluorescence. Fluorescent images were captured using a confocal microscope. The magnification used is 20X. The transmitted detector (TD) channel corresponds to the transmitted light channel (first row of panels), and the UV channel corresponds to the red channel (second row of panels).

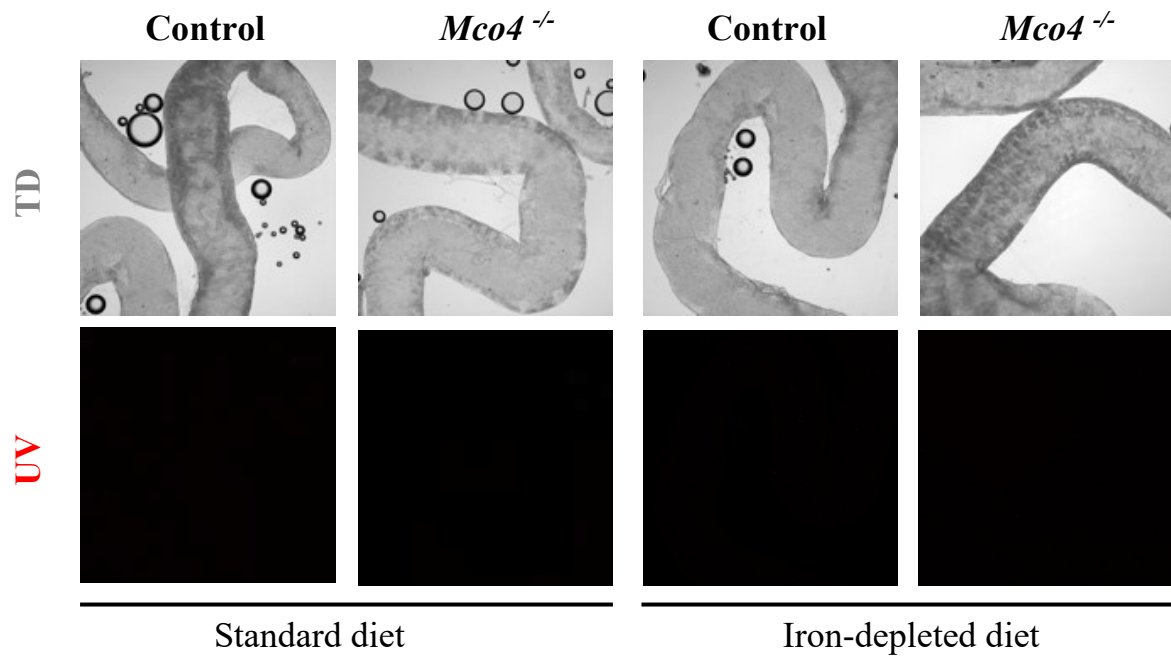


**Figure 31. Dissected midgut regions isolated from *Mco4*<sup>-/-</sup> larvae reared on standard and iron-depleted diets.** Third instar larvae guts were dissected, and the midgut region was assessed for red autofluorescence. Confocal microscopy was used to capture fluorescent images. The magnification used is 10X. The transmitted detector (TD) channel corresponds to the transmitted light channel (first row of panels), and the UV channel corresponds to the red channel (second row of panels).

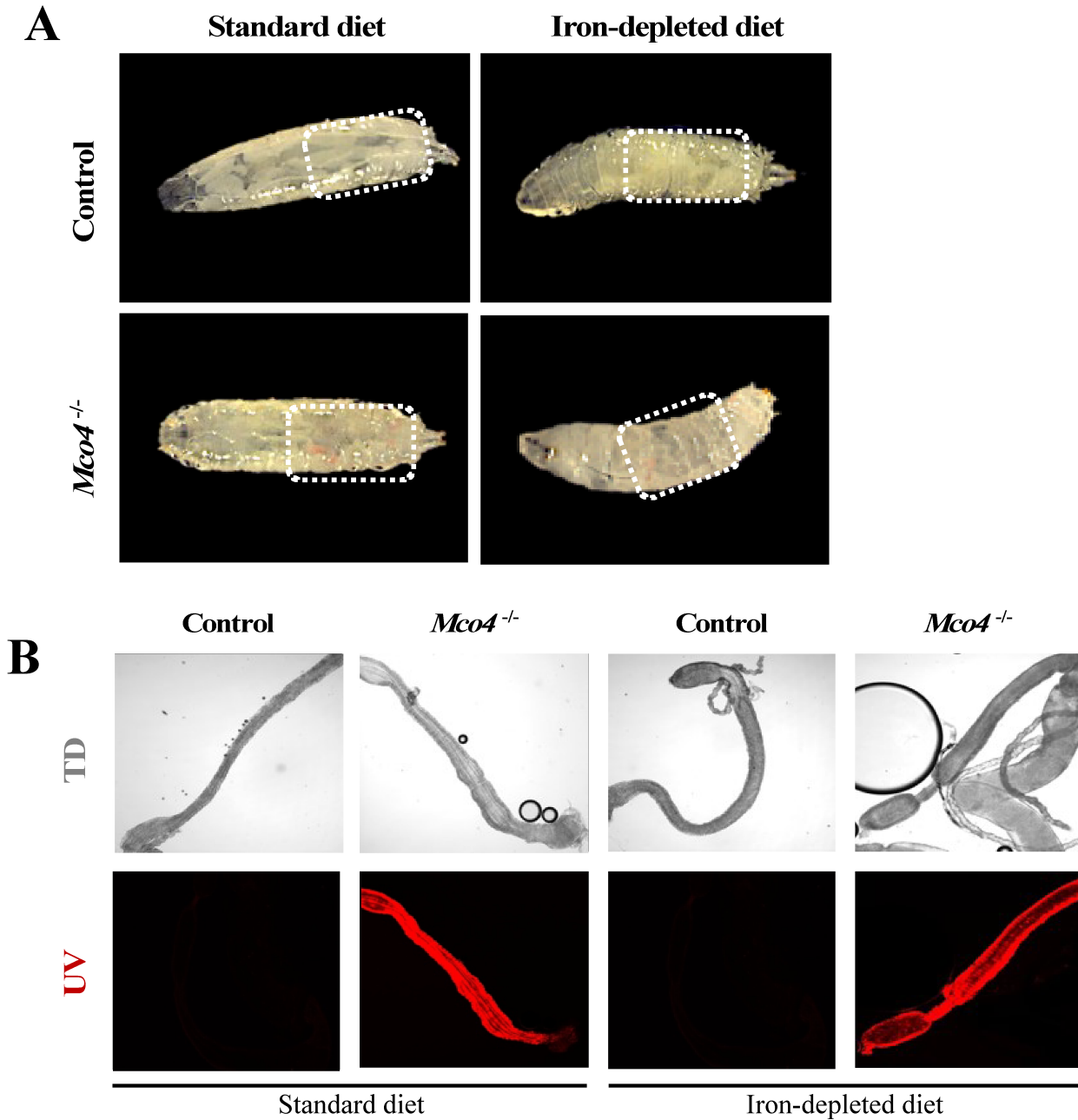


**Figure 32. Dissected hindguts isolated from *Mco4*<sup>-/-</sup> larvae reared on standard and iron-depleted food.** (A) *Mco4*<sup>-/-</sup> larvae reared under a standard and iron-chelated diet under brightfield settings. The images were acquired using an epifluorescence scope and a digital camera (LEICA DFC500 Camera), the magnification used was 3.2X. (B) Third instar larvae were reared under a standard and iron-depleted diet and dissected. Confocal microscopy was used to capture fluorescent images. The magnification used is 10X. The transmitted detector (TD) channel corresponds to the transmitted light channel (first row of panels), and the UV channel corresponds to the red channel (second row of panels).

## 6.4 Perl's Prussian Blue staining of whole guts isolated from *Mco4*<sup>-/-</sup> larvae

To study whether the iron import is impaired in the gut by complete deletion of *Mco4*, I conducted a Prussian Blue stain of the whole gut. The larvae were reared on an iron-chelated diet (100  $\mu$ M BPS) and an iron-loaded diet (1 mM FAC); *w*<sup>1118</sup> flies were used as a negative control.

### Results

I detected no visual difference in iron absorption in third instar larvae exposed to an iron-chelated and iron-loaded diet relative to the negative control *w*<sup>1118</sup> (Figure 33). Iron accumulation was not observed in the whole gut of larvae reared on an iron-depleted diet for *Mco4*<sup>-/-</sup> and the control. *Mco4*<sup>-/-</sup> larvae reared on an iron-loaded diet showed a dark Prussian blue pigment in the anterior region of the gut and the middle of the midgut region. A similar distribution was observed for the control *w*<sup>1118</sup>. Overall, iron accumulation observed with *Mco4*<sup>-/-</sup> larvae displayed the same stain intensity in the gut as the *w*<sup>1118</sup> control larvae.

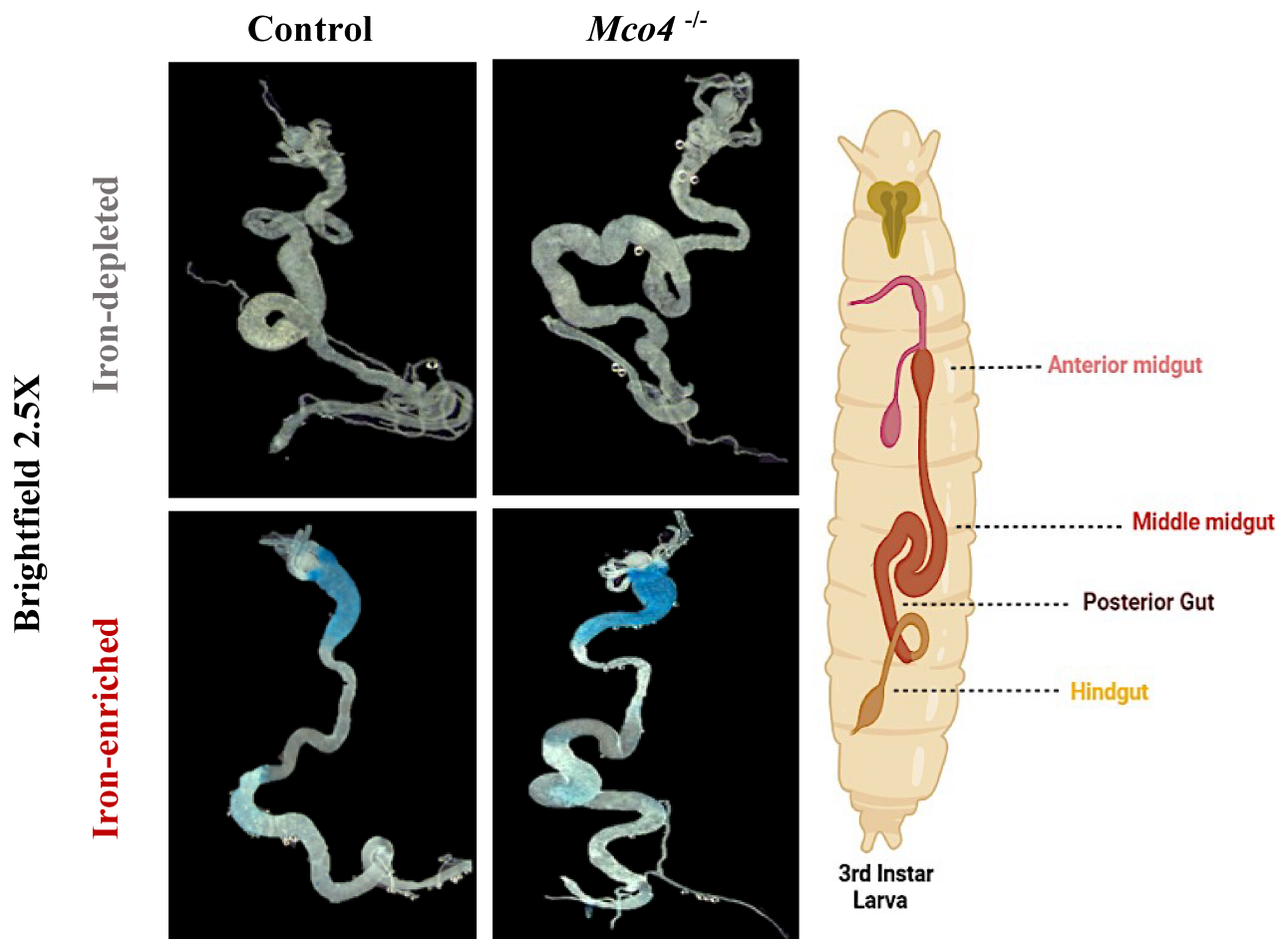


**Figure 33. Perl's Prussian blue staining of *Mco4*<sup>-/-</sup> larvae reared on iron-depleted and iron-enriched food.** Third instar larvae from an iron-depleted diet and an iron-loaded diet were dissected and stained with Perl's Prussian blue stain. The images were acquired using an epifluorescence camera (LEICA DFC500 Camera) under brightfield, and the magnification used was 2.5X.

## DISCUSSION

Compared to the *tubulin>Mco4*<sup>RNAi</sup> and *phm22>Mco4*<sup>RNAi</sup> knockdown results, the *Mco4* null animals displayed a significant decrease in survival rates. This finding is indicative that *Mco4* contributes to the survival of *Drosophila* flies. *Drosophila* acquires iron from the diet. Additionally, the mother also provides iron to the offspring in the embryo. A study completed by Sattar Soltani (manuscript in preparation) showed that when *w<sup>1118</sup>* flies are reared on an iron-chelated diet for five successive generations, a substantial decline in the fly's survival rate is seen in generation #6. The observed decrease in the survival rate signifies that it takes five generations for iron storage in the flies to be depleted (when using BPS as an iron chelator in the diet) and for the reared flies to experience iron deficiency phenotypes. Therefore, to explore whether *Mco4*<sup>-/-</sup> flies are sensitive to iron depletion on the hypothesis of *Mco4*'s involvement in iron transport. It would be prudent to test the survival rates of *Mco4*<sup>-/-</sup> flies reared for five successive generations in an iron-chelated diet. If *Mco4* were to be involved in iron transport, then theoretically, it should take less than five generations in iron-depleted conditions to observe a significant decline in the survival rates.

Notably, red fluorescence was observed in the CNS region of the brain and the hindgut region of the gut. Based on a published paper <sup>[136]</sup>, the donor plasmid promoter 3xP3 used to drive the DsRed marker (3xP3-DsRed) results in a spatiotemporal expression pattern of the fluorescent marker, seen in the CNS, hindgut and the anal plates of larvae in all three larval stages <sup>[136]</sup>. This correlates with the observed tissue distribution of the red fluorescence seen in the *Mco4*<sup>-/-</sup> larvae. A future experiment to study whether the auto-fluorescent phenotype observed in the CNS and hindgut directly results from the 3xP3-DsRed expression would be to use the Cre-loxP system. The DsRed marker found in the generated *Mco4* mutant line is flanked

by two loxP sites (Figure 27), and as such, DsRed can be removed by crossing *Mco4*<sup>-/-</sup> flies with Cre-lox flies. Cre-lox flies produce a Cre recombinase protein that recognizes the loxP site and excises the DNA sequence flanked by the two loxP sites [129], thereby removing the DsRed marker. The resulting offspring can then be screened for the red fluorescence in the CNS and the hindgut region of the larvae. Consequently, if the resulting offspring still retain the red fluorescence in the CNS and hindgut region of the gut, then the observed phenotype could be attributed to the complete deletion of the *Mco4* gene. In the absence of the red fluorescence, the observed phenotype could be attributed to the former presence of the DsRed marker.

## CHAPTER 7

### Summary and Significance

This thesis provides the first structural framework for identifying and understanding the Mco4 function as a possible candidate in *Drosophila* iron transport. The hypothesis that Mco4 functions as a high affinity iron importer is supported by Mco4's upregulated expression under iron-deprived conditions observed in three independent sets of RNA-Seq data, which I have further confirmed through qPCR in this thesis. This suggests that Mco4 expression is upregulated in cells exposed to iron-deprived conditions to ensure sufficient iron uptake, possibly via a high affinity iron import system. Along this line of thinking, the possibility of Mco4 functioning as a high affinity iron importer would be a central finding as no high affinity iron import system has ever been identified in higher eukaryotes.

To characterize the Mco4 function, I studied the subcellular localization both in *ex vivo* (Ac5-Mco4-C-4Myc and Ac5-Mco4- $\Delta$ SP-C-4Myc) and a *UAS-Mco4* model by generating Myc-tagged Mco4 constructs. Both the *ex vivo* and *UAS-Mco4*, Myc-tagged constructs showed subcellular localization in the plasma membrane of midgut and S2 cells. The observed plasma membrane localization was consistent with the predicted localization using the tool PSIPRED. Furthermore, the same tool also predicted a putative single transmembrane domain and a putative signal peptide in the Mco4 protein. A single putative transmembrane domain suggests Mco4 forms a complex with another transporter protein to facilitate iron import [137]. Similarly, the yeast ortholog Fet3p contains a single transmembrane domain and a signal peptide [137]. The existence of a putative signal peptide in Mco4 was determined *ex vivo*. S2 cells containing constructs with a deleted signal peptide (Ac5-Mco4- $\Delta$ SP-C-4Myc) showed localization in the cell's cytoplasm contrary to constructs with an intact signal peptide displaying a plasma membrane localization. As to other MCOs, Mco1 and Mco3 contain a putative signal peptide and a putative transmembrane domain [58,66,71]. Mco1 was found to be localized on the basal surface of midgut epithelial cells [66]. In comparison, Mco3 localized on the surface of salivary glands and mainly secreted and confined to the extracellular space [138].

To study the function of *Mco4* in *Drosophila*, I have analyzed the survival rate, development, and iron-dependent tissues (PG and gut) of *Mco4* RNAi and null mutant animals. I have validated the null mutant line at the genomic level using PCR/Sanger Sequencing and at the mRNA level using RT-qPCR. Additional validation of the generated null mutant line can be accomplished by performing a Western blot to validate at the protein level. The DsRed marker can be removed using the Cre-loxP system to address whether the red fluorescent phenotype observed in the CNS and hindgut tissues of the larvae is a direct result of the promoter 3xP3 used to drive the DsRed marker (3xP3-DsRed).

Nonetheless, the generated *Mco4*<sup>-/-</sup> line is significant as no deletion model of *Mco4* in *Drosophila* has been reported in the literature. Based on the hypothesis that *Mco4* function is or is part of a high affinity iron importer, I would expect that *Mco4* null mutants cause a reduction in available cellular iron, resulting in the developmental and porphyria-like phenotypes in flies. However, I did not observe any of the aforementioned phenotypes in *Mco4*<sup>-/-</sup> flies. Signifying that in the absence of *Mco4*, the heme biosynthetic pathway is not disrupted. Meaning sufficient iron requirements are still being met. In contrast, yeast models containing a Fet3p loss-of-function cannot grow in an iron-depleted medium [137]. A loss of Fet3p results in its partner protein, Ftr1p, failing to localize to the plasma membrane, resulting in Fet3p mutant inhibited growth [51]. When compared to other members of the MCO family in *Drosophila*, the knockdown of *Mco1* results in reduced iron abundance in the midgut region of the intestine and causes pupal lethality [66]. In comparison, *Mco3 / Malvolio double* mutants accumulate iron in the intestine midgut region, proposing the *Mco3* function to be involved in iron storage of the intestine midgut region [16,58].

The lack of *Mco4* resulted in a significant decrease in the survival rate of *Drosophila* flies reared under standard and iron-chelated diets (Figure 29). This reduction was not observed in the *Mco4* knockdown using two independent RNAi lines (Figure 15 & 17) and may be the result of the *Mco4*<sup>-/-</sup> line outperforming the RNAi lines in terms of silencing *Mco4* expression. Conversely, *Mco4*-loss-of-function may impact the survival of *Drosophila* flies through an unknown biological pathway. However, further experiments are needed to determine the impact of generational *Mco4* loss of function under iron-depleted conditions.

Additionally, not observing any phenotypes with the knockdown and removal of *Mco4* can be attributed to the already existing iron absorption pathways. Potentially the existing pathways can compensate for the lack of iron absorption resulting from the loss of *Mco4* function. In *Drosophila*, there are three potential iron absorption pathways: (1) Ferritin, (2) Transferrin and (3) Heme. The first pathway involves ferritin; in *Drosophila*, ferritin is localized to the hemolymph and secretory pathway (ER and Golgi) [61]. Knockdown analysis of *Fer1HCH* in the midgut shows systemic iron deficiency and iron accumulation in the gut [139]. Suggesting ferritin function to be involved in iron absorption and cellular iron export using the secretory pathway [61]. However, it's unknown whether ferritin is imported back into the cell. The second suggested pathway involves transferrin (*Tsf1*). *Tsf1* localizes to the gut surface and, when knocked down, results in iron accumulation in the gut and deficiency in the fat body [61]. Signifying, *Drosophila* transferrin's (*Tsf1*) potential function in iron transport from the gut to specific tissues and iron absorption [61]. However, no transferrin receptor homolog has been identified in *Drosophila* so far. The question of how tissues take up iron-bound to transferrin is unknown. The third potential pathway involves heme. In mammals, Heme-Fe is an essential source of dietary iron [140]. Whether dietary heme is a source of iron in *Drosophila* remains to be examined [18]. However, *Drosophila* does encode a heme oxygenase that has been characterized [18]. This pathway is particularly of significance in experiments where flies are reared on a standard diet containing no iron, but the flies appear to be healthy. The consumption of iron may result from larvae consuming heme found in the hemolymph of decaying larvae, suggesting heme as a source of iron (Figure 34). In summary, whether other pathways compensate for *Mco4* involvement in iron transport can be further examined by generating double mutants of *Mco4* and one of the other proteins (ferritin, transferrin and heme oxygenase).

Unregulated iron results in oxidative stress, which causes damage to many tissues in our body and is involved in several diseases and has been linked to neurodegenerative diseases and cancer [141-142]. A better understanding of how cells transport iron can provide us with the foundation to treat these diseases and possibly even prevent them. This thesis outlines a possible iron-transport system in *Drosophila*, mediated by exploring *Mco4*'s function by identifying its subcellular localization in the cell and characterizing a complete *Mco4*-loss-of-function model

using the profound gene-editing tool CRISPR/Cas9. Furthermore, considering the data shown here, the physiological significance of *Mco4* in relation to cellular iron homeostasis still requires further investigations to explore this promising lead. I am proposing a few future directions in chapter 8.

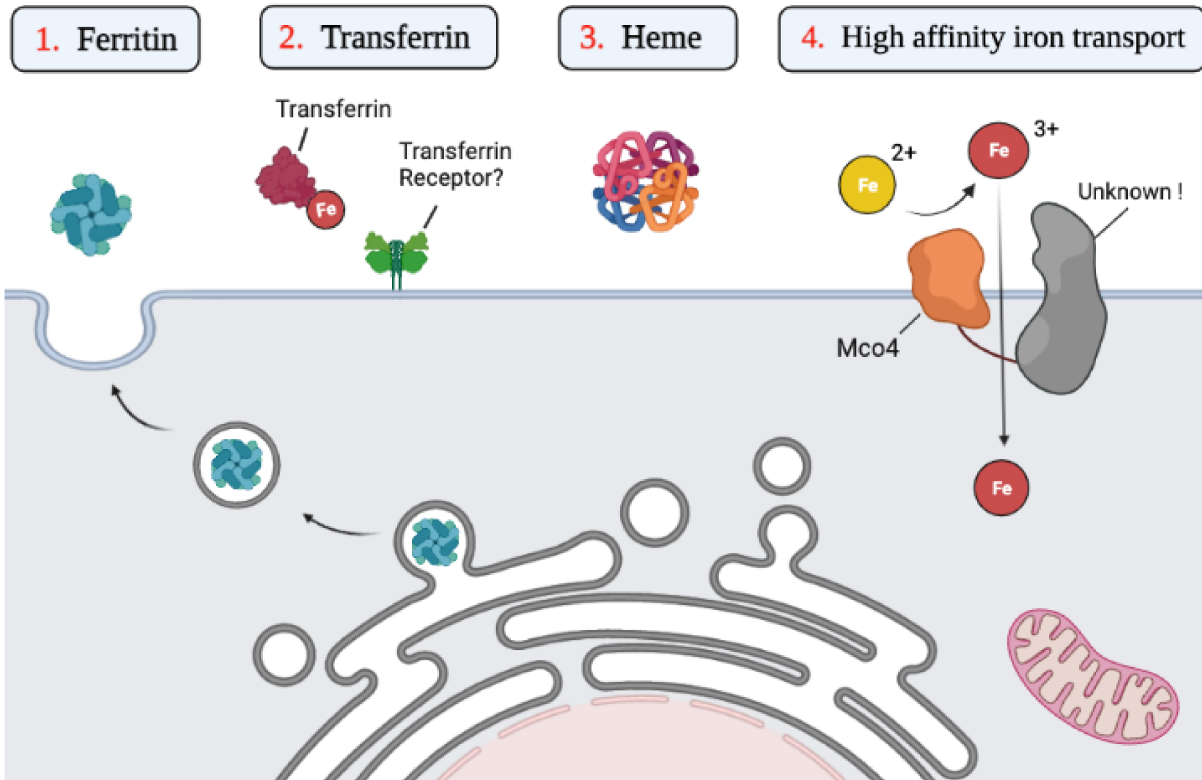


**Figure 34. Proposed model for high affinity iron transport in *Drosophila* during iron-deprived conditions.** In *Drosophila*, ferritin and transferrin have been identified as iron

transport/absorption candidates, and dietary heme is a potential source of iron in *Drosophila*. The work embodied in this thesis proposes a high affinity iron transporter in *Drosophila*. My hypothesis states that *Mco4* and an unknown protein function as a high affinity iron importer under iron-deprived conditions. This hypothesis requires further investigation to identify any interacting proteins working together with *Mco4* and whether *Mco4*<sup>-/-</sup> flies reared under an iron chelated diet for four or fewer successive generations exhibit early survival rate decline compared to the wildtype.

## CHAPTER 8

### Future Directions

#### *8.1 Study Mco4 null mutants under iron-chelated conditions over multiple generations*

Sattar Soltani found that when  $w^{1118}$  flies were reared for five successive generations under iron-chelated food, flies displayed a significant lethality of around fifty percent. This indicates that it takes five generations on iron-depleted conditions for wildtype flies iron stores to be depleted, affecting the animal's development and survival. When knocking out the *Mco4* gene in *Drosophila* flies, I observed a significant decrease in the survival rate of animals reared under an iron-chelated diet for one generation. Therefore, a proposed experiment would be to examine the number of successive generations *Mco4*<sup>-/-</sup> flies can endure surviving under iron-depleted conditions and if *Mco4*<sup>-/-</sup> flies would experience a drop in viability sooner than wildtype flies. These data would provide an informative insight into the consequences of loss-of-Mco4-function over multiple generations under iron-deprived conditions. That being said, if *Mco4* were to function as a high affinity iron importer under iron-deprived conditions as proposed, then theoretically, it should take less than five generations in iron-stressed conditions to observe a drop in survival rates compared to that of the control. The rationale is that upon removing *Mco4* function under iron-depleted conditions, larvae should experience inadequate intracellular iron concentration in tissues. This would hinder critical pathways in tissues that require large amounts of iron, such as the ecdysone pathway in the PG responsible for the growth and development of the larvae. This finding would demonstrate *Mco4*'s significance in *Drosophila* flies survival under iron-stressed conditions.

#### *8.2 Identifying proteins that interact with Mco4*

Consistent with Fet3p, Mco4 exhibited localization to the plasma membrane both in midgut cells (*tubulin* > *UAS-Mco4-3Myc*) and *ex vivo* (*Ac5-Mco4-C-4Myc*). Furthermore, using the bioinformatic tool PSIPRED, Mco4 was predicted to contain only one transmembrane domain [85], similar to that of Fet3p. Collectively these results provide a foundation for the

hypothesis that the Mco4 function is consistent with that of Fet3p. Fet3p forms a complex with a symporter protein, Ftr1p, to function as a highly specific iron importer<sup>[17]</sup>. However, no fly ortholog of Ftr1p has been identified so far<sup>[57]</sup>. Mco4 is unlikely to facilitate iron transport on its own because it lacks multiple membrane-spanning domains<sup>[143]</sup> and instead would need to interact with another transmembrane protein, as seen in the Fet3p/Ftr1p complex. As there are no orthologs to Ftr1p in *Drosophila*, a list of possible protein candidates can be identified using the co-IP method followed by mass spectrometry. This can be accomplished using the existing *UAS-Mco4* transgenic line crossed with a tubulin driver (*tubulin >UAS-Mco4-3Myc*) for co-IP. The protein of interest, in this case, Mco4, is isolated with an anti-Myc-tag antibody and separated via SDS-PAGE. Any interactions detected by this approach can be sent for mass spectrometry to be identified.

Alternatively, to complement the co-IP approach, one can utilize TurboID-mediated biotinylation (TurboID) in conjunction with mass spectrometry. TurboID is a technique used to identify protein-protein interactions within a living cell. TurboID is based on a biotin-ligase approach; ligase catalyzes the generation of a reactive biotin-5'-AMP intermediate from biotin and ATP<sup>[126]</sup>. The resulting intermediate biotin-5'-AMP biotinylates lysine residues of proteins proximal to the protein of interest<sup>[144]</sup>. In the case biotin does not bind to a protein, it is hydrolyzed within the cell<sup>[144]</sup>. The biotinylated target proteins are then pulled down using streptavidin beads with a strong biotin affinity, and the sample can then be sent for mass spectrometry<sup>[144]</sup>. The TurboID construct can be generated using the pUASst-V5-TurboID vector (addgene#116904), where the *Mco4* cDNA can be inserted into the pUASst vector using Gibson assembly cloning, following the Branon et al. (2018) protocol<sup>[145]</sup>. The constructed plasmid can then be confirmed by sequencing before injection into embryos. The generated line can be used to study Mco4 protein-protein interactions at different developmental stages and a variety of tissues using a tissue-specific Gal4-driver<sup>[126]</sup>. Transgenic flies are reared on a 100  $\mu$ M biotin supplemented diet to provide biotin for biotin-5'-AMP intermediate formation<sup>[126]</sup>.

Following mass spectrometry, the identified proteins can be screened, and any possible Mco4 interaction candidates identified using co-IP or TurboID can be verified and visualized through Förster resonance energy transfer (FRET). FRET is a technique used to identify protein-

protein interactions with proximity below 10 nm and is suitable for identifying membrane-associated protein complexes [146]. FRET measures the energy transfer between a donor and acceptor fluorophore [146]. To test this methodology, a donor plasmid can be constructed to contain the *Mco4* cDNA cloned in-frame to create a C-terminal mCerulean fusion protein, and the acceptor plasmid can be constructed to contain the potential candidate cDNA cloned in-frame to generate an N-terminal mVenus tag. The resulting constructs are confirmed through sequencing and transfected into S2 *Drosophila* cells. Furthermore, empty constructs of mVenus and mCerulean can serve as the negative controls. The emission spectra for the plasmids are, Cerulean is excited at 820 nm and has an emission of 475 nm, whereas Venus is excited at 940 nm and has an emission of 528 nm [147]. The samples are then excited at 820 nm to initiate FRET, and the emission will then be recorded at 528 nm [147]. Overall, if a magnitude of 528 nm wavelength emissions is observed, this will indicate that the Cerulean variant is directly exciting the Venus variant due to the *Mco4* and the identified candidate protein-protein interaction occurrence. At this stage, there are no candidates for *Mco4* protein interaction. It's fascinating to think of which proteins possibly interact with *Mco4* and are perhaps involved in iron transport.

### 8.3 Evaluate whether *Mco4* contains a ferroxidase activity

Fet3p is a multicopper ferroxidase in yeast that catalyzes the oxidation of  $\text{Fe}^{2+}$  to  $\text{Fe}^{3+}$ ; this is essential to facilitate iron uptake by the membrane permease Ftr1p [138]. In contrast, *Mco4* has not been proven to contain a ferroxidase activity to date. Evidence of *Mco4* functioning as a ferroxidase would be crucial in evaluating its function in relation to iron uptake in *Drosophila*. A method to measure ferroxidase activity has been described by Wong et al. (2014) and Wang et al. (2018) [138,148]. The assay spectrophotometrically measures the production of the  $\text{Fe}^{3+}$  substrate produced by the ferroxidase reaction [148]. The assay is done in a 96 well microplate, where the *Mco4* protein is added into an HBS reaction buffer, and ferrous ammonium sulfate is added to the assay as a substrate for the reaction. Absorbance readings are taken at 310 nm ( $A_{310}$ ) to reflect the production of ferric iron. Samples are blanked using the HBS buffer, and human ceruloplasmin can be used as a positive control. To control for autoxidation, a blank spectrum reading without the addition of *Mco4* should be recorded using the same time points used. Results are plotted, absorbance ( $A_{310}$ ) versus time (min) and statistically analyzed using Excel.

## 8.4 Conclusion

Our understanding of the potential role Mco4 may play in *Drosophila* physiology is unknown. My preliminary data show that Mco4 and Fet3p share similarities in localization, presence of a putative signal peptide and a putative single transmembrane domain. These are promising characteristics/results in supporting the hypothesis of Mco4 functioning in transporting iron across the plasma membrane to the cell's cytoplasm. However, further investigation is required to better understand whether Mco4 functions in the uptake of iron. Therefore, the proposed experiments mentioned in this chapter can help in functionally characterizing Mco4. Supporting the existence of a functional ferroxidase activity would be of fundamental importance in demonstrating Mco4 ability to oxidize  $\text{Fe}^{2+}$  to  $\text{Fe}^{3+}$  for iron transport. Identifying binding partners of Mco4 will provide us with potential candidates for the proposed high affinity *Drosophila* iron import system. Additionally, consolidating the impact of dietary iron changes over multiple generations in *Mco4*<sup>-/-</sup> flies can shed light on the importance of Mco4 under generational iron-depleted conditions. Finally, the described experiments would help broaden our knowledge and provide a framework in advancing our understanding of Mco4 function in relation to iron metabolism. Therefore, additional experiments are needed to resolve the role of Mco4 in *Drosophila* iron transport.

## Literature Cited

1. Abbaspour, N., Hurrell, R., & Kelishadi, R. (2014). Review on iron and its importance for human health. *Journal of Research in Medical Sciences: The Official Journal of Isfahan University of Medical Sciences*, 19(2), 164.
2. Li, Y., Huang, X., Wang, J., Huang, R., Wan, D., & Yang, G. (2020). Regulation of Iron Homeostasis and Related Diseases. *Mediators of Inflammation*, 2020. <https://doi.org/10.1155/2020/6062094>
3. Steinbicker, A. U., & Muckenthaler, M. U. (2013). Out of Balance—Systemic Iron Homeostasis in Iron-Related Disorders. *Nutrients*, 5(8), 3034-3061. <https://doi.org/10.3390/NU5083034>
4. Sarkar, J., Potdar, A. A., & Saidel, G. M. (2018). Whole-body iron transport and metabolism: Mechanistic, multi-scale model to improve treatment of anemia in chronic kidney disease. *PLOS Computational Biology*, 14(4), e1006060. <https://doi.org/10.1371/JOURNAL.PCBI.1006060>
5. Hamilton, J. L., & Kizhakkedathu, J. N. (2015). Polymeric nanocarriers for the treatment of systemic iron overload. *Molecular and Cellular Therapies*, 3(1). <https://doi.org/10.1186/s40591-015-0039-1>
6. Lieu, P. T., Heiskala, M., Peterson, P. A., & Yang, Y. (2001). The roles of iron in health and disease. *Molecular Aspects of Medicine*, 22(1–2), 1–87. [https://doi.org/10.1016/S0098-2997\(00\)00006-6](https://doi.org/10.1016/S0098-2997(00)00006-6)
7. DeLoughery, T. G. (2017). Iron Deficiency Anemia. *Medical Clinics of North America*, 101(2), 319–332. <https://doi.org/10.1016/J.MCNA.2016.09.004>
8. Wallace, D. F. (2016). The Regulation of Iron Absorption and Homeostasis. *The Clinical Biochemist Reviews*, 37(2), 51-62.
9. Lopez, A., Cacoub, P., Macdougall, I. C., & Peyrin-Biroulet, L. (2016). Iron deficiency anaemia. *The Lancet*, 387(10021), 907–916. [https://doi.org/10.1016/S0140-6736\(15\)60865-0](https://doi.org/10.1016/S0140-6736(15)60865-0)
10. Ugur, B., Chen, K., & Bellen, H. J. (2016). Drosophila tools and assays for the study of human diseases. *DMM Disease Models and Mechanisms*, 9(3), 235-244. <https://doi.org/10.1242/dmm.023762>

11. Jacomin, A. C., Geraki, K., Brooks, J., Tjendana-Tjhin, V., Collingwood, J. F., & Nezis, I. P. (2019). Impact of autophagy and aging on iron load and ferritin in *Drosophila* brain. *Frontiers in Cell and Developmental Biology*, 7, 142.  
<https://doi.org/10.3389/FCELL.2019.00142>
12. Xiao Guiran, Liu Zhi-Hua, Zhao Mengran, Wang Hui-Li, & Zhou Bing. (2019). Transferrin 1 Functions in Iron Trafficking and Genetically Interacts with Ferritin in *Drosophila melanogaster*. *Cell Reports*, 26(3), 748–758.  
<https://doi.org/10.1016/j.celrep.2018.12.053>
13. Ou, Q., Magico, A., & King-Jones, K. (2011). Nuclear Receptor DHR4 Controls the Timing of Steroid Hormone Pulses During *Drosophila* Development. *PLoS Biology*, 9(9), e1001160. <https://doi.org/10.1371/journal.pbio.1001160>
14. Gilbert, L. I. (2004). Halloween genes encode P450 enzymes that mediate steroid hormone biosynthesis in *Drosophila melanogaster*. *Molecular and Cellular Endocrinology*, 215(1–2), 1–10. <https://doi.org/10.1016/J.MCE.2003.11.003>
15. Huynh, N., Ou, Q., Cox, P., Lill, R., & King-Jones, K. (2019). Glycogen branching enzyme controls cellular iron homeostasis via Iron Regulatory Protein 1 and mitoNEET. *Nature Communications*, 10(1), 5463. <https://doi.org/10.1038/s41467-019-13237-8>
16. Tang, X., & Zhou, B. (2013). Iron homeostasis in insects: Insights from *Drosophila* studies. *IUBMB Life*, 65(10), 863-872. <https://doi.org/10.1002/iub.1211>
17. Kosman, D.J. (2002). The Fet3 Protein: A Multicopper Ferroxidase Essential to Iron Metabolism in Yeast. In *Handbook of Copper Pharmacology and Toxicology*, 8(6), 153-175. <https://doi.org/10.1007/s00775-003-0456-5>
18. Mandilara, K, Pathmanathan, T., and Missirlis, F. (2013). Iron absorption in *Drosophila*. *Nutrients*, 5(5), 1622-1647. <https://doi.org/10.3390/nu5051622>
19. Hurrell, R., & Egli, I. (2010). Iron bioavailability and dietary reference values. *The American Journal of Clinical Nutrition*, 91(5), 1461-1467.  
<https://doi.org/10.3945/ajcn.2010.28674F>
20. Anderson, G. J., & Frazer, D. M. (2017). Current understanding of iron homeostasis. *The American Journal of Clinical Nutrition*, 106(6), 1559-1566.  
<https://doi.org/10.3945/AJCN.117.155804>

21. McKie, A. T., Barrow, D., Latunde-Dada, G. O., Rolfs, A., Sager, G., Mudaly, E., Mudaly, M., Richardson, C., Barlow, D., Bomford, A., Peters, T. J., Raja, K. B., Shirali, S., Hediger, M. A., Farzaneh, F., & Simpson, R. J. (2001). An Iron-Regulated Ferric Reductase Associated with the Absorption of Dietary Iron. *Science*, *291*(5509), 1755–1759. <https://doi.org/10.1126/SCIENCE.1057206>
22. Gunshin, H., Mackenzie, B., Berger, U. v., Gunshin, Y., Romero, M. F., Boron, W. F., Nussberger, S., Gollan, J. L., & Hediger, M. A. (1997). Cloning and characterization of a mammalian proton-coupled metal-ion transporter. *Nature*, *388*(6641), 482–488. <https://doi.org/10.1038/41343>
23. Southon, A., Farlow, A., Norgate, M., Burke, R., & Camakaris, J. (2008). Malvolio is a copper transporter in *Drosophila melanogaster*. *Journal of Experimental Biology*, *211*(5), 709–716. <https://doi.org/10.1242/jeb.014159>
24. Doig, K. (2020). Iron kinetics and laboratory assessment. *Rodak's Hematology* (p. 104–116). Elsevier. <https://doi.org/10.1016/b978-0-323-53045-3.00017-9>
25. Abboud, S., & Haile, D. J. (2000). A Novel Mammalian Iron-regulated Protein Involved in Intracellular Iron Metabolism. *Journal of Biological Chemistry*, *275*(26), 19906–19912. <https://doi.org/10.1074/JBC.M000713200>
26. Richardson, D. R., Lane, D. J. R., Becker, E. M., Huang, M. L.-H., Whitnall, M., Rahmanto, Y. S., Sheftel, A. D., & Ponka, P. (2010). Mitochondrial iron trafficking and the integration of iron metabolism between the mitochondrion and cytosol. *Proceedings of the National Academy of Sciences*, *107*(24), 10775–10782. <https://doi.org/10.1073/PNAS.0912925107>
27. He, D., & Marles-Wright, J. (2015). Ferritin family proteins and their use in bionanotechnology. *New Biotechnology*, *32*(6), 651–657. <https://doi.org/10.1016/J.NBT.2014.12.006>
28. Alkhateeb, A. A., & Connor, J. R. (2010). Nuclear ferritin: A new role for ferritin in cell biology. *Biochimica et Biophysica Acta*, *1800*(8), 793–797. <https://doi.org/10.1016/J.BBAGEN.2010.03.017>
29. Imam, M., Zhang, S., Ma, J., Wang, H., & Wang, F. (2017). Antioxidants Mediate Both Iron Homeostasis and Oxidative Stress. *Nutrients*, *9*(7), 671. <https://doi.org/10.3390/nu9070671>

30. Hider, R. C., & Kong, X. L. (2011). Glutathione: A key component of the cytoplasmic labile iron pool. *BioMetals*, 24(6), 1179–1187. <https://doi.org/10.1007/S10534-011-9476-8>
31. Awadallah, S. (2013). Protein Antioxidants in Thalassemia. *Advances in Clinical Chemistry* (p. 85–128). Elsevier. <https://doi.org/10.1016/B978-0-12-407681-5.00003-9>
32. Ganz, T. (2013). Systemic Iron Homeostasis. *Physiological Reviews*, 93(4), 1721–1741. <https://doi.org/10.1152/Physrev.00008.2013>
33. Sintusek, P., Kyrana, E., & Dhawan, A. (2019). Diagnosis of Hepatic Wilson Disease. *Wilson Disease* (p. 125–138). Academic Press. <https://doi.org/10.1016/B978-0-12-811077-5.00011-6>
34. Jiang, R., Hua, C., Wan, Y., Jiang, B., Hu, H., Zheng, J., Fuqua, B. K., Dunaief, J. L., Anderson, G. J., David, S., Vulpe, C. D., & Chen, H. (2015). Hephaestin and Ceruloplasmin Play Distinct but Interrelated Roles in Iron Homeostasis in Mouse Brain. *The Journal of Nutrition*, 145(5), 1003–1009. <https://doi.org/10.3945/JN.114.207316>
35. Suh, Y. J., & David, S. (2006). Age-related changes in iron homeostasis and cell death in the cerebellum of ceruloplasmin-deficient mice. *The Journal of Neuroscience : The Official Journal of the Society for Neuroscience*, 26(38), 9810–9819. <https://doi.org/10.1523/JNEUROSCI.2922-06.2006>
36. Harris, Z. L. (2019). Ceruloplasmin. *Clinical and Translational Perspectives on WILSON DISEASE* (p. 77–84). Academic Press. <https://doi.org/10.1016/B978-0-12-810532-0.00009-4>
37. Vashchenko, G., & MacGillivray, R. T. A. (2013). Multi-Copper Oxidases and Human Iron Metabolism. *Nutrients*, 5(7), 2289–2313. <https://doi.org/10.14288/1.0378644>
38. Chen, H., Attieh, Z. K., Syed, B. A., Kuo, Y., Stevens, V., Fuqua, B. K., Andersen, H. S., Naylor, C. E., Evans, R. W., Gambling, L., Danzeisen, R., Bacouri-Haidar, M., Usta, J., Vulpe, C. D., & McArdle, H. J. (2010). Identification of Zyklopen, a New Member of the Vertebrate Multicopper Ferroxidase Family, and Characterization in Rodents and Human Cells. *The Journal of Nutrition*, 140(10), 1728–1735. <https://doi.org/10.3945/JN.109.117531>
39. Ervasti, M., Sankilampi, U., Heinonen, S., & Punnonen, K. (2009). Early signs of maternal iron deficiency do not influence the iron status of the newborn, but are

- associated with higher infant birthweight. *Acta Obstetricia et Gynecologica Scandinavica*, 88(1), 83–90. <https://doi.org/10.1080/00016340802595993>
40. Helman, S. L., Wilkins, S. J., McKeating, D. R., Perkins, A. v, Whibley, P. E., Cuffe, J. S. M., Simmons, D. G., Fuqua, B. K., Vulpe, C. D., Wallace, D. F., O’Callaghan, J. L., Pelzer, E. S., Anderson, G. J., & Frazer, D. M. (2021). The Placental Ferroxidase Zyklopen Is Not Essential for Iron Transport to the Fetus in Mice. *The Journal of Nutrition*, 151(9), 2541–2550. <https://doi.org/10.1093/JN/NXAB174>
  41. Pierre, J. L. & Fontecave, M. (1999). Iron and activated oxygen species in biology: the basic chemistry. *Biometals*, 12(3), 195-199. <https://doi.org/10.1023/a:1009252919854>
  42. Wessling-Resnick, M. (2017). Excess iron: Considerations related to development and early growth. *American Journal of Clinical Nutrition*, 106(6), 1600-1605. <https://doi.org/10.3945/ajcn.117.155879>
  43. Repetto, M., Semprine, J., & Boveris, A. (2012). Lipid Peroxidation: Chemical Mechanism, Biological Implications and Analytical Determination. *Lipid Peroxidation*. IntechOpen. <https://doi.org/10.5772/45943>
  44. Mailloux, R. J. (2015). Teaching the fundamentals of electron transfer reactions in mitochondria and the production and detection of reactive oxygen species. *Redox Biology*, 4, 381–398. <https://doi.org/10.1016/J.REDOX.2015.02.001>
  45. Mylonas, C., & Kouretas, D. (1999). Lipid Peroxidation and Tissue Damage. *In Vivo*, 13(3), 295–309.
  46. Gruer, M. J., Artymiuk, P. J., & Guest, J. R. (1997). The aconitase family: three structural variations on a common theme. *Trends in Biochemical Sciences*, 22(1), 3–6. [https://doi.org/10.1016/S0968-0004\(96\)10069-4](https://doi.org/10.1016/S0968-0004(96)10069-4)
  47. Rouault, T. A. (2006). The role of iron regulatory proteins in mammalian iron homeostasis and disease. *Nat Chem Biol.*, 2(8), 406-414. [10.1038/nchembio807](https://doi.org/10.1038/nchembio807)
  48. Wilkinson, N. & Pantopoulos, K. (2014). The IRP/IRE system in vivo: insights from mouse models. *Front Pharmacol.*, 5, 176. <https://doi.org/10.3389/fphar.2014.00176>
  49. Dix D. R., Bridgham J. T., Broderius M. A., Byersdorfer C. A., Eide D. J. (1994). The FET4 gene encodes the low affinity Fe(II) transport protein of *Saccharomyces cerevisiae*. *J Biol Chem*, 269(42), 26092–26099. [https://doi.org/10.1016/s0021-9258\(18\)47163-3](https://doi.org/10.1016/s0021-9258(18)47163-3)

50. Askwith, C., Eide, D., van Ho, A., Bernard, P. S., Li, L., Davis-Kaplan, S., Sipe, D. M., & Kaplan, J. (1994). The FET3 gene of *S. cerevisiae* encodes a multicopper oxidase required for ferrous iron uptake. *Cell*, 76(2), 403–410. [https://doi.org/10.1016/0092-8674\(94\)90346-8](https://doi.org/10.1016/0092-8674(94)90346-8)
51. Stearman R., Yuan D. S., Yamaguchi-Iwai Y., Klausner R. D., Dancis A. (1996). A permease–oxidase complex involved in high-affinity iron uptake in yeast. *Science*, 271(5255), 1552–1557. [10.1126/science.271.5255.1552](https://doi.org/10.1126/science.271.5255.1552)
52. Martins, T. S., Costa, V., & Pereira, C. (2018). Signaling pathways governing iron homeostasis in budding yeast. *Molecular Microbiology*, 109(4), 422-432. <https://doi.org/10.1111/mmi.14009>
53. Shakoury-Elizeh, M., Tiedeman, J., Rashford, J., Ferea, T., Demeter, J., Garcia, E., Rolfes, R., Brown, P. O., Botstein, D., & Philpott, C. C. (2004). Transcriptional Remodeling in Response to Iron Deprivation in *Saccharomyces cerevisiae*. *Molecular Biology of the Cell*, 15(3), 1233-1243. <https://doi.org/10.1091/MBE03-09-0642>
54. Blaiseau, P. L., Lesuisse, E., & Camadro, J. M. (2001). Aft2p, a novel iron-regulated transcription activator that modulates, with Aft1p, intracellular iron use and resistance to oxidative stress in yeast. *The Journal of Biological Chemistry*, 276(36), 34221–34226. <https://doi.org/10.1074/JBC.M104987200>
55. Rutherford, J. C., Jaron, S., Ray, E., Brown, P. O., & Winge, D. R. (2001). A second iron-regulatory system in yeast independent of Aft1p. *Proceedings of the National Academy of Sciences of the United States of America*, 98(25), 14322–14327. <https://doi.org/10.1073/PNAS.261381198>
56. Puig, S., Vergara, S. v., & Thiele, D. J. (2008). Cooperation of two mRNA-binding proteins drives metabolic adaptation to iron deficiency. *Cell Metabolism*, 7(6), 555–564. <https://doi.org/10.1016/J.CMET.2008.04.010>
57. Hu, Y., Flockhart, I., Vinayagam, A., Bergwitz, C., Berger, B., Perrimon, N., & Mohr, S. E. (2011). An integrative approach to ortholog prediction for disease-focused and other functional studies. *BMC Bioinformatics*, 12(1), 1-16. <https://doi.org/10.1186/1471-2105-12-357>
58. Bettedi, L., Aslam, M. F., Szular, J., Mandilaras, K., & Missirlis, F. (2011). Iron depletion in the intestines of malvolio mutant flies does not occur in the absence of a

- multicopper oxidase. *Journal of Experimental Biology*, 214(6), 971-978.  
<https://doi.org/10.1242/jeb.051664>
59. Xiao, G., & Zhou, B. (2018). ZIP13: A Study of *Drosophila* Offers an Alternative Explanation for the Corresponding Human Disease. *Frontiers in Genetics*, 8, 234.  
<https://doi.org/10.3389/FGENE.2017.00234>
60. Xiao, G., Wan, Z., Fan, Q., Tang, X., & Zhou, B. (2014). The metal transporter ZIP13 supplies iron into the secretory pathway in *Drosophila melanogaster*. *eLife*, 3, e03191.  
<https://doi.org/10.7554/ELIFE.03191>
61. Xiao Guiran, Liu Zhi-Hua, Zhao Mengran, Wang Hui-Li, & Zhou Bing. (2019). Transferrin 1 Functions in Iron Trafficking and Genetically Interacts with Ferritin in *Drosophila melanogaster*. *Cell Reports*, 26(3), 748–758.  
<https://doi.org/10.1016/j.celrep.2018.12.053>
62. Tiklova, K., Senti, K. A., Wang, S., Graslund, A., and Samakovlis, C. (2010). Epithelial septate junction assembly relies on melanotransferrin iron binding and endocytosis in *Drosophila*. *Nat. Cell. Biol.*, 12(11), 1071-1077. [10.1038/ncb2111](https://doi.org/10.1038/ncb2111)
63. K. Mandilaras, F. Missirlis. (2012). Genes for iron metabolism influence circadian rhythms in *Drosophila melanogaster*. *Metallomics*, 4(9), 928–936.  
<https://doi.org/10.1039/c2mt20065a>
64. Hamburger, A. E., West, A. P. Jr., Hamburger, Z. A., Hamburger, P., and Bjorkman, P. J. (2005). Crystal structure of a secreted insect ferritin reveals a symmetrical arrangement of heavy and light chains. *Journal of Molecular Biology*, 349(3), 558–569.  
<https://doi.org/10.1016/j.jmb.2005.03.074>
65. Marra, A., Masson, F., & Lemaitre, B. (2021). The iron transporter Transferrin 1 mediates homeostasis of the endosymbiotic relationship between *Drosophila melanogaster* and *Spiroplasma poulsonii*. *MicroLife*, 2, uqab008.  
<https://doi.org/10.1093/FEMSML/UQAB008>
66. Lang, M., Braun, C. L., Kanost, M. R., & Gorman, M. J. (2012). Multicopper oxidase-1 is a ferroxidase essential for iron homeostasis in *Drosophila melanogaster*. *Proceedings of the National Academy of Sciences*, 109(33), 13337–13342.  
<https://doi.org/10.1073/PNAS.1208703109>

67. Iatsenko, I., Marra, A., Boquete, J.-P., Peña, J., & Lemaitre, B. (2020). Iron sequestration by transferrin 1 mediates nutritional immunity in *Drosophila melanogaster*. *Proceedings of the National Academy of Sciences*, *117*(13), 7317–7325.  
<https://doi.org/10.1073/PNAS.1914830117>
68. Singh, R. S., Singh, T., & Pandey, A. (2019). Microbial Enzymes—An Overview. *Biomass, Biofuels, Biochemicals: Advances in Enzyme Technology* (p. 1–40). Elsevier.  
<https://doi.org/10.1016/B978-0-444-64114-4.00001-7>
69. Dittmer, N. T., & Kanost, M. R. (2010). Insect multicopper oxidases: Diversity, properties, and physiological roles. *Insect Biochemistry and Molecular Biology*, *40*(3), 179–188. <https://doi.org/10.1016/J.IBMB.2010.02.006>
70. Riedel, F., Vorkel, D., & Eaton, S. (2011). Megalin-dependent yellow endocytosis restricts melanization in the *Drosophila* cuticle. *Development*, *138*(1), 149–158.  
<https://doi.org/10.1242/DEV.056309>
71. Sansbury, B. M., Hewes, A. M., & Kmiec, E. B. (2019). Understanding the diversity of genetic outcomes from CRISPR-Cas generated homology-directed repair. *Communications Biology*, *2*(1), 1-10. <https://doi.org/10.1038/s42003-019-0705-y>
72. Lind, M. I., Missirlis, F., Melefors, Ö., Uhrigshardt, H., Kirby, K., Phillips, J. P., Söderhäll, K., & Rouault, T. A. (2006). Of Two Cytosolic Aconitases Expressed in *Drosophila*, Only One Functions as an Iron-regulatory Protein. *Journal of Biological Chemistry*, *281*(27), 18707-18714. <https://doi.org/10.1074/jbc.M603354200>
73. Nhan Huynh. (2020). Characterizing new players involved in iron homeostasis during *Drosophila* larval development: Shifting the classic paradigm of iron metabolism. Doctor of Philosophy Thesis: University of Alberta, 120-140.
74. Campillos, M., Cases, I., Hentze, M. W., & Sanchez, M. (2010). SIREs: searching for iron-responsive elements. *Nucleic Acids Research*, *38*(Web Server issue), W360.  
<https://doi.org/10.1093/NAR/GKQ371>
75. Hyun, S. (2018). Body size regulation by maturation steroid hormones: a *Drosophila* perspective. *Frontiers in Zoology*, *15*(1), 1–9. <https://doi.org/10.1186/S12983-018-0290-9>
76. Whirledge, S., & Cidlowski, J. A. (2019). Steroid Hormone Action. In J. F. Strauss & R. L. Barbieri (Eds.), *Yen & Jaffe's Reproductive Endocrinology: Physiology*,

- Pathophysiology, and Clinical Management* (p. 115-131.e4). Elsevier.  
<https://doi.org/10.1016/B978-0-323-47912-7.00005-6>
77. Riddiford L. (1993). Hormones and Drosophila development. *The development of Drosophila melanogaster*, 2, 899–939.
  78. Ou, Q., Zeng, J., Yamanaka, N., Brakken-Thal, C., O'Connor, M. B., & King-Jones, K. (2016). The Insect Prothoracic Gland as a Model for Steroid Hormone Biosynthesis and Regulation. *Cell Reports*, 16(1), 247–262.  
<https://doi.org/10.1016/J.CELREP.2016.05.053>
  79. Kannangara, J. R., Mirth, C. K., & Warr, C. G. (2021). Regulation of ecdysone production in Drosophila by neuropeptides and peptide hormones. *Open Biology*, 11(2), e200373. <https://doi.org/10.1098/RSOB.200373>
  80. Chiabrando, D., Vinchi, F., Fiorito, V., Mercurio, S., & Tolosano, E. (2014). Heme in pathophysiology: A matter of scavenging, metabolism and trafficking across cell membranes. *Frontiers in Pharmacology*, 5, 1-24.  
<https://doi.org/10.3389/fphar.2014.00061>
  81. Neuberger, A., & Scott, J. J. (1953). Aminolævulinic Acid and Porphyrin Biosynthesis. *Nature*, 172(4389), 1093–1094. <https://doi.org/10.1038/1721093a0>
  82. Jordan, P. M. & Seehra, J. S. (1979). The biosynthesis of uroporphyrinogen III: Order of assembly of the four porphobilinogen molecules in the formation of the tetrapyrrole ring. *FEBS Letters*, 104(2), 364-366. [https://doi.org/10.1016/0014-5793\(79\)80853-4](https://doi.org/10.1016/0014-5793(79)80853-4)
  83. Jordan, P. M., Burton, G., Nordlöv, H., Schneider, M. M., Pryde, L., & Scott, A. I. (1979). Pre-uroporphyrinogen: a substrate for uroporphyrinogen III cosynthetase. *Journal of the Chemical Society, Chemical Communications*, 5, 204–205.  
<https://doi.org/10.1039/C39790000204>
  84. R Poulson, & W J Polglase. (1975). The enzymic conversion of protoporphyrinogen IX to protoporphyrin IX. Protoporphyrinogen oxidase activity in mitochondrial extracts of *Saccharomyces cerevisiae*. *J Biol Chem*, 250(4), 1269–1274.  
<https://pubmed.ncbi.nlm.nih.gov/234450/>
  85. Taketani, S. (1994). Molecular and genetic characterization of ferrochelatase. *STEM CELLS*, 12(1), 41–54. <https://doi.org/10.1002/STEM.5530120707>

86. Buchan DWA, Jones DT (2019). The PSIPRED Protein Analysis Workbench: 20 years on. *Nucleic Acids Research*, 47(1), 402-407. <https://doi.org/10.1093/nar/gkz297>
87. Zimmermann, R. (2009). Post-Targeting Functions of Signal Peptides. *Protein Transport into the Endoplasmic Reticulum* (p. 21-36). CRC Press. <https://doi.org/10.1201/9781498714013-6>
88. Alberts, B., Johnson, A., Lewis, J., Raff, M., Roberts, K., and Walter, P. (2002). The Compartmentalization of Cells. In *Molecular biology of the cell* (4<sup>th</sup> Edition). Garland Science. Retrieved from <https://www.ncbi.nlm.nih.gov/books/NBK26907/>
89. Lodish, H., Berk, A., Zipursky, S. L., Matsudaira, P., Baltimore, D., & Darnell, J. (2000). Overview of the Secretory Pathway. In *Molecular Cell Biology* (4<sup>th</sup> Edition). W.H. Freeman. <https://www.ncbi.nlm.nih.gov/books/NBK21471/>
90. Noriega, T. R., Tsai, A., Elvekrog, M. M., Petrov, A., Neher, S. B., Chen, J., Bradshaw, N., Puglisi, J. D., & Walter, P. (2014). Signal Recognition Particle-ribosome Binding Is Sensitive to Nascent Chain Length \*. *Journal of Biological Chemistry*, 289(28), 19294–19305. <https://doi.org/10.1074/JBC.M114.563239>
91. Walter, P., Ibrahimi, I., & Blobel, G. (1981). Translocation of Proteins Across the Endoplasmic Reticulum I. Signal Recognition Protein (SRP) Binds to In-Vitro-Assembled Polysomes Synthesizing Secretory Protein. *The Journal of Cell Biology*, 91(2), 545–550. <https://doi.org/10.1083/jcb.91.2.545>
92. Prehn, S., Nürnberg, P., & Rapoport, T. A. (1981). A receptor for signal segments of secretory proteins in rough endoplasmic reticulum membranes. *FEBS Letters*, 123(1), 79–84. [https://doi.org/10.1016/0014-5793\(81\)80024-5](https://doi.org/10.1016/0014-5793(81)80024-5)
93. Gilmore R, Walter P, Blobel G. (1982). Protein translocation across the endoplasmic reticulum. II. Isolation and characterization of the signal recognition particle receptor. *The Journal of Cell Biology*, 95(2), 470-477. <https://doi.org/10.1083/jcb.95.2.470>
94. Blobel, G., and Dobberstein, B. (1975). Transfer of proteins across membranes. I. Presence of proteolytically processed and unprocessed nascent immunoglobulin light chains on membrane-bound ribosomes of murine myeloma. *Journal of Cell Biology*, 67(3), 835–851. <https://doi.org/10.1083/jcb.67.3.835>
95. Molhoj, M., and Dal Degan, F. (2004). Leader sequences are not signal peptides. *Nature Biotechnology*, 22(12), 1502–1502. <https://doi.org/10.1038/nbt1204-1502>

96. Von Heijne, G. (1990). The signal peptide. *The Journal of Membrane Biology*, 115(3), 195–201. <https://doi.org/10.1007/BF01868635>
97. Von Heijne, G. (1998). Protein transport - Life and death of a signal peptide. *Nature*, 396(6707), 111–113. <https://doi.org/10.1038/24036>
98. Weihofen, A., Lemberg, M. K., Ploegh, H. L., Bogyo, M., & Martoglio, B. (2000). Release of signal peptide fragments into the cytosol requires cleavage in the transmembrane region by a protease activity that is specifically blocked by a novel cysteine protease inhibitor. *Journal of Biological Chemistry*, 275(40), 30951-30956. <https://doi.org/10.1074/jbc.M005980200>
99. Farquhar, M.G. (1985). Progress in unraveling pathways of Golgi traffic. *Annu. Rev. Cell Biol.*, 1, 447-488. <https://doi.org/10.1146/annurev.cb.01.110185.002311>
100. Mellman, I. and Simons, K. (1992). The Golgi complex: in vitro veritas? *Cell*, 68(5), 829-840. [https://dx.doi.org/10.1016%2F0092-8674\(92\)90027-A](https://dx.doi.org/10.1016%2F0092-8674(92)90027-A)
101. Wang, J. W., Beck, E. S., & McCabe, B. D. (2012). A modular toolset for recombination transgenesis and neurogenetic analysis of Drosophila. *PLoS ONE*, 7(7), e42102. <https://doi.org/10.1371/journal.pone.0042102>
102. Gratz, S. J., Rubinstein, C. D., Harrison, M. M., Wildonger, J., & O'Connor-Giles, K. M. (2015). CRISPR-Cas9 genome editing in Drosophila. *Current Protocols in Molecular Biology*, 111(1), 31.2.1-31.2.20. <https://doi.org/10.1002/0471142727.mb3102s111>
103. Livak, K. J., & Schmittgen, T. D. (2001). Analysis of Relative Gene Expression Data Using Real-Time Quantitative PCR and the 2- $\Delta\Delta$ CT Method. *Methods*, 25(4), 402–408. <https://doi.org/10.1006/METH.2001.1262>
104. Xiao, G., Liu, Z.-H., Zhao, M., Wang, H.-L., & Zhou, B. (2019). Transferrin 1 Functions in Iron Trafficking and Genetically Interacts with Ferritin in Drosophila melanogaster. *CellReports*, 26(3), 748-758.e5. <https://doi.org/10.1016/j.celrep.2018.12.053>
105. Stephen F. Altschul, Thomas L. Madden, Alejandro A. Schäffer, Jinghui Zhang, Zheng Zhang, Webb Miller, and David J. Lipman. (1997). Gapped BLAST and PSI-BLAST: a new generation of protein database search programs. *Nucleic Acids Res*, 25, 3389-3402.
106. Stephen F. Altschul, John C. Wootton, E. Michael Gertz, Richa Agarwala, Aleksandr Morgulis, Alejandro A. Schäffer, and Yi-Kuo Yu. (2005). Protein database searches

- using compositionally adjusted substitution matrices. *FEBS J.*, 272(20), 5101-5109.  
<https://doi.org/10.1111/j.1742-4658.2005.04945.x>
107. Fire, A., Xu, S., Montgomery, M. K., Kostas, S. A., Driver, S. E., & Mello, C. C. (1998). Potent and specific genetic interference by double-stranded RNA in *Caenorhabditis elegans*. *Nature*, 391(6669), 806–811. <https://doi.org/10.1038/35888>
  108. Heigwer, F., Port, F., & Boutros, M. (2018). RNA Interference (RNAi) Screening in *Drosophila*. *Genetics*, 208(3), 874. <https://doi.org/10.1534/GENETICS.117.300077>
  109. Pan, H., Yang, X., Bidne, K., Hellmich, R. L., Siegfried, B. D., & Zhou, X. (2015). Selection of reference genes for RT-qPCR analysis in the monarch butterfly, *Danaus plexippus* (L.), a migrating bio-indicator. *PLoS ONE*, 10(6), e0129482.  
<https://doi.org/10.1371/journal.pone.0129482>
  110. Rual, J.-F., Klitgord, N., & Achaz, G. (2007). Novel insights into RNAi off-target effects using *C. elegans* paralogs. *BMC Genomics*, 8(1), 1–8. <https://doi.org/10.1186/1471-2164-8-106>
  111. Gelbart, W.M., Emmert, D.B. (2013). FlyBase High Throughput Expression Pattern Data.
  112. Corrin, B. (1981). Carleton's Histological Technique. *Journal of Clinical Pathology*, 34(5), 572. <https://doi.org/10.1136/jcp.34.5.572-d>
  113. Missirlis, F., Kosmidis, S., Brody, T., Mavrakis, M., Holmberg, S., Odenwald, W. F., Skoulakis, E. M. C., & Rouault, T. A. (2007). Homeostatic mechanisms for iron storage revealed by genetic manipulations and live imaging of *Drosophila* ferritin. *Genetics*, 177(1), 89-100. <https://doi.org/10.1534/genetics.107.075150>
  114. Nagalakshmi, U., Wang, Z., Waern, K., Shou, C., Raha, D., Gerstein, M., & Snyder, M. (2008). The Transcriptional Landscape of the Yeast Genome Defined by RNA Sequencing. *Science (New York, N.Y.)*, 320(5881), 1344-1349.  
<https://doi.org/10.1126/SCIENCE.1158441>
  115. Costa, C., Giménez-Capitán, A., Karachaliou, N., & Rosell, R. (2013). Comprehensive molecular screening: from the RT-PCR to the RNA-seq. *Translational Lung Cancer Research*, 2(2), 87-91. <https://doi.org/10.3978/J.ISSN.2218-6751.2013.02.05>
  116. Meissner, B., Rogalski, T., Viveiros, R., Warner, A., Plastino, L., Lorch, A., Granger, L., Segalat, L., & Moerman, D. G. (2011). Determining the sub-cellular localization of

- proteins within *Caenorhabditis elegans* body wall muscle. *PLoS ONE*, 6(5), e19937.  
<https://doi.org/10.1371/journal.pone.0019937>
117. Peng, C., & Gao, F. (2014). Protein localization analysis of essential genes in prokaryotes. *Scientific Reports*, 4(1), 1-7. <https://doi.org/10.1038/srep06001>
  118. *SignalP - 5.0 - Services - DTU Health Tech*. (n.d.). Retrieved October 21, 2021, from <https://services.healthtech.dtu.dk/service.php?SignalP-5.0>
  119. Fritze, C. E., & Anderson, T. R. (2000). Epitope tagging: General method for tracking recombinant proteins. In J. Thorner, S. D. Emr, & J. N. Abelson (Eds.), *Methods in Enzymology* (p. 3-16). Academic Press. [https://doi.org/10.1016/S0076-6879\(00\)27263-7](https://doi.org/10.1016/S0076-6879(00)27263-7)
  120. LaJeunesse, D. R., Buckner, S. M., Lake, J., Na, C., Pirt, A., & Fromson, K. (2004). Three new *Drosophila* markers of intracellular membranes. *BioTechniques*, 36(5), 784-790. <https://doi.org/10.2144/04365st01>
  121. Rutz, C., Klein, W., & Schüle, R. (2015). N-Terminal Signal Peptides of G Protein-Coupled Receptors: Significance for Receptor Biosynthesis, Trafficking, and Signal Transduction. *Progress in Molecular Biology and Translational Science* (p. 267–287). Academic Press. <https://doi.org/10.1016/BS.PMBTS.2015.03.003>
  122. Bieli, D., Alborelli, I., Harmansa, S., Matsuda, S., Caussinus, E., & Affolter, M. (2016). Development and Application of Functionalized Protein Binders in Multicellular Organisms. In J. Kang W. (Ed.), *International Review of Cell and Molecular Biology* (p. 181-213). Academic Press. <https://doi.org/10.1016/BS.IRCMB.2016.02.006>
  123. Bolognesi, B., & Lehner, B. (2018). Protein Overexpression: Reaching the limit. *eLife*, 7, e39804. <https://doi.org/10.7554/eLife.39804>
  124. Prelich, G. (2012). Gene overexpression: Uses, mechanisms, and interpretation. In *Genetics*, 190(3), 841-854. <https://doi.org/10.1534/genetics.111.136911>
  125. Yamabhai, M., Buranabanyat, B., Jaruseranee, N., & Songsiriritthigul, C. (2011). Efficient *E. coli* expression systems for the production of recombinant  $\beta$ -mannanases and other bacterial extracellular enzymes. *Bioengineered Bugs*, 2(1), 45-49. <https://doi.org/10.4161/bbug.2.1.13419>
  126. Zhang, B., Zhang, Y., & Liu, J. L. (2021). Highly effective proximate labeling in *Drosophila*. *G3: Genes, Genomes, Genetics*, 11(5), jkab077. <https://doi.org/10.1093/g3journal/jkab077>

127. Bischof, J., Maeda, R. K., Hediger, M., Karch, F., & Basler, K. (2007). An optimized transgenesis system for *Drosophila* using germ-line-specific  $\phi$ C31 integrases. *Proceedings of the National Academy of Sciences of the United States of America*, *104*(9), 3312-3317. <https://doi.org/10.1073/pnas.0611511104>
128. Reinke, A. W., Mak, R., Troemel, E. R., & Ben, E. J. (2017). In vivo mapping of tissue- and subcellular-specific proteomes in *Caenorhabditis elegans*. *Science Advances*, *3*(5), e1602426. <https://doi.org/10.1126/SCIADV.1602426>
129. Farkaš, R., Beňová-Liszeková, D., Mentelová, L., Beňo, M., Babišová, K., Trusínová-Pečeňová, L., Raška, O., Chase, B. A., & Raška, I. (2018). Endosomal vacuoles of the prepupal salivary glands of *Drosophila* play an essential role in the metabolic reallocation of iron. *Development, Growth & Differentiation*, *60*(7), 411–430. <https://doi.org/10.1111/DGD.12562>
130. Solis, G. P., Radon, Y., Sempou, E., Jechow, K., Stuermer, C. A. O., & Málaga-Trillo, E. (2013). Conserved Roles of the Prion Protein Domains on Subcellular Localization and Cell-Cell Adhesion. *PLoS ONE*, *8*(7), e70327. <https://doi.org/10.1371/journal.pone.0070327>
131. Huang, Y., Wilkinson, G. F., & Willars, G. B. (2010). Role of the signal peptide in the synthesis and processing of the glucagon-like peptide-1 receptor. *British Journal of Pharmacology*, *159*(1), 237-251. <https://doi.org/10.1111/j.1476-5381.2009.00517.x>
132. Bolognesi, B., & Lehner, B. (2018, August 10). *Protein Overexpression: Reaching the limit*. ELife. <https://doi.org/10.7554/ELIFE.39804>
133. Kintaka, R., Makanae, K., & Moriya, H. (2016). Cellular growth defects triggered by an overload of protein localization processes. *Scientific Reports 2016 6:1*, *6*(1), 1–11. <https://doi.org/10.1038/srep31774>
134. Aksoy, Y. A., Yang, B., Chen, W., Hung, T., Kuchel, R. P., Zammit, N. W., Grey, S. T., Goldys, E. M., & Deng, W. (2020). Spatial and Temporal Control of CRISPR-Cas9-Mediated Gene Editing Delivered via a Light-Triggered Liposome System. *ACS Applied Materials & Interfaces*, *12*(47), 52433–52444. <https://doi.org/10.1021/ACSAMI.0C16380>
135. Caporale, N., & Testa, G. (2019). At the Intersection of Epigenetics and Regeneration: An Analysis of the Experimental Outlook of Organoid Technology. In D. Palacios (Ed.),

- Epigenetics and Regeneration* (p. 385–402). Academic Press.  
<https://doi.org/10.1016/B978-0-12-814879-2.00017-0>
136. Horn, C., Jaunich, B., & Wimmer, E. A. (2000). Highly sensitive, fluorescent transformation marker for *Drosophila* transgenesis. *Development Genes and Evolution*, 210(12), 623-629. <https://doi.org/10.1007/s004270000111>
  137. Spizzo, T., Byersdorfer, C., Duesterhoeft, S., & Eide, D. (1997). The yeast *FET5* gene encodes a *FET3*-related multicopper oxidase implicated in iron transport. *Mol Gen Genet*, 256(5), 547-556. <https://doi.org/10.1007/pl00008615>
  138. Wang, X., Yin, S., Yang, Z., & Zhou, B. (2018). *Drosophila* multicopper oxidase 3 is a potential ferroxidase involved in iron homeostasis. *Biochimica et Biophysica Acta (BBA) - General Subjects*, 1862(8), 1826–1834.  
<https://doi.org/10.1016/J.BBAGEN.2018.04.017>
  139. Tang, X., & Zhou, B. (2013). Ferritin is the key to dietary iron absorption and tissue iron detoxification in *Drosophila melanogaster*. *FASEB Journal: Official Publication of the Federation of American Societies for Experimental Biology*, 27(1), 288–298.  
<https://doi.org/10.1096/FJ.12-213595>
  140. le Blanc, S., Garrick, M. D., & Arredondo, M. (2012). Heme carrier protein 1 transports heme and is involved in heme-Fe metabolism. *American Journal of Physiology. Cell Physiology*, 302(12). <https://doi.org/10.1152/AJPCELL.00080.2012>
  141. Ndayisaba, A., Kaindlstorfer, C., & Wenning, G. K. (2019). Iron in Neurodegeneration – Cause or Consequence? *Frontiers in Neuroscience*, 13.  
<https://doi.org/10.3389/FNINS.2019.00180>
  142. Torti, S. v., & Torti, F. M. (2013). Iron and cancer: more ore to be mined. *Nature Reviews Cancer*, 13(5), 342-355. <https://doi.org/10.1038/NRC3495>
  143. Robert A, S., & Culotta, V. (Eds.). (2013). *Metals in Cells* (p. 255). John Wiley & Sons.  
<https://www.wiley.com/en-us/Metals+in+Cells-p-9781119953234>
  144. Cho, K. F., Branon, T. C., Udeshi, N. D., Myers, S. A., Carr, S. A., & Ting, A. Y. (2020). Proximity labeling in mammalian cells with TurboID and split-TurboID. *Nature Protocols* 2020, 15(12), 3971–3999. <https://doi.org/10.1038/s41596-020-0399-0>
  145. Branon, T. C., Bosch, J. A., Sanchez, A. D., Udeshi, N. D., Svinkina, T., Carr, S. A., Feldman, J. L., Perrimon, N., & Ting, A. Y. (2018). Efficient proximity labeling in living

- cells and organisms with TurboID. *Nature Biotechnology*, 36(9), 880–887.  
<https://doi.org/10.1038/nbt.4201>
146. Mahalingam, M., & Fessenden, J. D. (2015). Methods for Labeling Skeletal Muscle Ion Channels Site-Specifically with Fluorophores Suitable for FRET-Based Structural Analysis. *Methods in Enzymology*, 556, 455–474.  
<https://doi.org/10.1016/BS.MIE.2014.11.049>
147. Koushik, S. v., Chen, H., Thaler, C., Puhl, H. L., & Vogel, S. S. (2006). Cerulean, venus, and venusY67C FRET reference standards. *Biophysical Journal*, 91(12), 99–101.  
<https://doi.org/10.1529/biophysj.106.096206>
148. Wong, B. X., Ayton, S., Lam, L. Q., Lei, P., Adlard, P. A., Bush, A. I., & Duce, J. A. (2014). A comparison of ceruloplasmin to biological polyanions in promoting the oxidation of Fe<sup>2+</sup> under physiologically relevant conditions. *Biochimica et Biophysica Acta (BBA) - General Subjects*, 1840(12), 3299–3310.  
<https://doi.org/10.1016/J.BBAGEN.2014.08.006>